

**ARTIFICIAL INTELLIGENCE BASED TOOL CONDITION
MONITORING IN MACHINING**

**ARTIFICIAL INTELLIGENCE BASED TOOL CONDITION
MONITORING IN MACHINING**

By

Md. Shafiul Alam, B.Sc.

(McMaster University, Canada)

A Thesis

Submitted to the School of Graduate Studies

in Partial Fulfilment of the Requirements

for the Degree

Master of Applied Science

McMaster University

© Copyright by Md. Shafiul Alam, December 2018

MASTER OF APPLIED SCIENCE (2018)

(Mechanical Engineering)

McMaster University

Hamilton, Ontario

TITLE:

**Artificial Intelligence based Tool Condition
Monitoring in Machining**

AUTHOR:

Md. Shafiul Alam, B.Sc.

SUPERVISOR:

Dr. Stephen C. Veldhuis

Department of Mechanical Engineering

McMaster University

NUMBER OF PAGES:

CXX, 120

Abstract

In a manufacturing environment, gradual and catastrophic failure of a cutting tool are common faults associated with a machining process. Left unmonitored these failures exhibit a high likelihood of triggering workpiece surface quality issues and reducing the overall productivity of the process. This research offers a comprehensive study of the design, development and implementation of a low-cost artificially intelligent (AI) tool condition monitoring (TCM) system for the turning operation of different workpiece material. As the characteristics of the signals from the fusion of multiple sensors differ from each individual sensor, fast Fourier transform (FFT) and wavelet transform (WT) were used to identify signal features which provided the most useful information about the cutting tool conditions. Pearson correlation coefficients (PCC) and principal component analysis (PCA) singled out the most sensitive features from the sensor fusion signals which play a pivotal role in monitoring gradual tool wear (flank wear) progression during machining. Experimental results indicated that the total harmonic distortion (THD), crest factor of the spindle motor current and certain spectral features from the vibration sensor signal had a significant correlation with cutting tool flank wear under different cutting conditions and when machining different materials. Furthermore, a data-driven artificial neural network (ANN) and an adaptive neuro-fuzzy inference system (ANFIS) were studied to investigate their prediction accuracy for cutting tool conditions (tool wear). The ANFIS prediction model outperformed the ANN prediction in terms of accuracy. As a result, the developed (trained and validated) ANFIS based TCM system was implemented in the material turning

process. In addition, the adaptability of the supervised ANFIS based TCM system was shown to further increase the reliability of tool wear prediction.

Acknowledgements

I would like to express my profound appreciation to my supervisor Dr. Stephen C. Veldhuis for his supervision and continuous guidance at all stages of this research work. I also acknowledge the financial support from the Natural Sciences and Engineering Research Council of Canada (NSERC) and the Canadian Network for Research and Innovation in Machining Technology (CANRIMT) and the McMaster Manufacturing Research Institute (MMRI) for its state of the art research facilities.

Additionally, I would like to express my gratitude to Dr. Abul fazal Arif, Dr. Maryam Aramesh, Dr. José Mario Fernandes Paiva JR. for their detailed guidance and constructive suggestions in every step of the research work. I would also like to thank MMRI colleagues and staff, especially Terry Wagg, Simon Oomen-Hurst, Brady Semple & Steve Remilli for their technical support during my research work.

Finally, I thank my parents, my siblings, my brother-in-law Dr. A Z M Shahriar Muttalib and my uncle Brig. Gen. Shamsur Rahman for their continued support and encouragement throughout my entire life.

Table of Contents

Abstract	iii
Acknowledgements	v
Table of Contents	vi
List of Figures	x
List of Tables	xiii
Nomenclature	xiv
Chapter 1. Introduction	1
1.1. Research Motivation	1
1.2. Research Objectives	2
1.3. Dissertation Outline.....	2
Chapter 2. Literature Review	4
2.1. Introduction	4
2.2. Tool Condition Monitoring (TCM).....	5
2.2.1. Sensors	8
2.2.2. Signal Processing and Feature Extraction.....	12
2.2.3. Artificial Intelligence (AI) Decision Making Techniques	15
2.2.4. Conclusions.....	18
Chapter 3. TCM System Design and Architecture	19

3.1.	Introduction	19
3.2.	Framework of the TCM System Architecture	19
3.3.	Selection of Sensors/ Sensor Fusions	22
3.3.1.	Three (3)-Component Cutting Force Sensor	23
3.3.2.	Vibration Sensor	24
3.3.3.	Transformer-based Current Sensor	25
3.3.4.	Sensor Signal Acquisition System	27
Chapter 4. Experimental Work & Data Acquisition		28
4.1.	Experimental Details	28
4.1.1.	Machine Tools	28
4.1.2.	Workpiece Material & Cutting Tools	29
4.1.3.	Experiment Setup	31
4.1.4.	Tool Wear Measurement	31
4.1.5.	Design of Experiment	35
4.2.	Experimental Results and Discussion	36
4.2.1.	Test Reports	36
4.2.2.	Effect of Tool-wear on Spindle Current	41
4.2.3.	Effect of Tool-wear on Forces	46
4.2.4.	Effect of Tool-wear on Vibration	47

Chapter 5. Signal Processing & Features Extraction	49
5.1. Signal Acquisition & Pre-Processing	49
5.2. Fourier Transforms (FT)	52
5.3. Wavelet Transform (WT) Analysis	53
5.4. Feature Extraction & Dimensionality Reduction	58
5.4.1. Pearson’s Correlation Coefficient (PCC) Analysis.....	62
5.4.2. Principal Component Analysis (PCA)	63
5.5. Discussion	69
Chapter 6. AI-based Decision-Making Module	70
6.1. Introduction to Artificial Intelligence (AI) in Machining	70
6.2. Multi-layer Perceptron based Artificial Neural Network.....	70
6.2.1. Comprehensive Evaluation of Major Clusters from PCC and PCA.....	73
6.3. Adaptive Neuro-Fuzzy Inference System (ANFIS)	82
6.3.1. Comprehensive Evaluation of Major Clusters from PCC and PCA	88
6.4. Comparison between AI Techniques for TCM	92
Chapter 7. Implementation of the Developed TCM System.....	95
7.1. Introduction	95
7.2. Implementation Methodology of the TCM System	95
7.3. TCM System for Different Workpiece Material	98

7.3.1. Case Study- 1	99
7.3.2. Case Study- 2	101
7.3.3. Discussion	102
7.4. Adaptability of the TCM System	105
Chapter 8. Conclusions and Future Work.....	108
8.1. Summary of the Research	108
8.2. The contribution of the Research	111
8.3. Future Work and Recommendations	113
References	114

List of Figures

Figure 1: Cutting tool conditions during machining.....	7
Figure 2: Key features in the TCM system.....	8
Figure 3: Sources of AE in machining [9].....	10
Figure 4: Vibration signals in machining (time & frequency domain) [14].....	11
Figure 5: Effect of tool wear on spindle motor current signals [15].....	11
Figure 6: Influence of bits and sampling rate in signal processing [18].....	13
Figure 7: Fourier and wavelet transform in signal processing.....	15
Figure 8: Architecture of the designed TCM systems	20
Figure 9: Three (3)-component dynamometer setup in the turning operation.....	23
Figure 10: Kistler© 8742A shock accelerometer setup in the turning operation	25
Figure 11: Installation of a split-core AC-current sensor [58].....	26
Figure 12: Installed split-core AC-current sensor over spindle motor wiring.....	26
Figure 13: (a) National Instrument© 9125 DAQ and (b) Kistler© 5010 amplifier.....	27
Figure 14: Nakamura- Tome CNC turning centre	29
Figure 15: Experimental setup for the turning operation using sensor fusion.....	31
Figure 16: Types of tool wear [60]	32
Figure 17: Stages of cutting tool flank wear.....	33
Figure 18: Optical microscopy used in this research.....	34
Figure 19: Tool wear curve development from standard tests.....	37
Figure 20: Tool wear curve development from severe cutting tests.....	39
Figure 21: Influence of harmonic in a signal	43

Figure 22: Effect of ‘aliasing’ in signal	43
Figure 23: Variation of THD in a tool life study (T4) (see Table 10)	45
Figure 24: Crest factor variation in the tool life study ((T4) (see Table 10).....	46
Figure 25: Variation of forces in a tool life study (T4) (see Table 10).....	47
Figure 26: Variation of vibration (RMS) in a tool life study (T1) (see Table 10).....	48
Figure 27: An example of sensor fusion raw signals	50
Figure 28: Data Segmentation (event detection) of a raw signal	51
Figure 29: An extracted event from the raw signals	51
Figure 30: Power spectrum of the extracted vibration signals (T7) (see Table 10).....	53
Figure 31: 3-level of wavelet packet decomposition tree of the measured signal	56
Figure 32: 3-level WPD of the vibration signal at flank wear 124 μ m.....	57
Figure 33: 3-level WPD of the vibration signal at flank wear 411 μ m.....	58
Figure 34: PCA analysis procedure	66
Figure 35: Scree plot (based on all dataset)	66
Figure 36: Score plot of the 1 st and 2 nd principal components (based on all dataset).....	67
Figure 37: Three-layer feed-forward neural network	72
Figure 38: Major clusters from PCC analysis	74
Figure 39: Major Clusters based on PCA	74
Figure 40: Effect of ML algorithms on the NN success rate	77
Figure 41: Effect of hidden layer node number on NN success rate	77
Figure 42: Evaluation of PCC based clusters in the Neural Network (NN)	78
Figure 43: Effect of cluster type on NN success rate.....	79

Figure 44: Evaluation of PCA based clusters in the Neural Network (NN)	80
Figure 45: RMSE based evaluation of all cluster in NN modelling	82
Figure 46: ANFIS architecture.....	83
Figure 47: Flowchart of ANFIS modelling.....	86
Figure 48: A general overview of the ANFIS interface.....	87
Figure 49: ANFIS validation results with RMSE.....	89
Figure 50: Evaluation of PCC and PCA based cluster on ANFIS modelling.....	92
Figure 51: Comparison among AI based prediction model	94
Figure 52: Experiment setup for validation (including tool holder)	96
Figure 53: TCM system implementation flowchart.....	97
Figure 54: The architecture of the data-driven TCM system.....	98
Figure 55: Prediction comparison of the TCM system (PCC-cluster-1 based)	100
Figure 56: Prediction comparison of the TCM system (PCA-cluster-1 based)	100
Figure 57: Prediction comparison of the TCM system (PCC-cluster-1 based)	101
Figure 58: Prediction comparison of the TCM system (PCA-cluster-1 based)	102
Figure 59: Error comparison of the TCM system.....	105
Figure 60: Adaptability of the Supervised TCM system	107

List of Tables

Table 1: Common sensing variable to monitor faults in machining	6
Table 2: A summary of signal processing techniques from the literature	15
Table 3: A summary of diagnostics tool usage from featured researches	17
Table 4: Technical specifications of the three-component dynamometer	23
Table 5: Technical specification of the shock accelerometer	25
Table 6: Technical specifications of the current sensor (ACT005-42L-S).....	26
Table 7: Technical specifications of the data acquisition system	27
Table 8: List of workpiece materials used in this research	30
Table 9: Tool holders and Cutting tools	30
Table 10: Design of experiment (Taguchi L9 orthogonal array)	35
Table 11: Offline monitoring results (standard cutting tests)	38
Table 12: Offline monitoring results (severe cutting tests)	40
Table 13: List of extracted features from the processed sensor signal	60
Table 14: Correlations between extracted features and cutting tool wear	63
Table 15: List of significant features based on PCA score	68
Table 16: ANFIS Learning Structure.....	88
Table 17: ANFIS structure Information.....	90
Table 18: Experiment details for the TCM system implementation.....	97
Table 19: Summary of the offline monitoring results.....	103

Nomenclature

TCM - Tool Condition Monitoring

FFT- Fast Fourier Transform

WT- Wavelet Transform

AC- Alternating Current

AI- Artificial Intelligence

Vb- Flank Wear

Vc- Cutting Speed

f- Feed Rate

doc- Depth of Cut

CBN- Cubic Boron Nitride

PCA- Principal Component Analysis

PCC- Pearson Correlation Coefficient

ANN- Artificial Neural Network

LM- Levenberg Marquardt

SCG- Scaled Conjugate Gradient

GDX- Variable Learning Rate Backpropagation

ANFIS- Adaptive Neuro-Fuzzy Inference System

RMS- Root Mean Square

Chapter 1. Introduction

1.1. Research Motivation

Prediction of cutting tool condition (tool wear) during the machining process has been a topic of research for decades. Several techniques were introduced and implemented such as numeric methods and simulations. Very few methods have been fully validated in practice. Even if they were implemented, their reliability was observed to degrade compared to lab-based testing in the actual manufacturing environment. In current industrial practice, worn out cutting tools are generally removed based on: machining time, the operator's experience, periodic offline measurements of the tool or workpiece surface finish many of which are based on recommendations provided by the cutting tool supplier. Also, indirect measurement technologies are currently being used in the manufacturing industry. However, in most cases, indirect measurement costs, setup or data analytics are simply not efficient enough for an automated manufacturing environment. An efficient and low-cost based cutting tool wear monitoring system can provide an advantage for small to medium scale industries.

This research investigates a low-cost tool wear monitoring system. It provides a solution which uses a comprehensive and adaptive model, that expends minimal effort on feature extraction while incorporating real-time sensor data. The goal of this study is to propose a standard gradual tool wear monitoring system which could be implemented in other material machining processes.

1.2. Research Objectives

The key goals of this research are

1. A comprehensive study of an artificial intelligence (AI) based tool condition monitoring system for machining applications.
2. Design & development of a low-cost tool condition monitoring (TCM) system for turning operations.
3. Implementation of the developed tool condition monitoring (TCM) system in turning operations of different workpiece material.

1.3. Dissertation Outline

This thesis is arranged in eight (8) chapters. The summary of each chapter is as follows:

CHAPTER 1: Research motivation and objectives.

CHAPTER 2: Introduction to the concept of the tool condition monitoring (TCM), literature review and description of the research potential in this field.

CHAPTER 3: Outline of the methodology and the architecture of the system. System level design using sensor fusion methods.

CHAPTER 4: Details of the experimental procedure and the data acquisition system. The first section of this chapter introduces every element of the TCM system, including the design of experiment. The second section highlights the impact of online monitoring on cutting tool conditions and explains the effect of cutting tool conditions on the sensor fusion signal.

CHAPTER 5: Signal processing techniques and feature extraction. In the first section, signal processing was applied to evaluate the acquired signal. The next section explains the data analytics procedure for feature extraction and dimensionality reduction techniques.

CHAPTER 6: A comparative study of two artificial intelligence (AI) techniques during development of TCM system architecture's decision-making levels. Comprehensive evaluation of the model produced from the sensor fusion signal and cutting tool conditions.

CHAPTER 7: Implementation of the developed TCM system in machining through several case studies. This chapter also demonstrates the wide-ranging adaptability of the TCM system.

CHAPTER 8: Conclusions drawn from the current research and prospects of its future extension.

Chapter 2. Literature Review

2.1. Introduction

The metal cutting operation is one of the most significant operations in manufacturing systems when tight dimensional tolerances and surface finishes are required. Generally, metal cutting or machining operation (conventional or non- conventional) can be affected by various known or unknown disturbances which can interact in complex ways due to the machining process's inherent non-linearity. Therefore, there is always a necessity for efficient decision-making capability to support the machining process operation. This is due to the ever-increasing demand for improved productivity, part quality and process reliability. For many decades, the application of automation in decision-making has been a focus of considerable research attention in both the manufacturing industry and academia. The recent trend of incorporating automation in the process level of machining operations has extended to introducing artificial intelligence (AI) based techniques. The decision-making capabilities of a human operator is the result of long-term training and practice over time. In the case of the automated manufacturing system, the training and the practice comes from the mathematical model based on the relationship of the sensor data and the physics of the metal cutting processes.

For an automated machining process, monitoring and decision making are fundamental functions. Without this functionality, a machining process cannot be adjusted intelligently to maintain and improve the machining process over time. Therefore, a machine monitoring

and decision-making system are required in a machining setup and named a ‘Tool Condition Monitoring System’ or TCM system for the purposes of this thesis.

2.2. Tool Condition Monitoring (TCM)

The recent trend of modern machining industries is geared towards reducing production costs by targeting higher productivity with reduced cost, particularly in terms of human effort. The ultimate goal however is to achieve the most advanced and automated manufacturing system in the industry appropriately leveraging human expertise and machine capabilities.

Cutting tools are a critical component of a machining system. A cutting tool can undergo two different types of faults during machining, such as, hard faults and soft faults. Hard faults are the sudden fault (catastrophic tool failure) while soft faults develop gradually over time (i.e. gradual tool wear). Table 1 shows several common sensing variables used to monitor these faults in machining. An intelligent manufacturing system cannot be possible without a proper tool management system. Cutting tool failure influences the quality of the surface finish, dimensions of the machined parts and the production time. Tool failure causes significantly interruption to the machining environment [1]. Previous research showed that for modern machine tools, cutting tool failure can result in approximately 20% downtime in addition to reduced productivity and economic losses due to scrapping or reworking of defective parts [2]. A tool condition monitoring (TCM) system has two objectives. One is to make an accurate evaluation of the tool's condition, and the other is the real-time detection of catastrophic tool failure. Tool

wear during machining is a natural part of the material removal process, and it is challenging to estimate its level. Catastrophic tool breakage is the most crucial phenomenon in machining since it can irreversibly damage the product's surface. Therefore, estimation of tool wear leading up to catastrophic failure is also an important part of ensuring satisfactory final product surface quality.

Determining the cutting tool condition also has value for predicting the surface roughness of the final product. If tight tolerances are set for the surface quality of the final product, these tolerances can be inferred from the tool's cutting condition if it can be continuously monitored. Thus, effective tool wear estimation is essential to ensure the tool can last until the end of the process. Knowing whether or not the cutting tool can perform over the entire process enables manufacturers to determine if the cutting tool or the cutting condition need to be changed.

Table 1: Common sensing variables used to monitor faults in machining

Sensing Variables for Hard Fault	Sensing Variables for Soft Fault
Noise from cutting tool breakage Presence of coolant or not	Spindle motor current/ power Feed drive current Force Acceleration or vibrations Displacement Temperature Vision System

TCM related research has been intensively conducted in recent years. Among several possible tool faults, the three most common in machining processes are:

Tool wear directly influences the dimension and accuracy of the finished surface. Excessive tool wear leads to catastrophic **tool breakage** which can often render the final part unusable.

Chatter (caused by the instability of the cutting processes) is another phenomenon which limits the material removal rate during machining while deteriorating the finish surface quality of the workpiece. Figure 1 shows the standard type of tool conditions considered during machining.

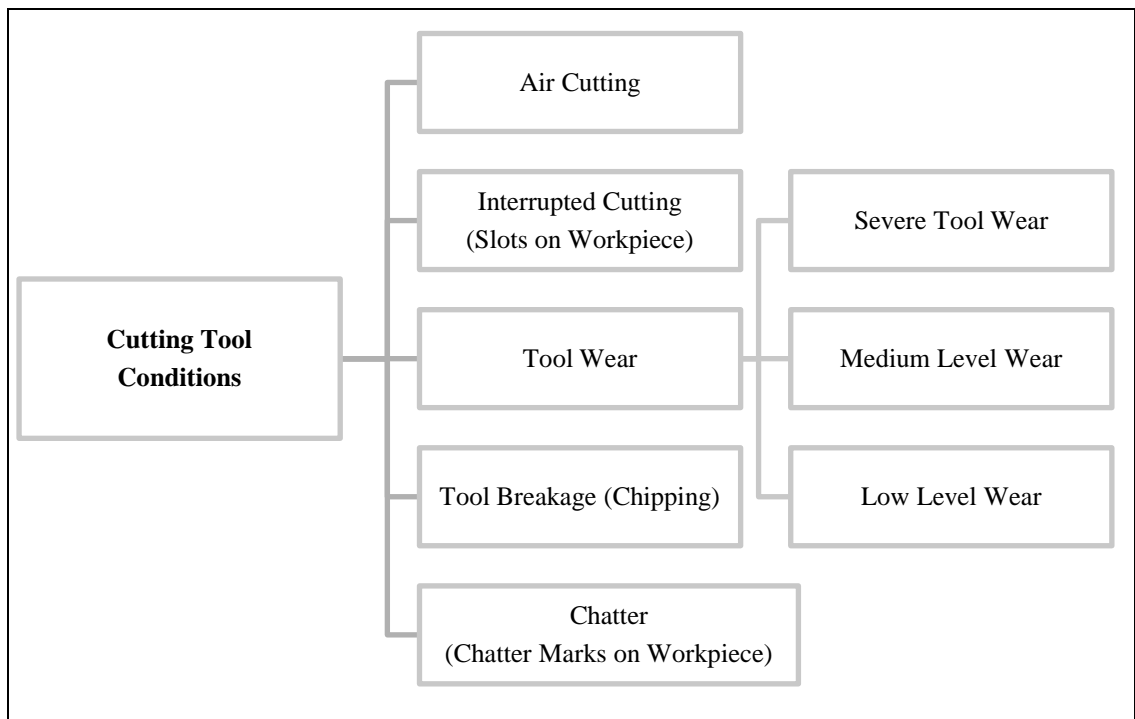


Figure 1: Cutting tool conditions during machining

Therefore, a tool fault detection system is crucial for rapidly detecting faults to prevent workpiece surface damage or machine tool degradation. Traditional analytical methods (assumption based) have limited tool wear prediction accuracy since the gradual tool failure is a complicated part of the machining process [4]. In general, four components, shown in Figure 2 are considered to be the critical features for developing an intelligent tool wear monitoring system in machining [5].

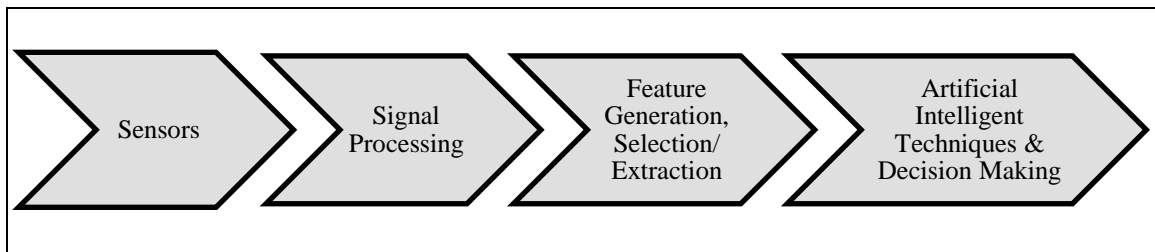


Figure 2: Key features in the TCM system

2.2.1. Sensors

A sensor transforms a physical quantity into a corresponding electrical signal. Selecting the best sensor and process variable is an essential step in TCM. An ideal variable highly sensitive to a failure feature, can provide a reliable fault detection system. Applicability and reliability in the industrial environment, as well as sensor cost, are the other factors to be considered in this regard [6]. Different types of monitoring methods were demonstrated in a wide range of TCM related research fields. An offline monitoring method is a direct tool wear monitoring system capable of measuring tool wear directly with a vision system. However, implementation of offline tool wear monitoring (or, direct) system in a manufacturing environment is not an easy task. Indirect methods (use of sensors) can be

applied online during the machining process to sense the nature of the wear progression and its impact on the measured signal.

Measurement of machining forces is a way to monitor the tool wear progression. The reason for measuring the torque and feed forces is that these dynamic parameters generally increase during machining as the cutting tool gradually wears out. In [7], Heinemann et al. observed that in the drilling operation, torque and thrust force are the most important dynamic parameters for obtaining drill wear information. Their research showed that torque monitoring is well suited for tool condition monitoring in drilling. In addition to cutting parameters, workpiece and tool materials also affect the cutting forces during machining [8]. For example, a faster feed rate generates higher cutting forces, either due to tool wear or changes in the cutting conditions. Therefore, it is suggested that the proposed method is affected specific experimental conditions.

Acoustic emission (AE) occurs when a material is displaced from a surface produces stress waves from the rapid release of the surface material's energy [1]. Thus, AE signal is a promising candidate for tool wear monitoring. Li's turning study reported that the significant advantage of AE sensor use for tool wear monitoring is that the AE signal's frequency range is much higher than other noise sources during machining and is therefore less sensitive to other noise associated with the cutting operation [9]. Jantunen observed that AE is limited by multi-path distortion caused by machine tool's structure joints and the need for the mounting location of the AE sensor to be very close to the tool or workpiece in machining [1].

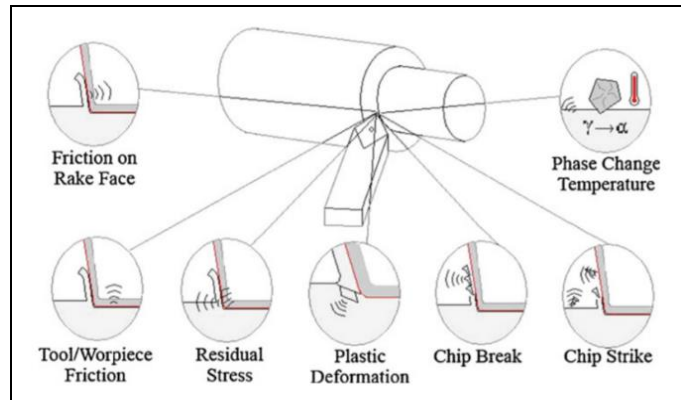


Figure 3: Sources of AE in machining [9]

In metal cutting, vibration data is commonly collected to predict tool wear level and assess the process. For example, the vibration signal from an accelerometer has been shown to exhibit strong correlation with tool wear during machining. Therefore, they have been widely used in the literature as a way to assess tool condition. In addition, machine tool-workpiece dynamic interactions and the state of machine tool components can also be effectively assessed using accelerometers. Dimla's research indicated that AE is more suited for detecting catastrophic tooltip breakage rather than the subtler gradual tool wear that commonly occurs during machining. He recommended the vibration signal as being the most reliable and prompt responsive factor for developing a tool wear monitoring system [11].

Wang et al. researched vibration signals and used SVM (Support Vector Machine) as an online tool condition monitoring system [12]. Also, Rao et al. worked with vibration signals in a boring operation using a Doppler vibrometer for tool wear monitoring [13].

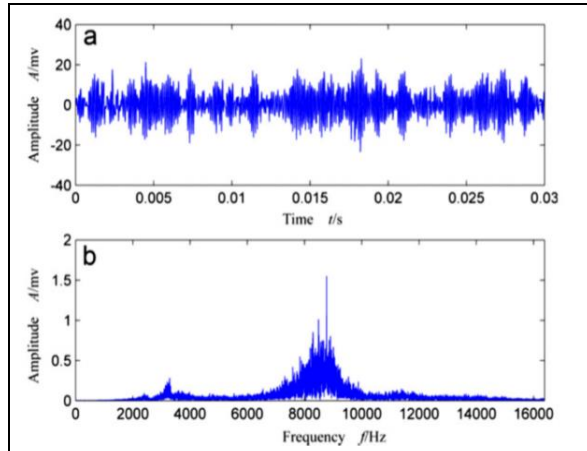


Figure 4: Vibration signals in machining (time & frequency domain) [14]

Spindle motor current is also used as a reliable and low-cost sensor as a worn tool requires more machining force than a sharp one, which necessitates greater input power. The waveform of an electric current signal while cutting with a worn tool is usually distorted in comparison with the cutting signal obtained from a sharp tool. Gasca et al. studied the spindle current or power in relation to the cutting tool wear in drilling [15]. He quantified signal distortion with an asymmetric parameter and stated that the asymmetrical properties of the current signal change proportionally with the tool wear condition.

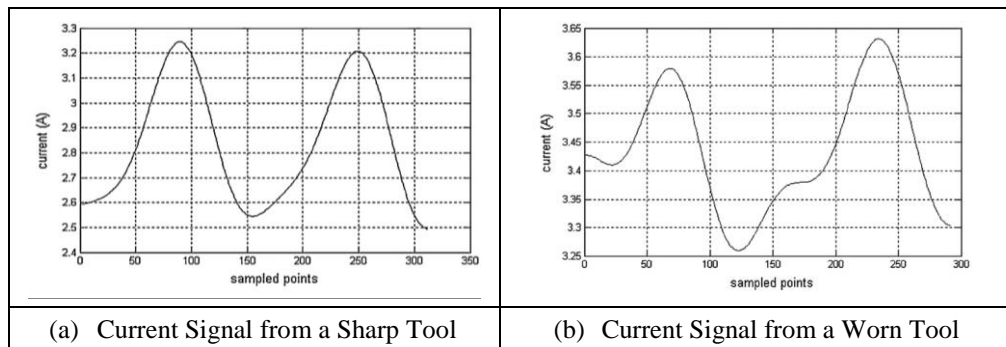


Figure 5: Effect of tool wear on spindle motor current signals [15]

Previous research showed that motor current measurement techniques are widely adopted due to their low cost and low disturbance levels during the machining process. Also, the current sensor does not require pre-assembly for signal acquisition, unlike other sensors which are generally used in the TCM system. Lee et al. used a current sensor to monitor the gradual tool wear in the end milling process of SMC45 steel with coated HSS (high-speed steel) cutting tool. However, in his research he only used statistical features of the current signal to monitor the gradual tool wear progression [16]. Bennett examined the use of spindle motor power measurement to detect the end of useful tool life in a milling operation. This study also indicated that changes in the cutting tool wear rate are linearly related to spectral energy in the fluctuating part of the spindle motor power consumption [17].

2.2.2. Signal Processing and Feature Extraction

To acquire meaningful information from an enormous set of data provided by sensor signals, various signal processing techniques have been used. The common dilemma is that the more sophisticated techniques require more processing power and are slow to respond and thus impractical (tool breakage detection). Conversely, elementary signal processing techniques are fast but often fail to extract sufficient information about changes in cutting conditions from the data.

For a successful monitoring system, the choice of signal processing devices is significant. Researchers should check the range and measurement resolution according to

system requirements. The resolution refers to the number of ADC binary levels that can be used to represent a signal.

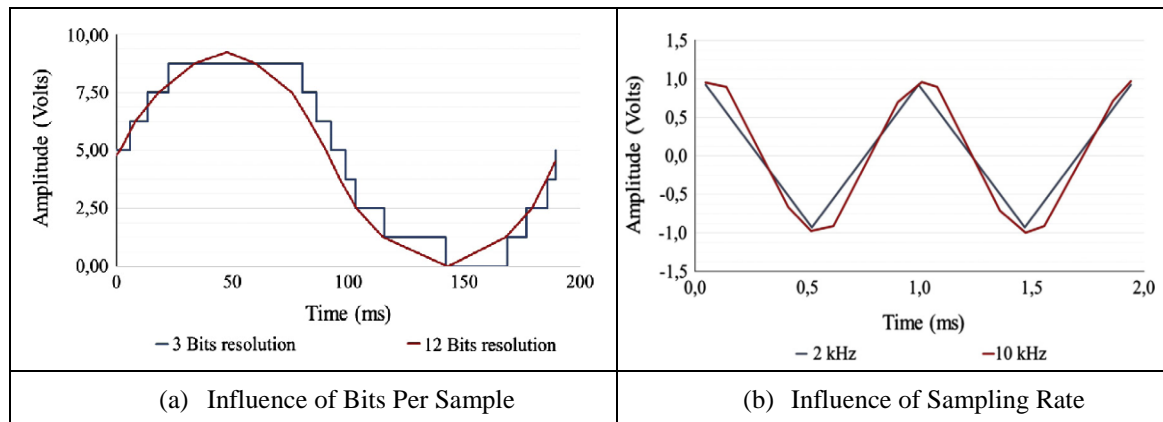


Figure 6: Influence of bits and sampling rate in signal processing [18]

The resolution of the device is determined by the smallest detectable change in this signal (Figure 6-a). The sampling frequency should be clearly defined during data acquisition and be chosen based on the process. To avoid aliasing, the ‘Nyquist theorem’ is applied to ensure a sufficiently high sampling rate is used to measure a specific event. Several researchers also suggested sampling at least ten times the maximum frequency of interest to be able to recombine the event to better visualize it on a graph (Figure 6-b).

Several signal processing techniques were used in the past literature. A list of these techniques is depicted in Table 2. Compared to frequency domain signals, the time domain signal is usually considered to be less informative and not as time-consuming. The time domain analysis of force signals does not show a strong correlation with the drilling tool wear [1]. However, statistical features from the time domain analysis can provide useful

information. The thrust force signal gradient was identified as one such suitable process parameter for the prediction of tool failure. The RMS value of the spindle motor current signals also provides essential features for online tool wear prediction.

The fast Fourier transforms (FFT), short-time Fourier transforms (STFT), and the discrete Fourier transforms (DFT) are commonly used in Fourier transform analysis. They serve to characterize the frequency content of a measured signal. In particular, when the power spectrum of the FFT during signal processing is considered, the power (or amplitude) content of the cutting force associated with the high frequencies increases as the cutting tool gradually wears out. Therefore, the fast Fourier transform analysis acts as a pivotal index to detect the failure of the cutting tool [1]. Liu et al. used FFT in their research to detect and avoid vibrational noise in the machining signal. Also, X. Liu et al. used FFT to identify unwanted frequencies including interpolation points which causes excessive vibration in machining [19].

The wavelet transform (WT) analysis was also applied to various TCM related research studies with great success, see Table 2. The most prominent feature of the WT is that it can provide the most natural shape of the signal, which is more informative compared with the sine function used in Fourier analysis. The wavelet transform is usually considered as the most effective tool for many applications in tool condition monitoring related research. Chen and Li applied wavelet transform analysis while processing the signal from an acoustic emission (AE) sensor to monitor the tool wear during the turning operation. They used wavelet multi-resolution analysis to obtain the frequency band which contains the main energy of AE signals [20].

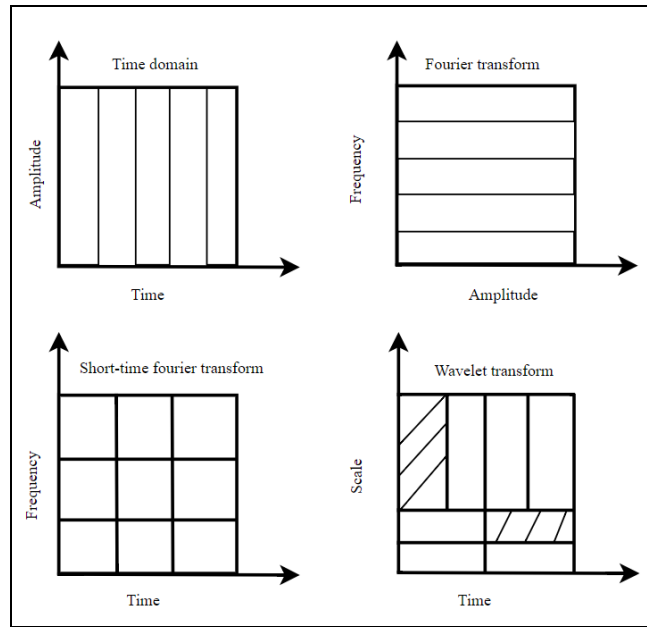


Figure 7: Fourier and wavelet transform in signal processing

Table 2: A summary of signal processing techniques from the literature

Applied Signal Processing Techniques	Featured Research Work
Fourier Transform Analysis	16, 21, 22, 23, 24, 26, 27, 28, 29, 30
Time Domain Analysis	29, 31, 32, 33, 34, 35, 36
Wavelet Transform Analysis	4, 15, 20, 23, 37, 38, 39, 40, 41, 42
Other Signal Processing Analysis	43, 44, 45, 46, 47

2.2.3. Artificial Intelligence (AI) Decision Making Techniques

A diagnostic tool plays an important role in developing a tool condition monitoring system. The decision-making tools or diagnostics tools classify or cluster previously acquired and processed signals in the tool condition monitoring system, acting as a human-

machine interface that can carry out prompt decisions based on conditions of tool wear. Different types of machine learning algorithms were introduced in this research field, though there remains an ample space for further contribution. An indirect monitoring system should be developed based on physical signals which provide information about the machining system and its faults. In this regard, a more complex and robust model is needed to monitor the machining system in real-time and simultaneously interpret the sensor data. Such a model can eliminate unwanted details while identifying signal anomalies to make an appropriate decision.

Fuzzy logic or a fuzzy inference system (FIS) is generally used in specific applications where the experimental dataset consists of a relatively small number of samples. The FIS model is developed using previously measured data. This approach can be used when the system's knowledge is already established and is sufficient to ensure the model's robustness. The accuracy of this system is generally less than that of a more extensive artificial neural network (ANN) (i.e. sometimes the fuzzy system provides a poor tool wear classification response). In recent years, ANNs have been successfully used to model the complex relationships between input feature sets of sensor signals, cutting conditions and tool wear data. ANNs is also promising for data or image clustering related applications. Another effective method of modelling dynamic systems is the use of Hidden Markov models (HMMs), which are generally used in modern speech-recognition systems. ANN can provide more accuracy without requiring prior knowledge of the process in many cases. In addition, it can handle a significant amount of sample data for training. Several studies reported in the literature mention that the ANN method is suitable for accurate cutting tool

flank wear and surface roughness prediction [5][6]. An adaptive neural fuzzy inference system (ANFIS) is a hybrid method which incorporates the theory underlying both fuzzy logic and artificial neural networks. It has the advantages of both decision-making techniques. ANFIS is generally used when previously developed systemic knowledge needs to be updated to account for changing system requirements and to extract knowledge otherwise concealed in the experimental data.

A support vector machine (SVM) is a modern machine learning algorithm based on statistical learning theory. The basic concept of SVM is to map training samples (which cannot be classified by a linear function) into a high-dimensional feature. The SVM is developed based on the structural risk minimization (SRM) principle. Currently, the support vector-based algorithm has been demonstrated to be proficient for condition monitoring since it can handle extensive feature extraction and classification processes.

Table 3 provides an overview of the diagnostical tools used in past research.

Table 3: A summary of diagnostics tool usage from featured researches

Applied Diagnostic Techniques	Featured Research Work
Linear Regression	17, 38, 45, 49, 50
Fuzzy Logic (FL)	36, 42, 49, 51, 52, 53
Neural Networks (NN)	4, 25, 29, 30, 32, 37, 51, 54, 55
Support Vector Machine (SVM)	35, 56, 57
Data Fusion	26, 53

2.2.4. Conclusions

Selection of sensors for tool wear monitoring system is a key decision. The implementation of sensor fusion techniques has shown promising results in past research studies and been demonstrated as a reliable approach for a condition monitoring system. However, a variety of obstacles still limit the implementation of this technology in actual manufacturing practice.

The literature review supports a high potential of introducing a low-cost, adaptive and online TCM for sensor fusion implementation, signal processing and decision-making in the turning process. However, the most effective and reliable methods of tool wear monitoring are poorly suited for detecting tool wear progression or catastrophic tool failures, often due to their long processing time. Therefore, a reliable and inexpensive tool wear monitoring system is designed and developed in this research to investigate tool wear progression in different workpiece materials with the goal of establishing a standard monitoring system capable of addressing a wide range of applications.

Chapter 3. TCM System Design and Architecture

3.1. Introduction

This chapter demonstrates the architecture of the tool condition monitoring (TCM) system in the present research. The first section provides an overview of the TCM system. The second section exhibits the system framework in terms of components, techniques and overall approach.

3.2. Framework of the TCM System Architecture

This section will detail the design of the sensor fusion-based tool condition monitoring (TCM) system for turning operations. The framework of the proposed system is composed of four main components.

The first component of the system is sensor selection and signal acquisition. Two types of monitoring approaches were introduced, online and offline. A sensor fusion approach was adopted to acquire the signals for online monitoring. Optical microscopy was used to analyze cutting tool conditions for offline monitoring. Amplifications and preprocessing techniques were adopted to improve the acquired signal's quality. Signal processing is the next component of the system. Different sensors were used with each requiring its own post-processing. The third component of the system is feature extraction and dimensionality reduction. Processed signals are used to extract features which detect faults in the system. Several correlation analysis techniques can obtain the best features.

The last TCM component is the decision-making system. Based on the condition monitoring database and other machining parameters, this component can decide whether or not to continue the machining process. Figure 8 demonstrates the detailed architecture of the sensor fusion based TCM system as designed for a turning operation.

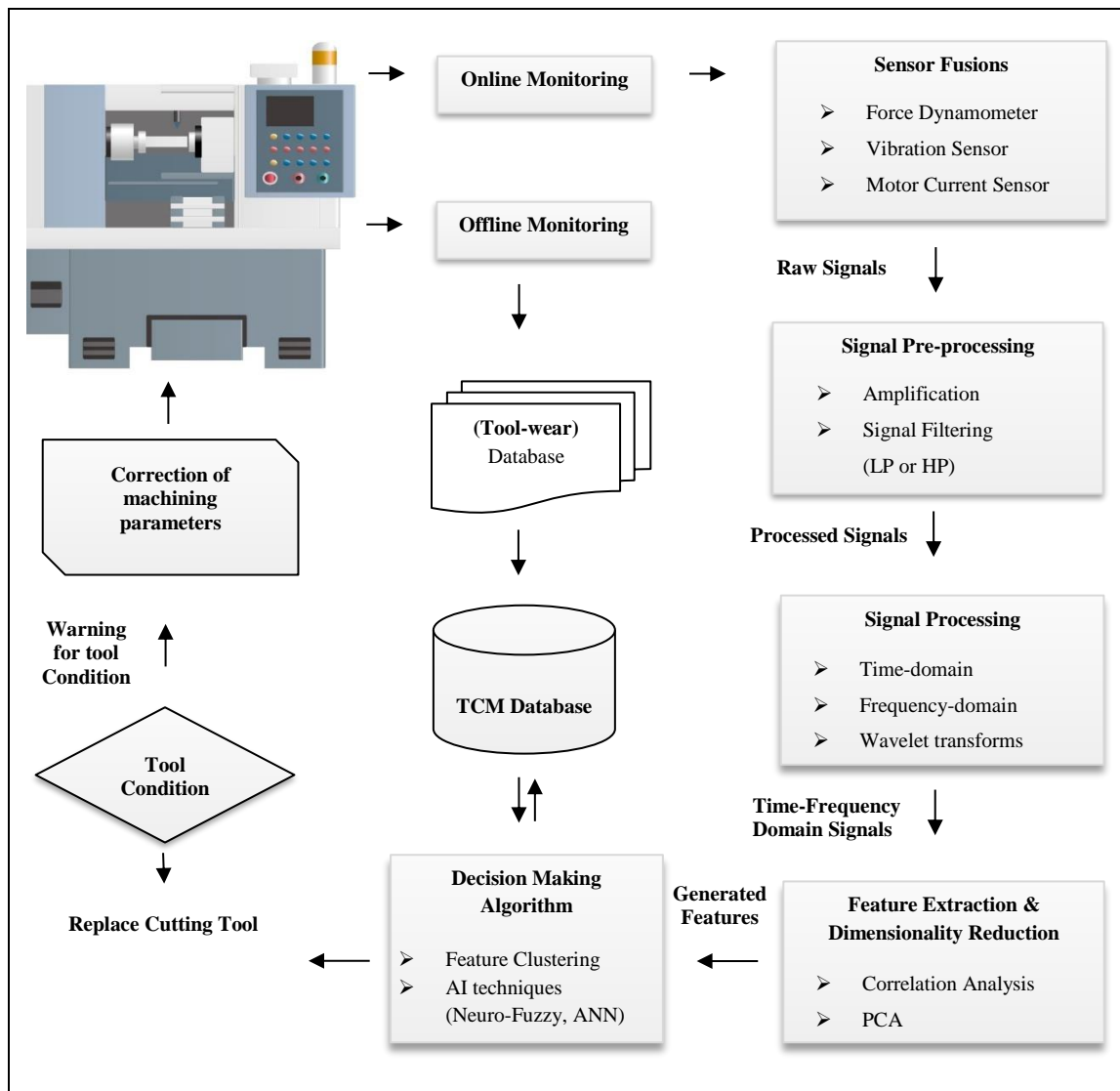


Figure 8: Architecture of the designed TCM systems

A sensor fusion approach for online monitoring consists of a force dynamometer, a vibration sensor and a low-cost sensor (transformer-based) spindle motor current sensor. The specifics of the sensor fusion structure are explained in the next section (section 3.3). Optical microscopy was used to record tool states (cutting tool flank wear). The tool states values were then stored in the TCM database.

The raw sensor signals are then pre-processed through amplification and signal filtering. Low pass (LP) filter (with a cut-off frequency of 200 Hz) were applied for spindle motor current sensor.

The next step is to process the signal for feature generation and extraction. The sensor fusion structure is composed of multiple sensors each with different operating principles. Therefore, to obtain vital information about the cutting tool state from the signal, more insight is required to process it. Selection of time domain, frequency domain and time-frequency domain analysis are critical aspects of the system.

In this section, features from a different domain are generated and extracted from the processed signal. Extracted features are then correlated with the cutting tool conditions. Dimensionality reduction is the critical concern of feature extraction. Pearson correlation coefficient analysis and principal component analysis techniques are used to reduce the dimension of the extracted features, providing the one best related to the cutting tool state. The extracted features are stored in the TCM system database for data training and validation.

The final stage of the design is the decision making or pattern recognition algorithm. This stage is the most crucial section of the architecture which best represents the

robustness of the monitoring system. In this section, AI techniques were implemented for developing a decision-making system which can predict the cutting tool state (flank wear) based on the sensorial data and the cutting parameters. Both an ANN and an ANFIS system were implemented as part of this decision-making system. The developed system is then applied for online monitoring of other workpiece materials to validate its tool wear prediction ability and demonstrate the TCM system's adaptability.

3.3. Selection of Sensors/ Sensor Fusions

During the machining process, changes in the cutting conditions or cutting parameters greatly affect the sensitivity and noise of the signal. Therefore, it is always helpful to use more than one sensor to avoid the uncertainty and increase reliability of the monitoring system. Two different approaches are considered to address this. A multiple sensor system without fusion uses multiple sensors with non-complementary information sharing to increase the reliability of the monitoring process, whereas a sensor fusion system uses multiple sensors with complementary information sharing to enhance robustness. Also, a proper sensor fusion system can overcome the disadvantages of one sensor over another while monitoring tool wear progression during the machining process.

This research uses sensor fusion techniques involving a transformer-based AC spindle motor current sensor, a vibration sensor (one-axis mechanical shock accelerometer) and a piezoelectric dynamometer (3-component force sensor).

3.3.1. Three (3)-Component Cutting Force Sensor

The cutting force sensor used in this research was a Kistler© 9121 three-component dynamometer. The piezoelectric dynamometer was used to measure the cutting forces (radial force, feed force and tangential force) in the turning operation. Figure 9 shows the placement of the tool holder inside the dynamometer fixture with minimum overhang.

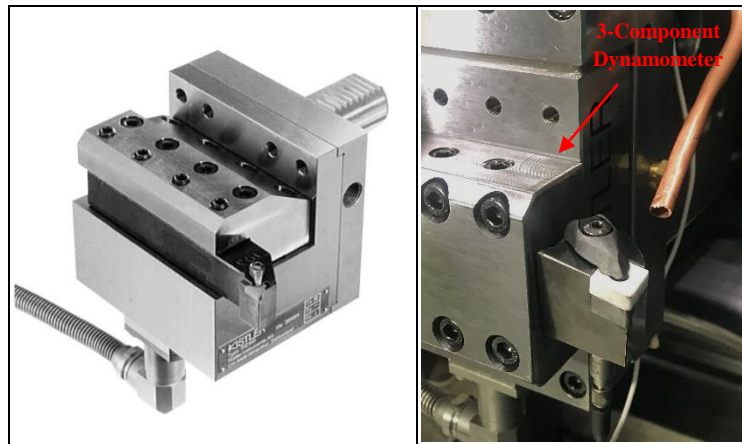


Figure 9: Three (3)-component dynamometer setup in the turning operation

Table 4: Technical specifications of the three-component dynamometer

Specifications	Values
Force application range	Fx, Fy (-3.0 to 3.0 kN); Fz (-6.0 to 6.0 kN)
Sensitivity	Fx, Fy (-7.9 pC/N); Fz (-3.9 pC/N)
Natural Frequency (clamped)	1000 Hz
Rigidity	Approx. 600 N/ μ m
Operating temperature range	0 to 70-degree C

The cutting force dynamometer signal was sampled at a 10kHz sampling rate and acquired and amplified by the Kistler© 5010 series dual-mode amplifier. Table 4 presents the technical specifications of the Kistler© 9121 dynamometer used in this research. The estimated cost of the Kistler© 9121 dynamometer (excluding all accessories) is approx. 28,000 CAD (estimated in December, 2018)

3.3.2. Vibration Sensor

The vibration sensor used in the experiment was a Kistler© 8742A shock accelerometer with a 10-32 threaded connector (Figure 10). This industrial-scale shock accelerometer incorporates a stable quartz sensor, which ensures accurate measurement of high-speed events with low transverse sensitivity and impedance. Also, to ensure the accurate vibration measurement during progressive tool wear or catastrophic tool failure, the sensor was placed in several positions on the tool holder to measure the response from all (cutting, feed and radial) direction. The most sensitive measurement was achieved from the cutting direction of the tool holder (Figure 10). Therefore, through a series of experiments, the sensor was placed at a position to measure the cutting direction vibration. Table 5 shows the technical specifications of the Kistler© 8742A20 shock accelerometer. The estimated cost of the Kistler© 8742A20 shock accelerometer (excluding all accessories) is approx. 6,500 CAD (estimated in December, 2018)

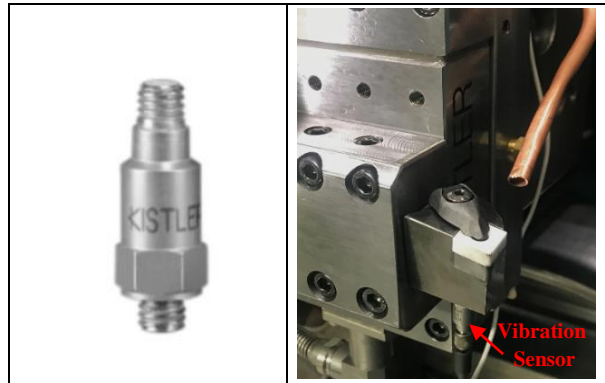


Figure 10: Kistler© 8742A shock accelerometer setup in the turning operation

Table 5: Technical specification of the shock accelerometer

Specifications	Values
Acceleration range	$\pm 20,000 \text{ g}$ ($g=9.8 \text{ m/s}^2$)
Sensitivity	0.25 mV/g
Natural frequency (clamped)	100 kHz
Operating temperature range	-55 to 100-degree C

3.3.3. Transformer-based Current Sensor

A cost-effective transformer-based current sensor was used to acquire the spindle motor current signal during the turning process. This technology is well suited to retrofit on a machine tool as it is easy to install and does not interfere with the process. The ACT-series AcuAMP© split-core current transducer (ACT005-42L-S) was placed over the spindle motor wiring. Figure 11 and Figure 12 shows images of the installed sensor. The estimated cost of the current transducer (ACT005-42L-S) (excluding all accessories) is approx. 220.00 CAD (estimated in December, 2018).

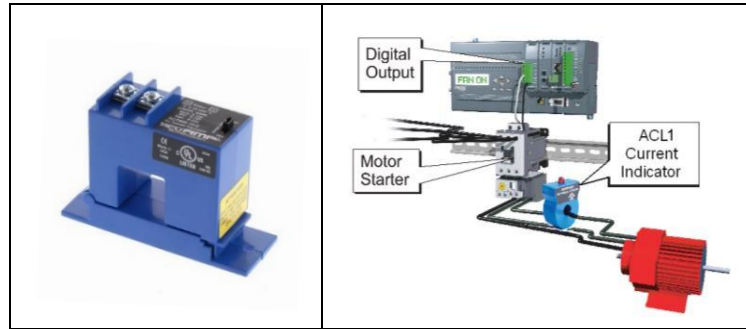


Figure 11: Installation of a split-core AC-current sensor [58]

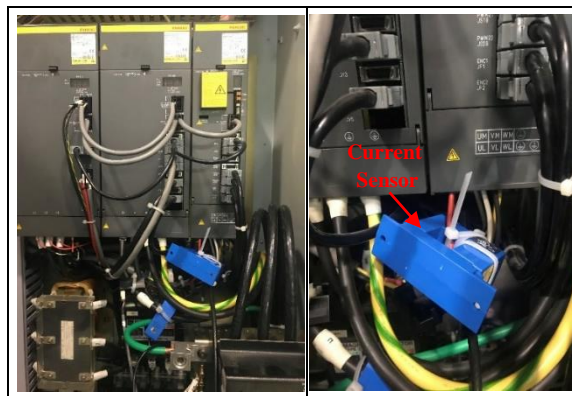


Figure 12: Installed split-core AC-current sensor over spindle motor wiring

Technical specifications of the AC- current sensor are presented in Table 6.

Table 6: Technical specifications of the current sensor (ACT005-42L-S)

Specifications	Values
Output signal	0 to 10 VDC
Input range	0 to 200 A
Response time	300 ms
Frequency range	20 Hz to 100 Hz
Operating temperature range	-20 to 50-degree C

3.3.4. Sensor Signal Acquisition System

To acquire the sensor signal for preprocessing and further post-processing, a data acquisition system was used in the experimental setup: Kistler© 5010 dual-mode amplifiers and National Instrument© 9125 DAQ-board for the signal acquisition system (see Figure 13). The signal acquisition system allows connecting all channels from the sensor fusion.

To avoid signal drifting (signal drifting happens due to the charge dissipation) over extended periods of time between cutting tests, a secondary switch was connected to reset the sensor before each cutting test. In all cases, the sampling rate was 10 kHz with most content of interest being limited to 5 kHz (to avoid aliasing, see Figure 22).

Table 7: Technical specifications of the data acquisition system

Specifications	Values
Channels	Five analogue input channel (used)
Resolutions	24 Bits
Maximum voltage range	$\pm 10V$

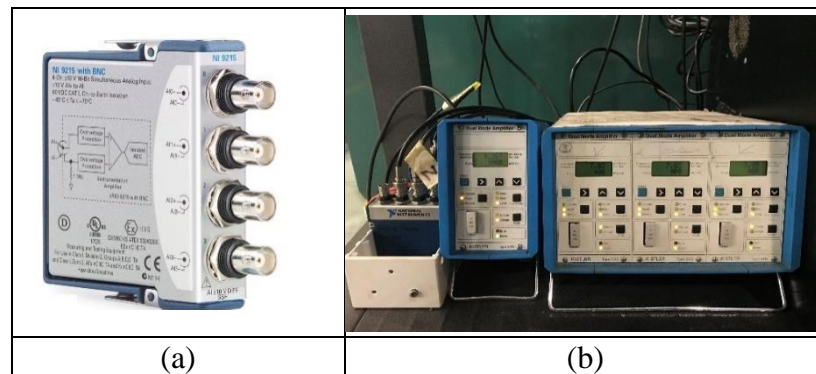


Figure 13: (a) National Instrument© 9125 DAQ and (b) Kistler© 5010 amplifier

Chapter 4. Experimental Work & Data Acquisition

4.1. Experimental Details

To start, a dry turning operation was performed, followed by the combination of a dry and wet procedure. In the dry turning test tool progression and catastrophic tool failure provided the distinguishable conditions and thus the most distinctive signals from the sensor.

A series of tests based on a design of experiments (DOE) (section 4.1.5) was performed on a CNC turning centre with the developed sensor fusion setup and data acquisition system. These tests were selected based on cutting tool and workpiece specifications for the semi-finish turning and final finish-turning operations.

4.1.1. Machine Tools

The machine tool employed for the experiment test was a Nakamura-Tome (SC-450) CNC turning centre (Figure 14). The maximum spindle speed is 2500 RPM. 30/22KW is the maximum output of the CNC center's spindle motor.

The spindle motor used on the Nakamura-Tome SC450 is a FANUC© A06B-0832 series α P-50, four pole 3-phase induction motor with a power factor of 77%.



Figure 14: Nakamura- Tome CNC turning centre

4.1.2. Workpiece Material & Cutting Tools

The key goal of the current research is to develop a tool wear monitoring system for a turning operation. The development of a data-driven artificial intelligence based TCM system requires a series of cutting tests to provide the data for training. Furthermore, the application of a TCM system was also considered during the experiment. In this research, a TCM system was designed and developed for a hard-turning test of AISI 4340 steel. Furthermore, other workpiece materials and cutting tools were used to validate and implement the TCM system.

Table 8 and Table 9 shows the list of workpiece materials and cutting tools used in this research.

Table 8: List of workpiece materials used in this research

Experiment Criteria	Workpiece Material	Chemical Composition (wt%) of the Workpiece Material
System design & development	AISI 4340 steel (50 ± 1.0 HRC)	0.38% C, 0.2% Mo, 0.15% Si, 0.6% Mn, 0.7% Cr, 0.17% Ni, Balanced %Fe
System Implementation	AISI D2 steel (46 ± 1.0 HRC)	1.5% C, 0.28% Mn, 0.32% Si, 11.4% Cr, 0.73% Mo, 0.3% Ni + Cu
System Implementation	ASTM A536 ductile iron (24 ± 1.0 HRC)	3.2% C, 0.4% Mn, 0.07% Cr, 0.4% Ni, 0.6% Cu, 0.03% Mg

Table 9: Tool holders and Cutting tools

Tool Holder	Cutting Tools
Kennametal© DCLNL 16 4D Rake angle= -6° ; Clearance angle= -5°	Pure alumina (cc620) CBN (cubic boron nitride)

4.1.3. Experiment Setup

The turning experiments were performed on a Nakamura Tome-SC 450 CNC machining centre. A similar experiment setup was used during validation tests as well.

Figure 15 shows the experimental setup with the sensor fusion based TCM system.

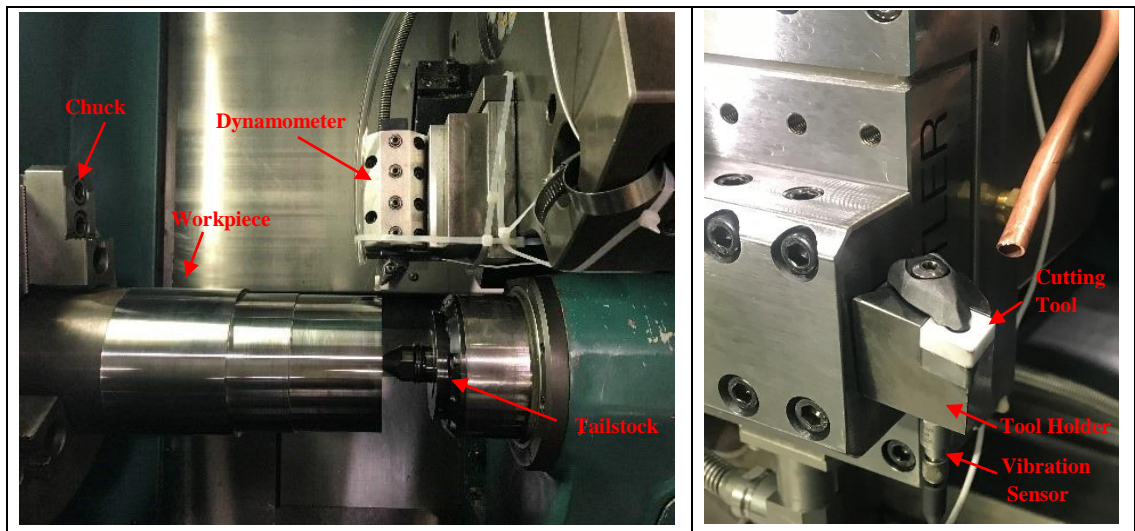


Figure 15: Experimental setup for the turning operation using sensor fusion

4.1.4. Tool Wear Measurement

The tool wear measurement during the experiment was performed according to ISO 3685:1993 [59], the international standard of tool-life testing. This ISO standard defines the tool wear on the flank and rake faces of a single-point cutting tool used in turning operations. Four different regions of the first cutting edge are considered for wear measurements. Region C, B, N and b showed in Figure 16 are the four regions being monitored as they impact tool performance the most. The width of the flank wear land

VB_B , maximum flank wear VB_{max} , and notch wear VB_N are generally measured during tool-life testing. The most common tool wear observed in this research is described below.

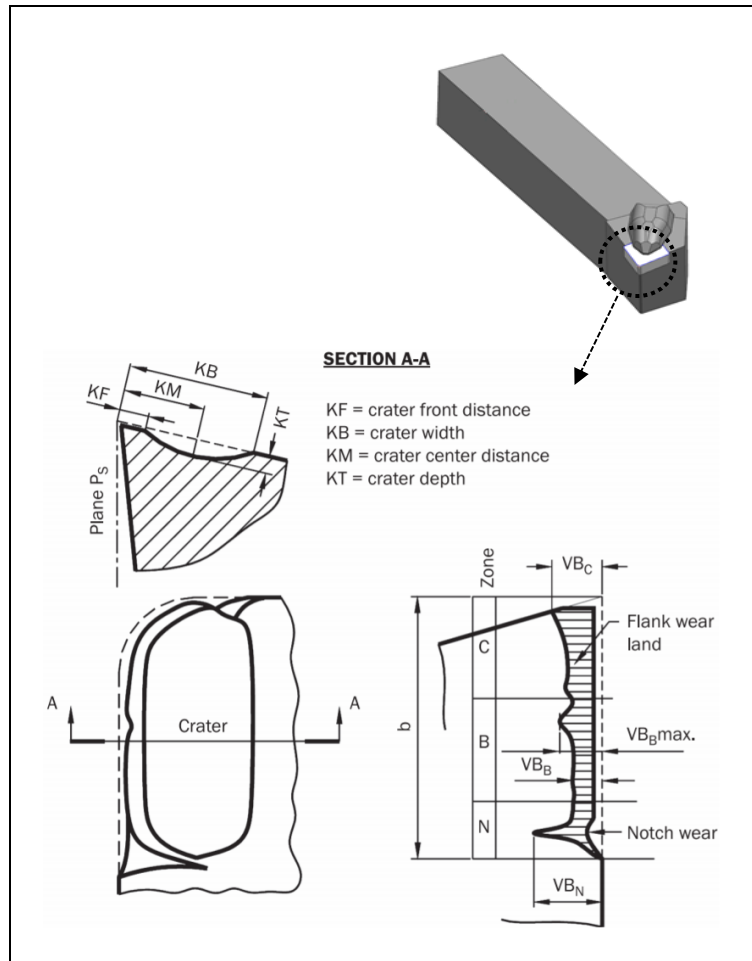


Figure 16: Types of tool wear [60]

Flank Wear

Flank wear is the wear on the flank (relief) face that in turn, causes land wear. Due to the abrasive wear mechanism, the wear land formation is not generally uniform along the cutting edge of the tool. Land wear reduces the dimensional accuracy and the surface

integrity of the workpiece material. The functional tool life criterion is generally set to be 300 μm of flank wear according to ISO 3685: 1993 [59].

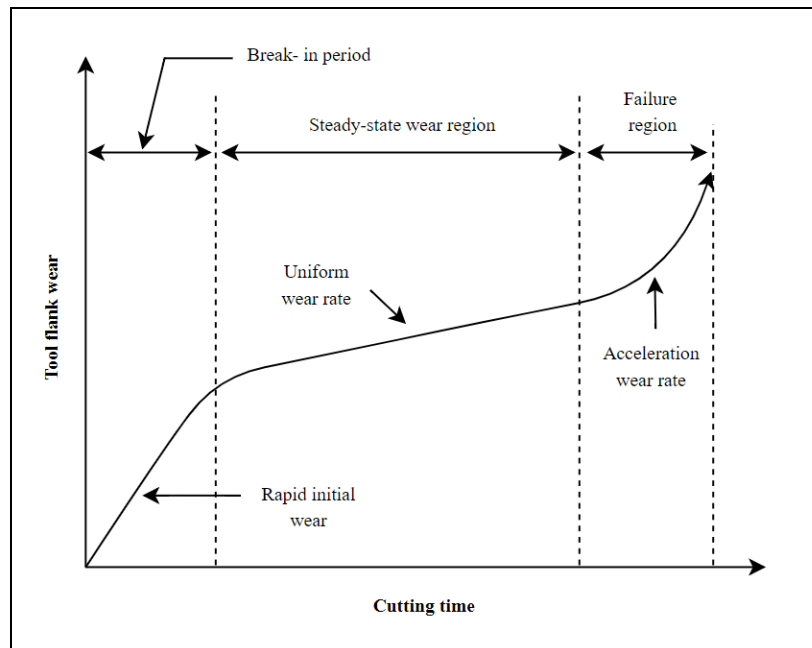


Figure 17: Stages of cutting tool flank wear

Crater Wear

During the machining process, the cutting chips flow over the rake face of the tool at a high temperature due to the sliding and sticking motion. This phenomenon results in diffusion of the tool material into the workpiece material generating crater wear on the surface of the tool. As crater wear increases the chance of catastrophic tool failure also increases as the support material and thus the strength of the cutting edge is reduced.

Notch Wear

Notch wear at the wear land's outer edge is the result of either oxidation or the presence of hard particles in the surface of the workpiece material. It is associated with the depth of cut (the uncut chip thickness). It can also occur due to the strain hardening of previously machined surfaces.

Chipping

Chipping of the cutting tool results in catastrophic tool failure during machining. Discontinuous cutting conditions and the brittleness of the cutting tool are some of the major reasons for this type of wear.

In this research, a KEYANCE VHX-5000 optical microscope was used to measure the cutting tool wear (resolution of $\pm 5.0 \mu\text{m}$) after each cut and with the tool wear measurements stored as offline monitoring data in the TCM database. Figure 18 (a) shows the optical microscope setup and a tool wear image measured as $217 \mu\text{m}$ of flank wear under a 200x magnification scale (Figure 18 (b)) from the T9 test outlined in Table 10.

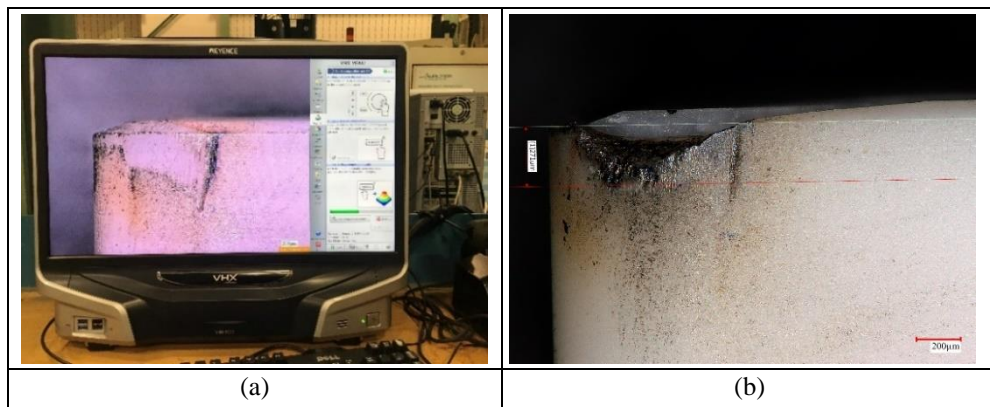


Figure 18: Optical microscopy used in this research.

4.1.5. Design of Experiment

The experiment results produce a training and testing dataset for the machine learning (ML) procedure. A wide range of cutting parameters were used to perform the hard-turning test on AISI 4340 steel with a pure alumina (cc620) ceramic cutting tool. To reduce the number of tests and understand the effect of cutting conditions on tool wear, a design of experiment (DOE) was undertaken based on a Taguchi L9 orthogonal array (Table 10). To improve the reliability of the TCM system database, design of the experiment was carried out four times (4x) under a similar experimental setup. The preliminary database of the TCM system consisted of 884 sets of data, with each dataset containing information from the cutting parameters, signals from all sensors channel and the flank wear values.

Table 10: Design of experiment (Taguchi L9 orthogonal array)

Test Title	Machining Parameters		
	Cutting Speed, V_c (m/min)	Feed Rate, f (mm/rev)	Depth of Cut, d_{oc} (mm)
T1	150	0.10	0.20
T2	150	0.15	0.30
T3	150	0.20	0.40
T4	250	0.10	0.20
T5	250	0.15	0.40
T6	250	0.20	0.30
T7	350	0.10	0.40
T8	350	0.15	0.20
T9	350	0.20	0.30

4.2. Experimental Results and Discussion

4.2.1. Test Reports

This section contains the offline monitoring test report (Flank wear values). Here, the design of experiments was organized based on the cutting conditions. Test 1 (T1) to test 4 (T4) from Table 10 were separated out as a standard cutting test, while test 5 (T5) to test 9 (T9) from Table 10 were considered to be cases with severe cutting conditions based on the cutting parameters (cutting speed, feed rate and depth of cut).

The test reports of the tool wear curve in this chapter are plotted against the number of cuts (each cut =100 m length of cut) in each test. The tool-wear curves of the standard tests (%error of flank wear values= 1.2 to 3.2) and severe cutting tests (%error of flank wear values= 1.4 to 5.2%) are presented in Figure 19 and Figure 20.

Each test report (maximum flank wear, VB_{max}) was obtained from a pure alumina (cc620) tool flank-wear measurement with optical microscopy according to the ISO standard (ISO 3685:1993). Each offline monitoring result (end of the test) from the standard and severe cutting tests is given in Table 11 and Table 12.

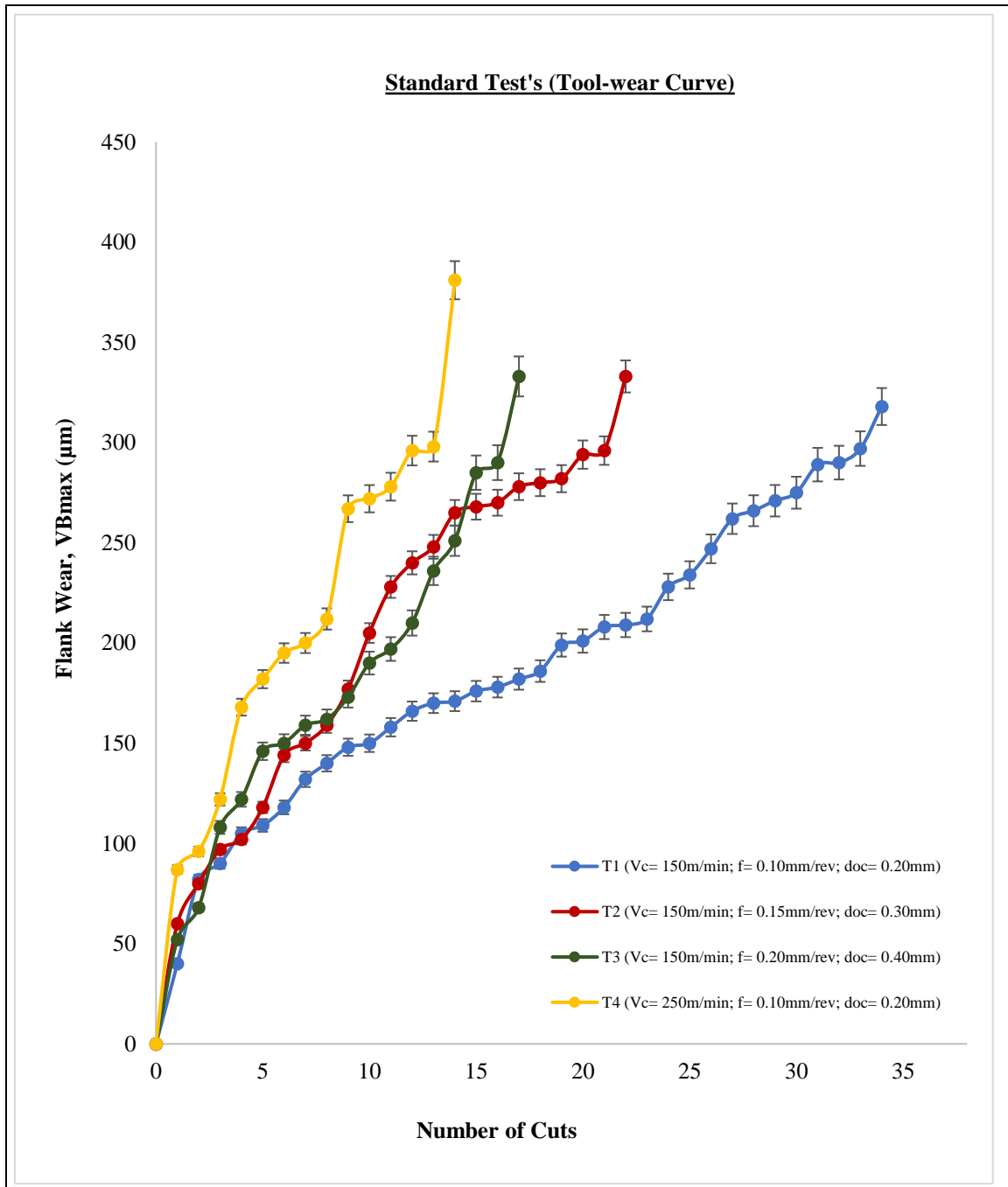
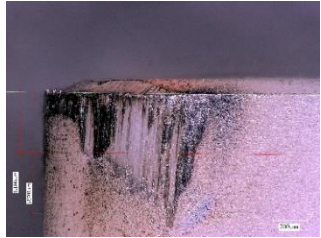
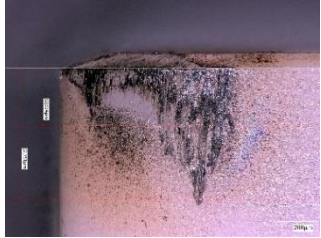




Figure 19: Tool wear curve development from standard tests

Table 11: Offline monitoring results (standard cutting tests)

Test Title	Cutting Condition	Tool Life (Number of cuts or cutting length)	Flank Wear Images (End of Test)
T1	$V_c = 150$ m/min, $f = 0.10$ mm/rev; $doc = 0.20$ mm	Total cut = 34 Cutting Length (3400 m)	
T2	$V_c = 150$ m/min, $f = 0.15$ mm/rev; $doc = 0.30$ mm	Total cut = 22 Cutting Length (2200 m)	
T3	$V_c = 150$ m/min, $f = 0.20$ mm/rev; $doc = 0.40$ mm	Total Cut = 17 Cutting Length (1700 m)	
T4	$V_c = 250$ m/min, $f = 0.10$ mm/rev; $doc = 0.20$ mm	Total Cut = 14 Cutting Length (1400 m)	

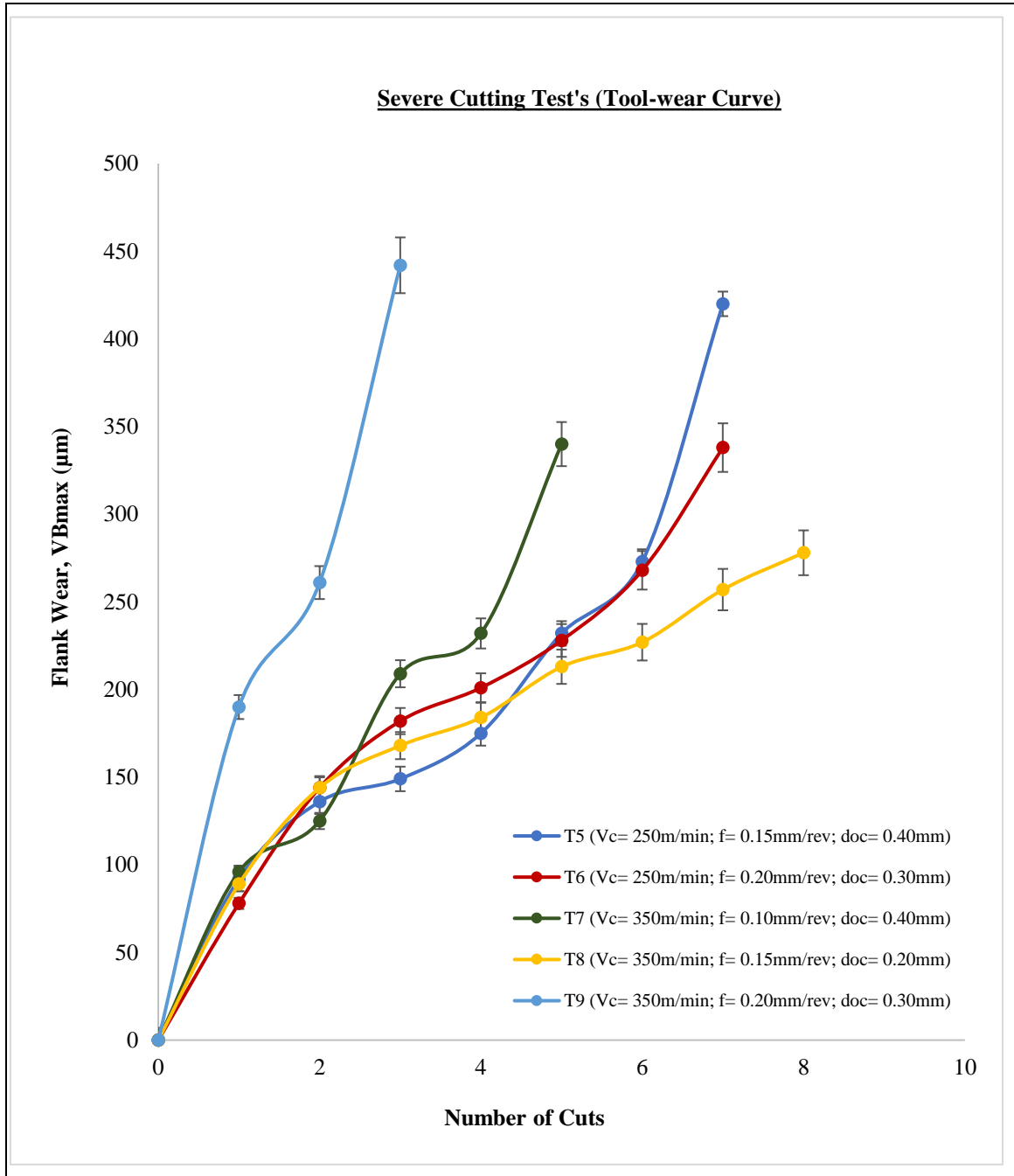
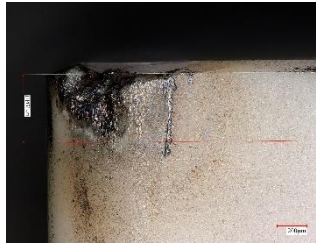

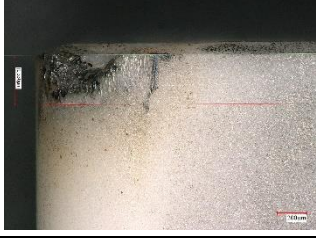




Figure 20: Tool wear curve development from severe cutting tests

Table 12: Offline monitoring results (severe cutting tests)

Test Title	Cutting Condition	Length of Cut	Flank Wear Images (End of Test)
T5	$V_c = 250$ m/min, $f = 0.15$ mm/rev; $d_{oc} = 0.40$ mm	Total cut = 07 Cutting length (700 m)	
T6	$V_c = 250$ m/min, $f = 0.20$ mm/rev; $d_{oc} = 0.30$ mm	Total cut = 07 Cutting length (700 m)	
T7	$V_c = 350$ m/min, $f = 0.10$ mm/rev; $d_{oc} = 0.40$ mm	Total cut = 05 Cutting length (500 m)	
T8	$V_c = 350$ m/min, $f = 0.15$ mm/rev; $d_{oc} = 0.20$ mm	Total cut = 09 Cutting length (900 m)	
T9	$V_c = 350$ m/min, $f = 0.20$ mm/rev; $d_{oc} = 0.30$ mm	Total cut = 03 Cutting length (300 m)	

4.2.2. Effect of Tool-wear on Spindle Current

The induction spindle motor is commonly used in the machine tool industry. Generally, an induction motor consists of two components: a stationary stator and a rotating rotor. The rotor is separated from the stator by a small air gap. A three-phase set of current flow is a result of voltages applied to the stator. These currents create a rotating magnetic field which effectively drags the spindle in the direction of the rotating magnetic field. The square of the induction motor's stator current is proportional to the developed torque for an induction style motor.

It is well known that the occurrence of tool failure causes a rise in cutting force acting on the cutting edge during machining. As a result, a considerable variation in torque is experienced by the induction motor as a result. Therefore, the stator current of the CNC spindle motor is considered to be the sensing signal for monitoring tool wear (or, failure) in this research.

The lathe used in this study has a three-phase four-pole induction spindle motor (Fanuc 6S- α P50 series). For this induction motor, the stator current signal for each phase is an AC-signal generated at the supply frequency. It has the same peak-to-peak amplitude but is displaced in time by a phase angle of 120° between each phase. Since all phases move synchronously in response to changes in torque only one of the stator current signals was measured by the ACT-series AcuAMP[©] split-core current transducer (ACT005-42L-S).

The frequency of the stator current 'f' can be expressed as:

$$F = N \cdot p / 120 \quad (1)$$

Where ' N ' is the synchronous speed (r.p.m.) and ' p ' is the number of poles on the rotor. The sensitivity of the stator current was analyzed by creating a transfer function between the square of the stator current and the cutting force acting on the tool. Total harmonic distortion and crest factor are two key parameters which are generally used for analyzing the induction motor current signal.

Total Harmonic Distortion (THD)

The harmonic is an integral component of the fundamental frequency. In an electrical system, the presence of a harmonic (due to non-linear load variations of any system) distorts an ideal sinewave signal. For instance, the presence of the fifth harmonic (300 Hz) (middle graph) in a 60Hz signal (top graph) can result in a distorted signal (bottom graph) that is depicted in Figure 21.

Fourier transform analysis can separate the harmonics into a periodic waveform series. It should be mentioned that the sampling rate should always be higher than the Nyquist frequency for the frequency of interest. Otherwise, the aliasing phenomena could emerge during the data acquisition period. Figure 22 shows an under-sampling scenario which highlights aliasing. Due to under-sampling, the high-frequency signal (300 Hz) is reflected (circled in Figure 22) into the low-frequency signal (60Hz). These signals became indistinguishable from each other because of the aliasing. Either a higher sampling rate or an anti-aliasing filter must be used to avoid aliasing during data acquisition.

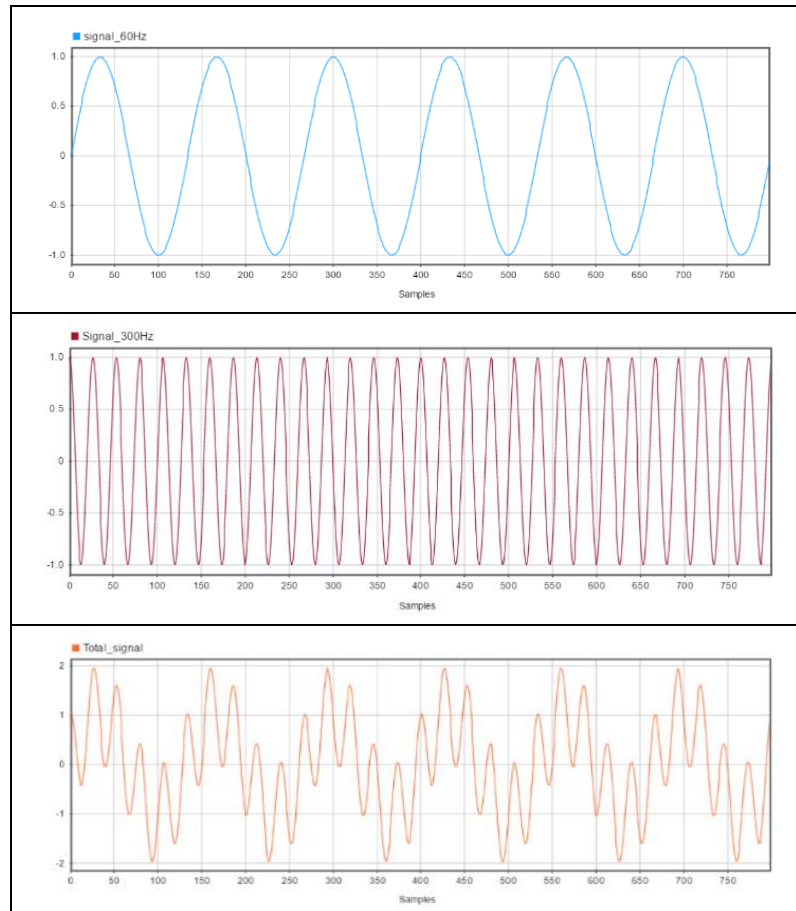


Figure 21: Influence of harmonic in a signal

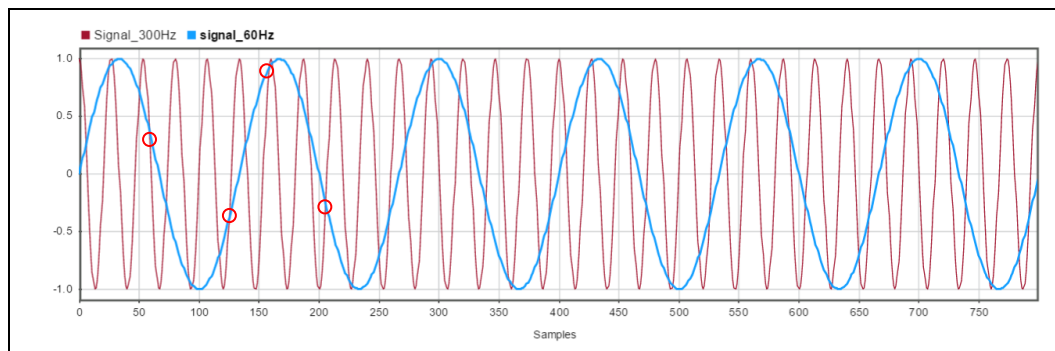


Figure 22: Effect of 'aliasing' in signal

Total harmonic distortion (THD) is a widely used measure of signal quality. In an electronic system, the term THD is an important parameter mostly used to detect a motor bearing fault [61]. THD can be used to represent current or voltage distortion. Generally, the measurement unit is in (- dB). THD is calculated as follows:

$$\text{THD (\%)} = \frac{\sqrt{I_2^2 + I_3^2 + \dots + I_n^2}}{I_1} \quad (2)$$

Here, ' I_n ' is the magnitude of the n^{th} harmonic and ' I_1 ' is the magnitude of the fundamental frequency. If the current waveform is an ideal sine wave, then the THD is zero.

Crest Factor (CF)

The ratio between the peak of the current (I_{max}) (or, voltage) and its RMS value (I_{rms}) is known as the crest factor. To evaluate the distortion in the waveform of a signal, the crest factor (CF) provides another source of measurement. If the signal does not have any harmonic distortion (an ideal case), then the current's peak value will be $\sqrt{2} * I_{\text{rms}}$. Therefore, the crest factor measurement of a pure sinusoidal signal is 1.414. The following Equation (3) relates the crest factor of a current signal.

$$\text{Crest Factor, CF} = \frac{I_{\text{max}}}{I_{\text{rms}}} \quad (3)$$

During the cutting process, motor shaft torque affects the motor power/current, which provides a comparative analysis for online tool wear monitoring. The higher the crest factor, the greater is the energy contained in the higher harmonics. Therefore, the peak values of the crest factor and THD are visible when the cutting torque has a sudden increase

due to tool wear. Figure 23 show the variation in total harmonic distortion (THD) (%error of THD values= 0.12) and Figure 24 present the crest factor (CF) (%error of CF values= 1.90) variation in a tool life study (plotted against the number of cuts) of test-1 (T1 from Table 10). In both cases, a significant increment of these features (from the motor current sensor) is clearly visible, at a time when the tool-wear curve reaches the steady-state wear zone and the catastrophic tool failure region, respectively. The THD value was measured as 24% during the no-cutting (or air-cutting) condition in T1.

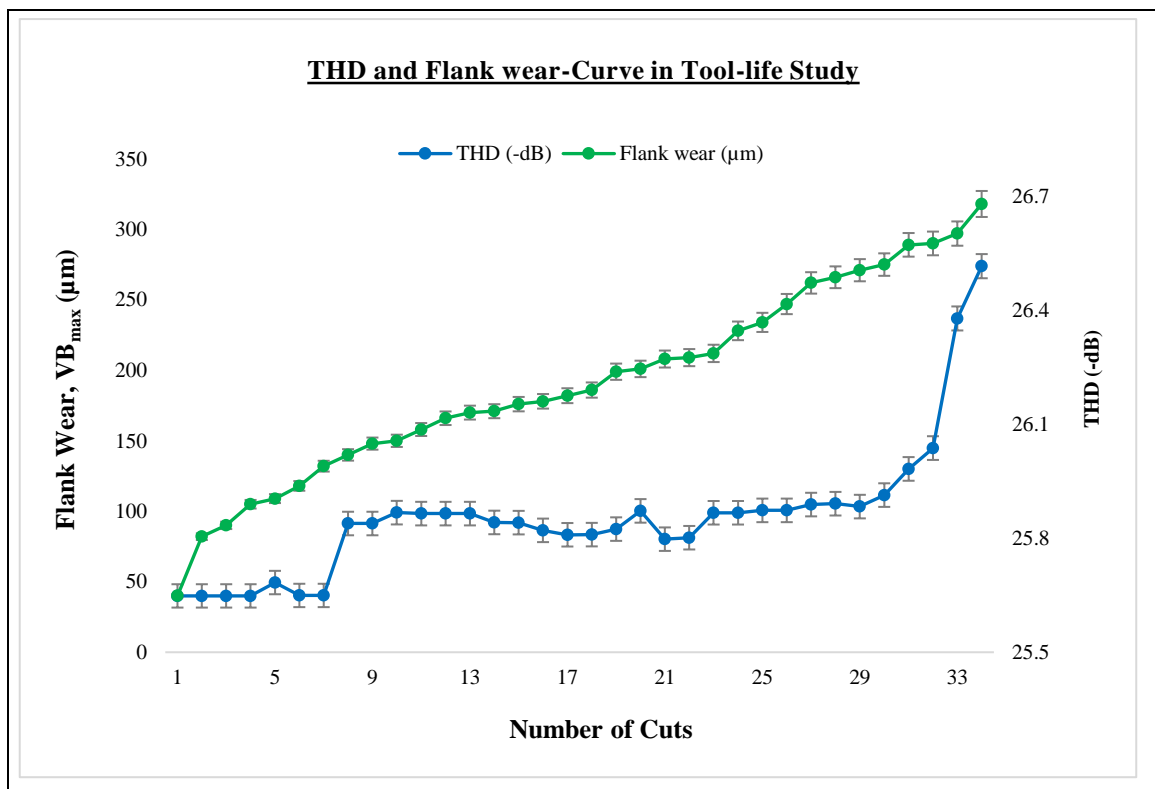


Figure 23: Variation of THD in a tool life study (T4) (see Table 10)

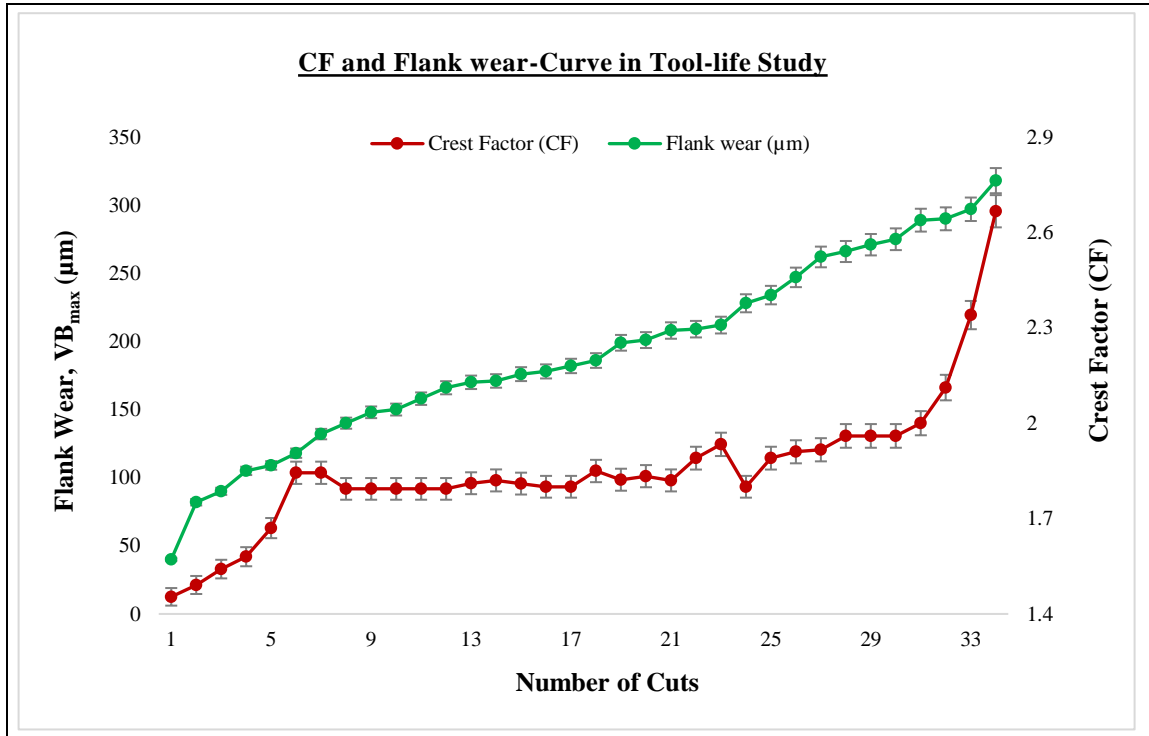


Figure 24: Crest factor variation in the tool life study ((T4) (see Table 10)

4.2.3. Effect of Tool-wear on Forces

Machining forces increase as the cutting tool gradually wears out, due to the increasing friction between the cutting tool and the workpiece. In dry turning, the radial force- F_x (%error of F_x values= 4.6) value was observed to be higher than the cutting force- F_z (%error of F_z values= 2.6) and feed force- F_y (%error of F_y values= 5.4). The entire force curve gradually increases throughout the tool life (Figure 25). The contact area between the workpiece and the tooltip grows larger due to sudden breakage, which causes a rapid increase in the turning process’s radial forces. Moreover, the contact area gradually increases in the stable tool wear region. Finally, catastrophic tool failure promotes a rapid rise in the radial and feed forces.

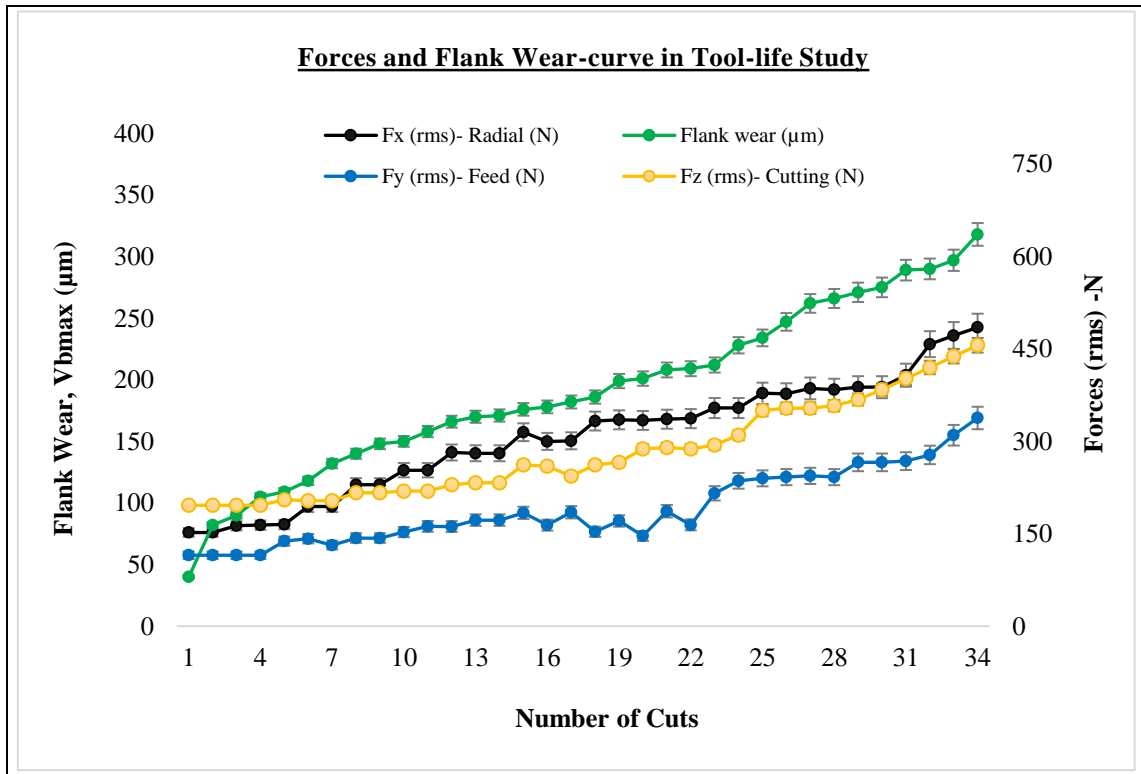


Figure 25: Variation of forces in a tool life study (T4) (see Table 10)

4.2.4. Effect of Tool-wear on Vibration

Vibration content in the cutting direction shows a gradual increase during the tool's life. A sudden increase in tool wear causes a rapid increase in the vibration content associated with the cutting direction. For example, when tool flank wear suddenly reaches the second stage of tool wear, vibration-rms (%error of vibration-rms values= 4.2) values increased (Figure 26). Further catastrophic failure or a rapid increase in tool wear with crater wear (i.e. a ceramic tool during the experiment) again increases vibration at the end of the tool-life study.

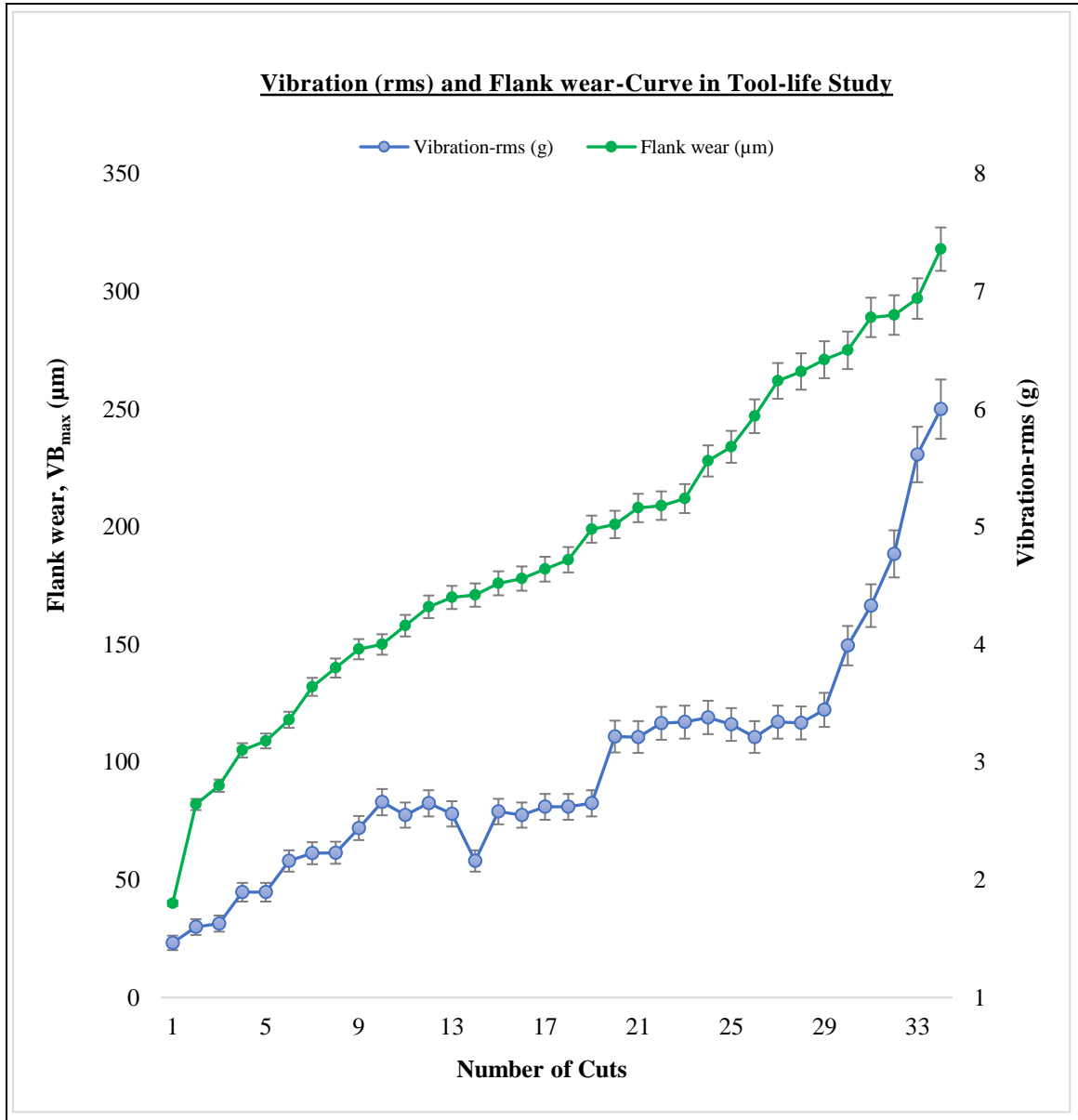


Figure 26: Variation of vibration (RMS) in a tool life study (T1) (see Table 10)

Chapter 5. Signal Processing & Features Extraction

This chapter summarizes the techniques of sensor signal acquisition, pre- and post-signal processing, considering the multifaceted nature of the sensor fusion process described in the first section (section 5.1 and section 5.3). The next section (section 5.4) offers a feature generation & extraction procedure. In addition, several feature dimensionality reduction methods are also presented in this section.

5.1. Signal Acquisition & Pre-Processing

Signal acquisition and pre-processing include signal conditioning and event detection of the signal acquired from the data acquisition system. During the turning test, the data acquisition system acquires the signals from the individual sensors, which are then directed to the appropriate Kistler amplifiers and the National Instrument (NI) DAQ board for analogue to digital conversion and preliminary signal conditioning. Transducer sensitivity and the measurement units (volts) were taken into account for the voltage gain (or loss) settings of each sensor signal. The sampling rate was set to 10 kHz (predetermined by Nyquist) based on the expected content generated in the cutting process.

National Instrument LabView© 2014 version software was used for data acquisition. The data acquisition software was able to acquire the signal considering the filtering (Low pass filter for the current sensor with a cut-off frequency of 200 Hz). In addition, the offset from the vibration signal (due to the relative orientation of gravity) was also removed during the signal conditioning.

The raw signals (Figure 27) from the sensors need to be pre-processed for further signal processing and feature extraction. The LabView© software was accordingly programmed to distinguish the event (only cutting data) from the acquired signal.

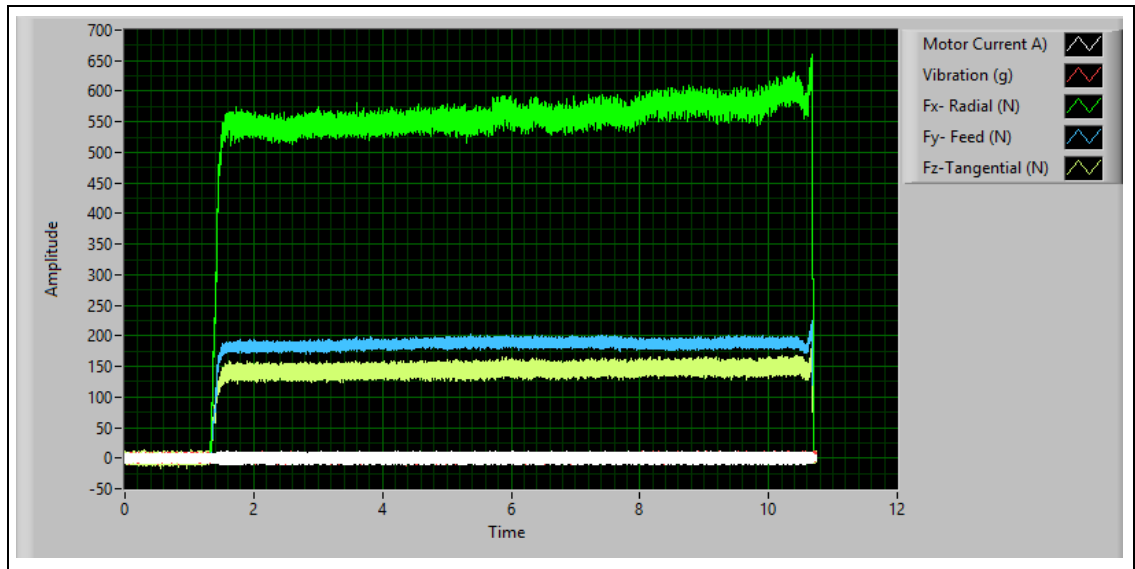


Figure 27: An example of sensor fusion raw signals

For example, each sensor fusion signal consists of four (4) segments of data (Figure 28). No cut (A), entry cut (B), continuous cut (C) and, exit cut (D), compose the segments of each raw signal from which only turning test cutting data (C) was obtained by the event detection program. Since segments A, B & D emerge from the tool approaching and moving away from the workpiece, they do not convey any relevant information about the cutting tool conditions (tool wear).

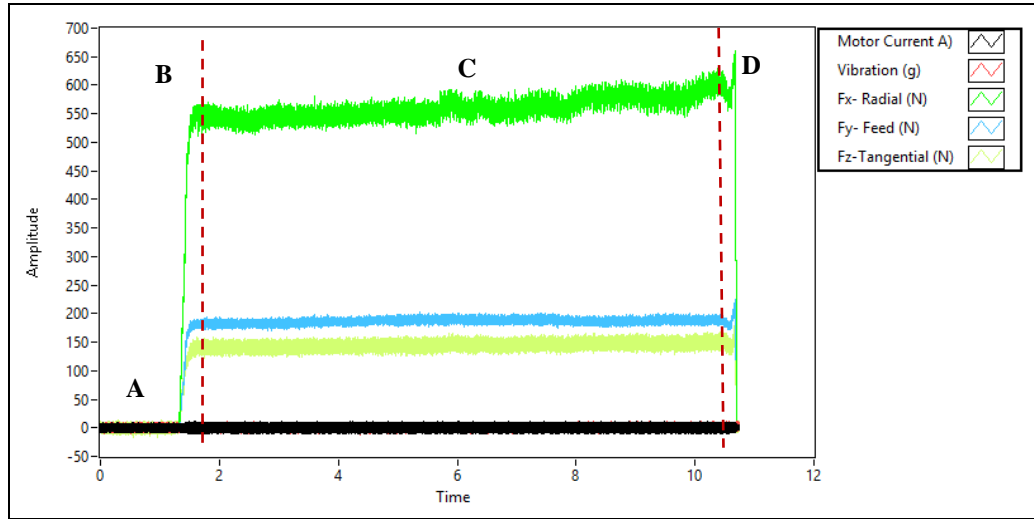


Figure 28: Data Segmentation (event detection) of a raw signal

Afterwards, this segmentation technique was carried out for all the acquired signals (Figure 29). In this way, all acquired signal segments that do not convey relevant information about the actual cutting test were removed. Furthermore, all channel signals (spindle motor current, vibration, 3-axis forces) were pre-processed in a likewise manner.

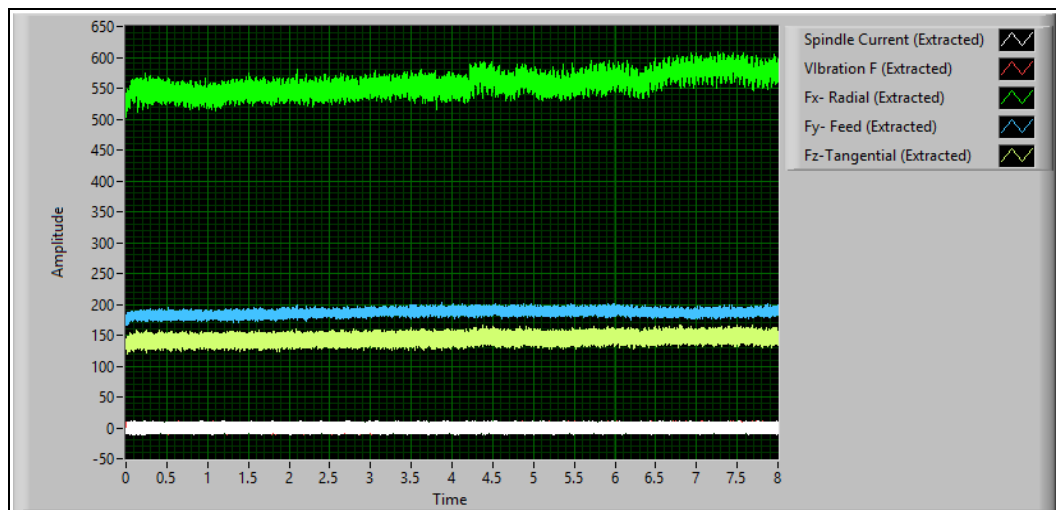


Figure 29: An extracted event from the raw signals

After pre-processing, the next step is to process the signal. The sensor signals can be presented in different domains (time, frequency and time-frequency). Signals from the sensors possess different properties. Therefore, to establish the best relationship between sensor signals and the tool-state, further signal processing is necessary.

5.2. Fourier Transforms (FT)

Fourier transforms (FT) are the most commonly used tools in signal analysis. To identify the source of any vibration and noise, FT can be useful because of its representation type (frequency-domain). Fourier transform analysis can decompose a limited energy signal. A time-domain signal $x(t)$ can be decomposed by the Fourier transform $X(\omega)$ as follows:

$$X(t) = 1/2\pi \int_{-\infty}^{+\infty} X(\omega) e^{i\omega t} dt \quad (4)$$

Where,

$$X(\omega) = \int_{-\infty}^{+\infty} f(t) e^{-i\omega t} dt \quad (5)$$

Equation (4) presents the Fourier transform whereas Equation (30) presents the inverse Fourier transform. In FT, the time-domain signal $x(t)$ is decomposed into a family of harmonics $e^{i\omega t}$ where, $X(\omega)$ represents the amplitude of that harmonics.

Sensor features were also extracted in the time-domain. Figure 30 shows a frequency-domain (power-spectrum) analysis. Here, vibration signals from cutting test 7 (T7) (see Table 10) were plotted in the frequency domain (normalized frequency). Two significant frequencies are shown, sourced from the accelerated flank wear (left cursor) and the tool

holder (right cursor). Both have a significant impact on accelerated tool wear. The 'RT7P51' signal represents tool failure.

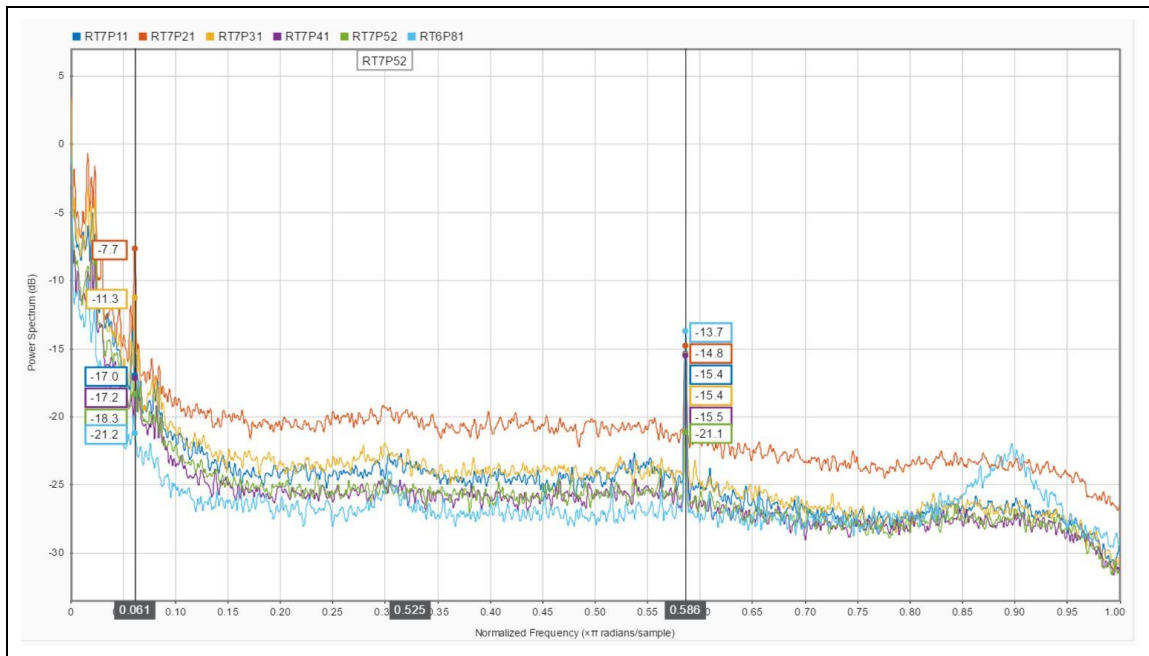


Figure 30: Power spectrum of the extracted vibration signals (T7) (see Table 10)

5.3. Wavelet Transform (WT) Analysis

Wavelet transform (WT) analysis is an advanced signal processing tool which decomposes the signal into various components at different time windows and frequency bands. Analyzing the signal in only the time or frequency domain is not efficient. To develop a robust tool-wear monitoring system, wavelet transform (WT) analysis was used in this research to acquire more information from the time-frequency domain signal.

In wavelet transform analysis, wavelets are used as the base component instead of a sinusoidal function. This decomposes a signal into sub-levels with different frequency

ranges under a time domain. Based on the decomposition level, any component of a signal can be obtained by the wavelet's scale and position. The wavelet transform is defined by

$$H^{(a,b)}(x) = |a|^{-1/2} h\left(\frac{x-b}{a}\right) \quad (6)$$

In Equation (6), a and b represent the frequency and the time shift or 'location' respectively. The 'mother wavelet function' is denoted as $h^{(a,b)}$. Wavelet transform analysis restructures the original signal with the following expression:

$$F = C \int \frac{da}{a^2} \int db \langle h^{(a,b)}, f \rangle h^{(a,b)} \quad (7)$$

Where ' f ' represents the original function and $\langle h^{(a,b)}, f \rangle$ are the wavelet's components.

During signal processing with the wavelet transform, signal decomposes in the 'approximation coefficient' (low-frequency component) and 'detail coefficient' (high-frequency component). In the next step (or level), the 'approximation coefficient' decomposes into the second level of 'approximation coefficient' and 'detail coefficient'. Moreover, this process is continued.

A wavelet packet $W_{j,n,k}$ is generated from the base function (MathWorks©, 2004) [62]:

$$W_{j,n,k}(x) = 2^{-\frac{j}{2}} W_n(2^{-j}x-k) \quad (8)$$

Here, j, n, k are the scale, oscillation and time-localization parameters respectively considering $(j, k) \in \mathbb{Z}$ and $n=0, 1, 2, 3 \dots, 2^{j-1}$. Generally, the functions of the wavelet packet (WP) are defined as follows:

$$W_{2n}(x) = \sqrt{2} \sum_k h(k) W_n(2x-k) \quad (9)$$

$$W_{2n+1}(x) = \sqrt{2} \sum_k g(k) W_n(2x-k) \quad (10)$$

Here, $h(k)$ is the low-pass and $g(k)$ is the high-pass filter given the scaling and wavelet function, $W_0(x)=\Phi(x)$ and $W_1(x)=\Psi(x)$ respectively.

In this research, Wavelet Packet Decomposition (WPD) was performed by MATLAB® R2017b with a built-in function for 1-D wavelet packet analysis. Mathematically, the discrete wavelet packet transform (DWPT) is expressed as

$$W_{j+1, 2n} = H W_{j, n} \quad (11)$$

$$W_{j+1, 2n+1} = G W_{j, n} \quad (12)$$

Where $H=\{h_l\}_{l \in \mathbb{Z}}$ are the low-pass filter matrices and $G=\{g_l\}_{l \in \mathbb{Z}}$ are the high-pass filter matrices. In general, W_{00} is the measured signal and $W_{j, n}$ is the wavelet packet in the j^{th} level and n^{th} position. The updated wavelet packet in each decomposition level and position can be expressed as follows:

$$W_{j, n} = H^* W_{j+1, 2n} + G^* W_{j+1, 2n+1} \quad (13)$$

Here, H^* and G^* is the conjugate matrix of 'H' and 'G', respectively.

The 'Haar' mother wavelet was used to estimate the wavelet packet coefficient. Figure 31 presents the third level of the extracted signal's wavelet packet decomposition tree. The signal acquired with a sample rate 10 kHz (i.e. 5 kHz useful bandwidth in the wavelet packet) is denoted as W_{00} and the 8-wavelet packets in the third level ($j=3$) of decomposition are denoted as $W_{30}, W_{31}, \dots, W_{37}$ respectively. To describe the tool wear condition, two types of information were extracted in this analysis. The RMS value of the

wavelet coefficients (approximation-level and detail-level) and the Shannon entropy of that signal at that decomposition level.

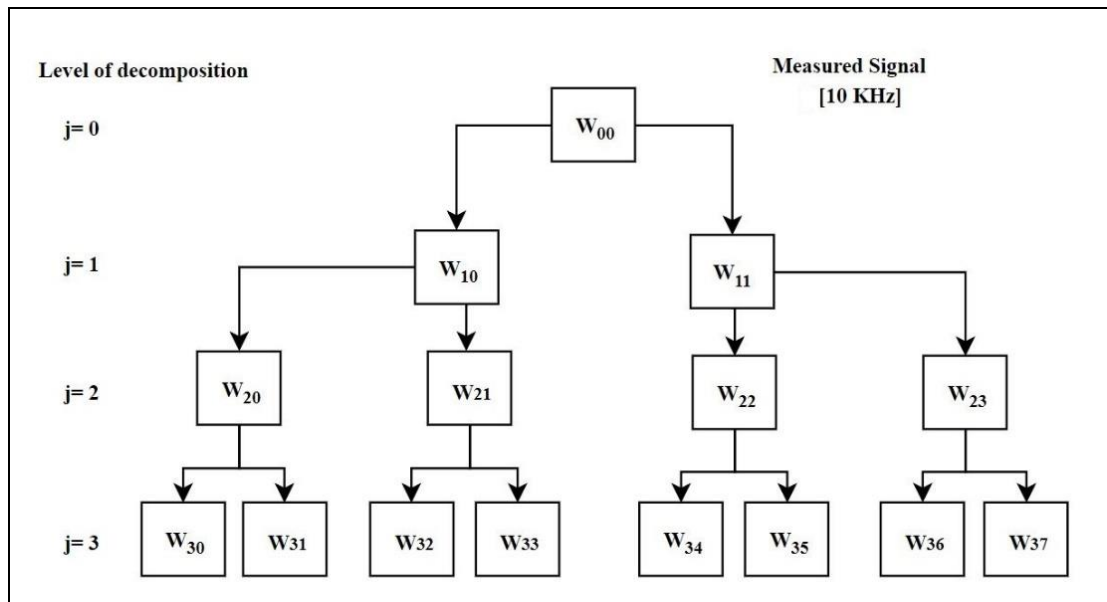


Figure 31: 3-level of wavelet packet decomposition tree of the measured signal

Figure 32 and Figure 33 represent the decomposition of the acquired signal into 8 (eight) frequency bands (8-wavelet packets) with 3 (three) levels of decomposition each. Both signals were acquired from the same machining condition test (Test 9 from Table 10). Figure 32 was the decomposed vibration signal when the tool flank wear was measured to be $124\mu\text{m}$, and Figure 33 is the decomposed vibration signal at a flank wear of $411\mu\text{m}$. The ‘approximation coefficient’ is denoted as ‘a’, the ‘detail coefficient’ is ‘d’ and the final decomposed signal is ‘s’. Both results show a significant difference at the 3rd - level of decomposition, especially in the approximation-level ‘ a_3 ’.

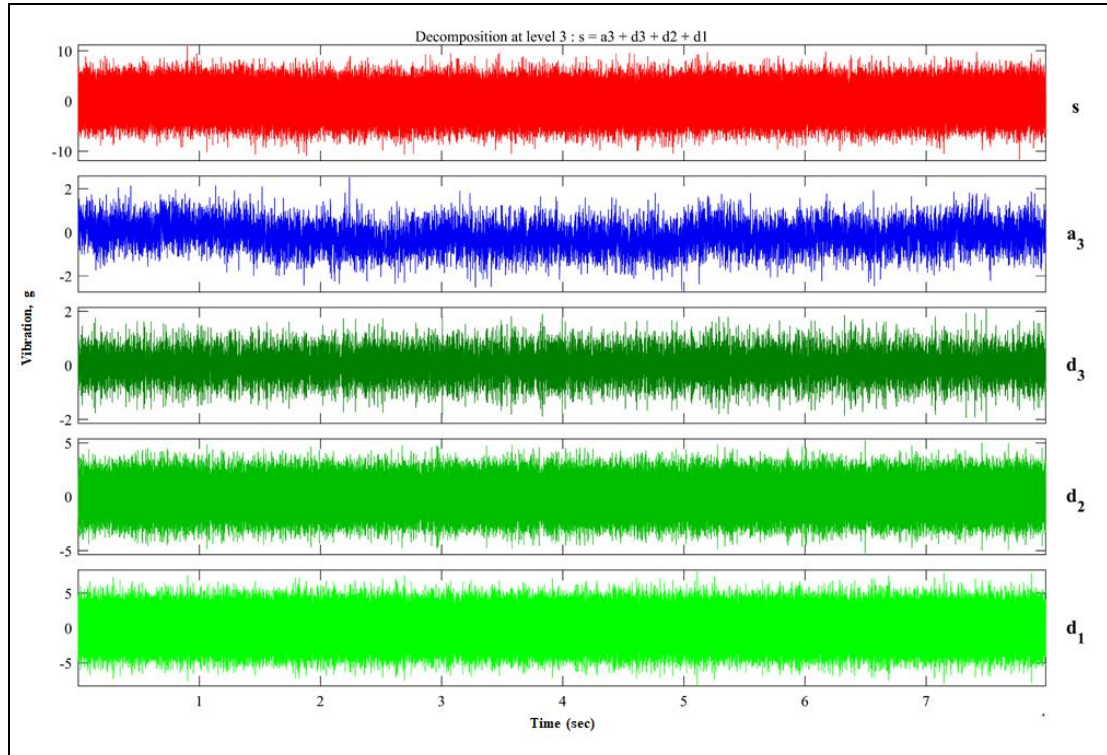


Figure 32: 3-level WPD of the vibration signal at flank wear 124µm

In Figure 33, the approximation-level ' a_3 ' of the decomposed signal significantly rises to the maximum amplitude (vibration = +8g, here $g= 9.8 \text{ ms}^{-2}$) whereas in Figure 32, the vibration level was quite low (in the decomposed signal of a_3) at a flank wear of 124µm.

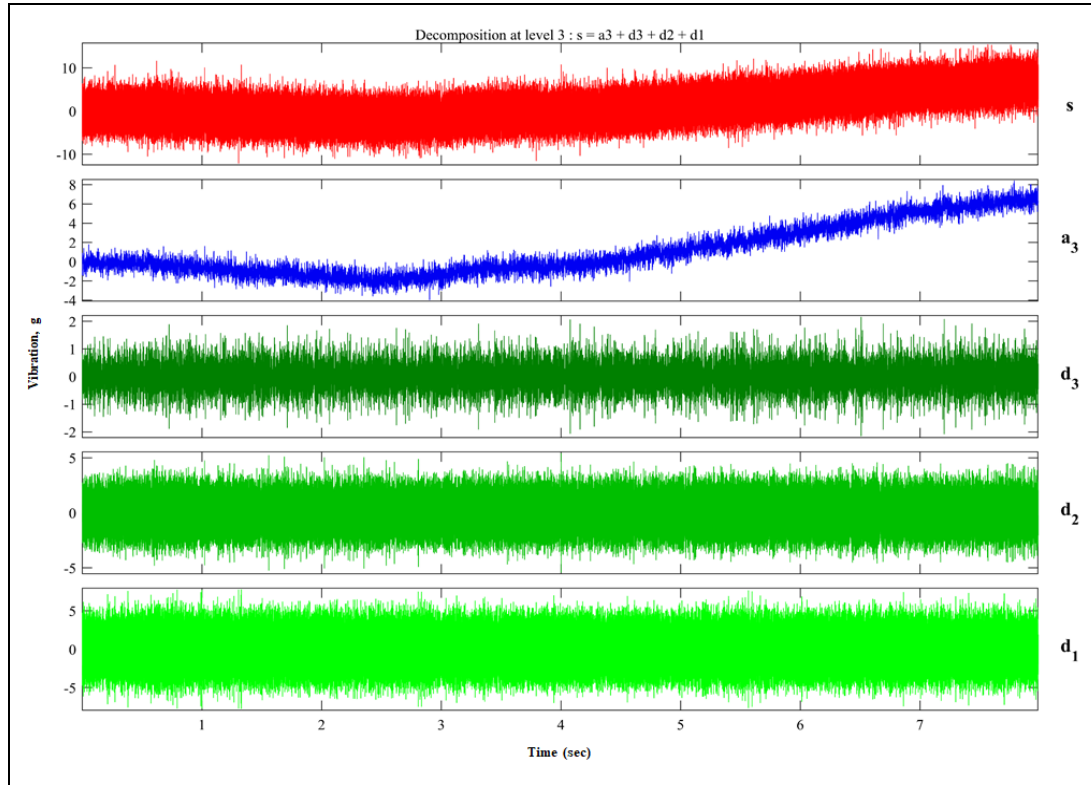


Figure 33: 3-level WPD of the vibration signal at flank wear 411 μm

5.4. Feature Extraction & Dimensionality Reduction

During the cutting test, the sensor's online measurements can act as an indirect indicator of the tool wear condition. Generally, it is always arduous to develop a relationship between the raw signal and the tool wear state, due to the low signal-to-noise ratio (SNR) of the acquired signal. Relevant features need to be extracted from the processed signal. It is important to note that tool wear can be different in two wear tests under identical machining conditions, cutting length and cutting time. However, with efficient feature extraction and a trained machine learning algorithm, it is possible to correlate the same features with a

similar amount of tool wear. Therefore, effective features need to be extracted from the processed signal and mapped to obtain a relationship (correlation) with the tool wear state.

In this research, custom MATLAB© code was implemented to generate and extract features from the processed signal acquired from all of the (5-channel) sensor channels. The different features from the different domains generated from the dataset are summarised in Table 13.

These listed features were extracted from the 5 channel signals (Spindle Motor Current, Vibration, Fx, Fy, Fz) of the data which were previously stored in the database. Seven (7) typical statistical features were selected. In frequency domain analysis, the power spectrum density, $S(f_j)$ was calculated by using the Welch method [63]. In all cases, total harmonic distortion, THD (frequency-domain), crest factor (CF) and peak-to-peak (statistical features) were extracted only from the spindle motor current channel signals. These three features were considered to be special features coming from motor current signals in this research.

Time-frequency domain analysis gives another perspective of the tool wear condition, which statistical features and frequency-domain features can't express as well. Further signal processing analysis (Fourier and wavelet transforms) were involved in extracting these features.

From the spindle motor current - channel, 7 (seven) statistical, 3 (three) frequency-domain and 2 (two) time-frequency domain features and from the vibration - channel, 5 (five) statistical, 2 (two) frequency-domain and 2 (two) time-frequency domain features were extracted.

Table 13: List of extracted features from the processed sensor signal

Feature Type	Features	Mathematical Expression
Statistical Features	Mean	$\bar{x} = 1/N \sum_{i=1}^N x_i $
	Variance	$x_{\text{var}} = 1/N \sum_{i=1}^N (x_i - \bar{x})^2$
	RMS	$x_{\text{rms}} = \sqrt{1/n (x_1^2 + x_2^2 + \dots + x_n^2)}$
	Kurtosis	$x_{\text{kurt}} = \frac{1}{n} \sum_{i=1}^n \left(\frac{x_i - \mu}{\sigma} \right)^4$
	Skewness	$x_{\text{skew}} = \frac{1/n \sum_{i=1}^n (x_i - \bar{x})^3}{\left(\sqrt{1/n \sum_{i=1}^n (x_i - \bar{x})^2} \right)^3}$
	CF (peak2rms)	$x_{\text{peak2rms}} = \frac{\ x\ _{\infty}}{\sqrt{1/N \sum_{n=1}^N x_n ^2}}$
	peak2peak	$x_{\text{peak2peak}} = (x_{\text{max}} - x_{\text{min}})$
Frequency-Domain Features	Spectral mean	$\bar{f} = \frac{\sqrt{\sum_{i=1}^k f_i^2 S(f_i)}}{\sum_{i=1}^k S(f_i)}$
	Spectral kurtosis	$f_{\text{kurtosis}} = \sum_{i=1}^k \left(\frac{f_i - \bar{f}}{\sigma} \right)^4 S(f_i)$
	Total Harmonic Distortion	$\text{THD (\%)} = \frac{\sqrt{I_2^2 + I_3^2 + \dots + I_n^2}}{I_{\text{fundamental}}}$
Time-Frequency Domain Features	Shannon entropy	$E(x) = - \sum_{k=1}^N S_k^2 \log(S_k^2)$
	Wavelet energy	$E_{\text{WT}} = \frac{\sum_{i=1}^N w t_{\varphi}^2(i)}{N}$
	Wavelet energy ratio	$R_{\text{WT}} = \frac{E_{\text{WT}}^Y}{E_{\text{WT}}^Z}$

Again, 5 (five) statistical, 2 (two) frequency-domain and 3 (three) time-frequency domain features were extracted from the Fx - channel. Furthermore, from the Fy and Fz - channel, 5 (five) statistical, 2 (two) frequency-domain and 2 (two) time-frequency domain features were extracted. As a result, in a total of 49 features were extracted and stored in the database for further analysis (dimensionality reduction).

Dimensionality reduction is the next post-processing step for implementing artificial intelligence (AI) techniques. The complexity of any AI algorithm depends on the number of input variables and the data sample size. The selection of the input variable number affects the computation time and space. Therefore, reducing the number of redundant input variables results in less data processing time.

In general, dimensionality reduction techniques may reduce certain features which are more responsive to the output variable. The objective is to acquire the best and least combination of input features that provide a strong relationship with the output variable.

For example, suppose the original dimension of the extracted feature is m . The objective of the dimensionality reduction technique is to derive a new set of n (where, $n < m$) dimensions given the most information and the leftover set ($m - n$). This research study uses two types of feature selection techniques. The first is a supervised technique (Pearson Correlation co-efficient) & the second is an unsupervised technique, principal component analysis (PCA).

5.4.1. Pearson's Correlation Coefficient (PCC) Analysis

Pearson's correlation coefficient was employed to evaluate the correlation between the extracted feature and the tool wear condition. This method measures the independence of two or more random variables providing a coefficient value (Pearson's correlation coefficient) called 'r' with a level of significance 'p'. In this study, the correlation analysis was calculated as follows:

$$r = \frac{\sum_{i=1}^n (x_i - \bar{x})(y_i - \bar{y})}{\sqrt{\sum_{i=1}^n (x_i - \bar{x})^2} \sqrt{\sum_{i=1}^n (y_i - \bar{y})^2}} \quad (14)$$

Where 'x' is the feature and 'y' is the condition of the tool (i.e. flank wear). The value of 'r' categorizes the correlation level according to class: weak correlation ($0 < r < 0.3$), moderate correlation ($0.3 < r < 0.5$), strong correlation ($0.5 < r < 1.0$). Features were selected based on strong to medium correlations. Table 14 represents the PCC analysis on extracted features with the common used 'statistical significant' level ($p < 0.05$).

The extracted features that show a strong correlation with tool wear propagation ($r > 0.5$) are: motor current (crest factor, THD, Shannon entropy, wavelet energy), vibration (mean, wavelet energy), Fx (mean, Shannon entropy), and Fy (variance, energy ratio). In this way, the 10 best features out of 49 were selected for the decision-making algorithm due to their strong correlation with the tool wear state. Furthermore, the extracted features that have a medium or greater correlation ($0.3 < r < 0.5$) are: motor current (mean), vibration (rms, spectral mean), Fx (variance, rms, wavelet energy), Fy (mean, rms, Shannon entropy), and Fz (variance, skewness, wavelet energy). In total, 12 out of 49

features have an average correlation with the tool wear state. These features will also be considered in the next chapter for further comparison.

Table 14: Correlations between extracted features and cutting tool wear

Extracted Features		Motor Current	Vibration	F _x	F _y	F _z
Statistical features	Mean	0.46	0.66	0.87	0.39	0.29
	Variance	0.20	0.20	0.48	0.76	0.42
	RMS	0.28	0.33	0.33	0.47	0.15
	Kurtosis	0.24	0.21	0.21	0.18	0.18
	Skewness	0.18	0.21	0.28	0.15	0.32
	Crest factor	0.76				
	Peak to Peak	0.41				
Frequency- domain features	Spectral mean	0.26	0.44	0.2	0.2	0.2
	Spectral kurtosis	0.22	0.18	0.18	0.18	0.2
	THD	0.89				
Time-frequency domain features	Shannon entropy	0.65	0.19	0.76	0.4	0.19
	Wavelet energy	0.51	0.54	0.35	0.21	0.35
	Energy ratio (F _x /F _z)			0.65		

5.4.2. Principal Component Analysis (PCA)

Principal component analysis (PCA), an unsupervised linear projection-based feature extraction method, is used to further reduce the dimensionality. It is one of the most widely used statistical techniques that converts a set of matrices with correlated variables into a set

of independent variables, known as principal components. In general, the first component has the highest possible variance. The analysis is mathematically derived from an orthogonal linear transformation that converts a data set into a new coordinate system, where the projected data with the greatest variance falls into the first component (first coordinate in the coordinate system), the second highest variance data falls into the second component (second coordinate in the coordinate system) and so on accordingly. PCA has the following goals:

- Extract the essential information from the dataset
- Reduce the size of the dataset considering important information
- Analyze the structure of the extracted features by simplifying the dataset.

The following mathematical expression can be developed according to the PCA algorithm presented in the literature [64].

A data matrix, $Y = \{y_1, y_2, \dots, y_N\}$, where $y_i^T = \{F_{ij}, j = 1, 2, 3, \dots, m\}$, can be constructed, given 'N' training samples consisting of 'm' dimensional features vectors (in this dataset, $m=49$). R_Y is the corresponding covariance matrix which is as follows:

$$R_Y = \sum_{I=1}^N (y_i - \bar{y})(y_i - \bar{y})^T \quad (15)$$

Where, \bar{y} is the mean feature vector of all samples of 'Y' and 'T' represents the transposition

$$\bar{Y} = \frac{1}{N} \sum_{I=1}^N y_I \quad (16)$$

The corresponding 'Y' matrix's eigenvalues can be obtained from the following equations:

$$\lambda v = R_Y v \quad (17)$$

Where ' λ ' are the eigenvalues and ' v ' is the eigenvector of R_Y respectively. During calculation, the eigenvalues are usually listed in descending order ($\lambda_1 \geq \lambda_2 \geq \dots \geq \lambda_d$) whereas the corresponding eigenvector of λ_j ($j = 1, 2, \dots, m$) is denoted as v_j ($j = 1, 2, \dots, m$). Therefore, the j^{th} -principal component feature ' F_{ij} ' of a sample pattern ' y_i ', can be obtained as follows:

$$F_{ij} = v_j^T (y_i - \bar{y}) \quad (18)$$

To classify the tool condition, each principal component score can be evaluated based on its contribution to the response (tool condition). In general, first ' n ' principal components are selected based on the eigenvalues. This method is called the accumulative contribution rate (ACR) which can be defined as [65]:

$$R_n = \frac{\sum_{i=1}^n \lambda_i}{\sum_{i=1}^m \lambda_i} \quad (19)$$

Where, ' R'_n ' is the percentage of the total variance which is explained by the first ' n ' component. According to the ACR method, the first ' n ' principal components are then selected as the updated (new) feature vectors.

In summary, the ' n ' principal components are selected to represent ' m ' features extracted from the machining test by the matrix transformation formula (Equation (18)) without any loss of information from the dataset. The flowchart in Figure 34 summarises the principal component analysis (PCA) procedure described in this chapter.



Figure 34: PCA analysis procedure

Principal component analysis from all datasets produced a scree plot (Figure 35) which envisions the size of the eigenvalues in relation to the number of principal components (eigenvalues as a function of principal components). The scree plot determines the number of components based on the size of the eigenvalues.

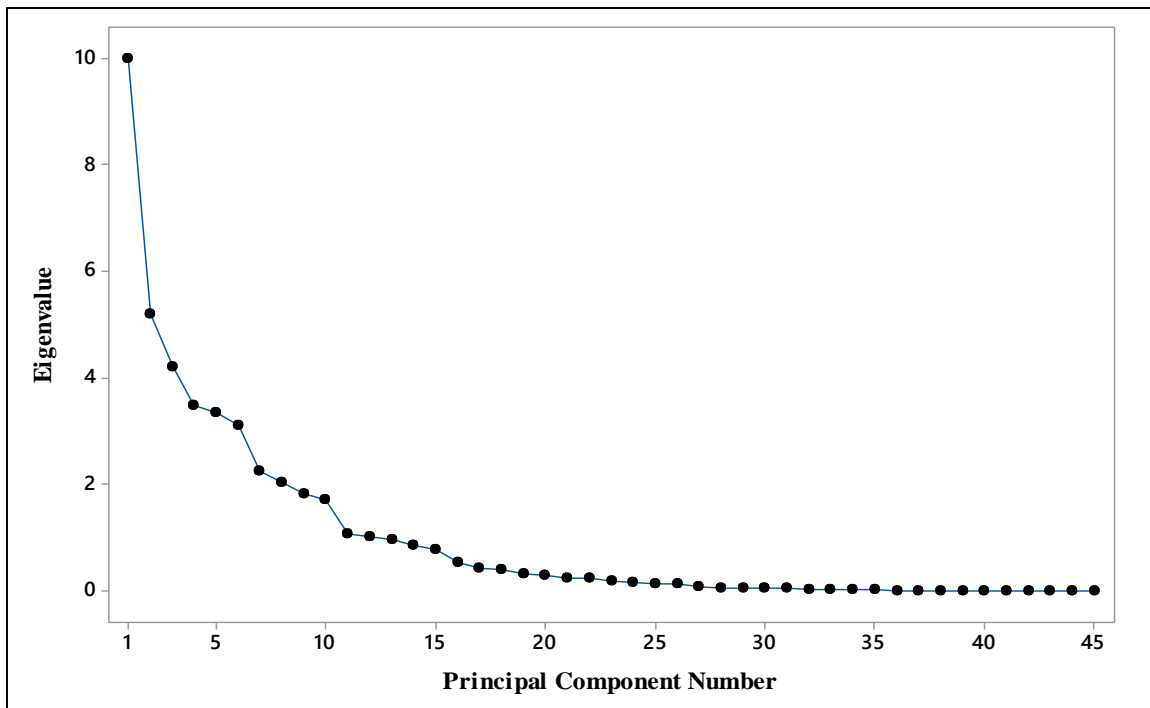


Figure 35: Scree plot (based on all dataset)

The results from the scree plot show that the first 11 principal component have eigenvalues greater than 1 (one). These components generally explain the highest variation in the dataset. The remaining principal components account for a decidedly lesser portion of the variability (close to zero) and are thus far less important for modelling.

The score plot (Figure 36) represents the first and second principal component scores. It assesses the data structure and detects the cluster of tool conditions (tool wear state). From the clustering distribution, it is evident that the 2nd principal component can better indicate more separate clusters in the dataset compared to the 1st principal component, but the first two components from PCA failed to classify a few critical clusters.

Furthermore, several outliers from the data set are also visible at the bottom of the plot, which represents the anomalies of a specific cluster of features in the dataset. Therefore, this study considered scores up until the 11th principal component, based on the scree and score plot results.

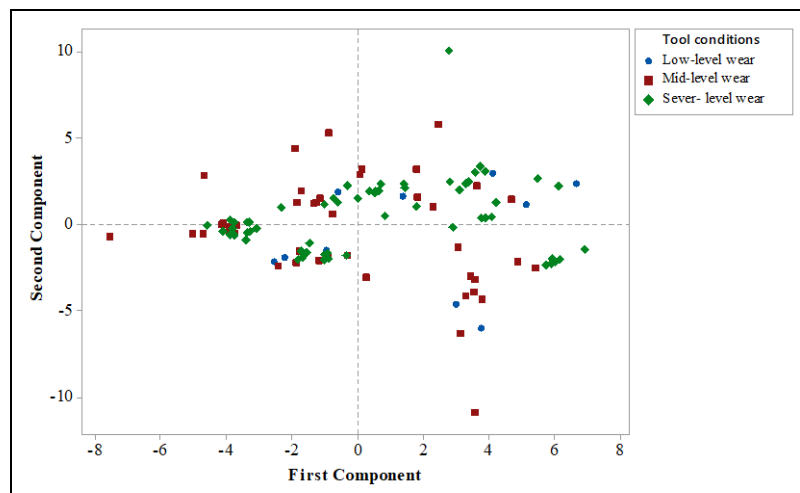


Figure 36: Score plot of the 1st and 2nd principal components (based on all dataset)

The results of the PCA procedure are summarised in Table 15. The table represents significant feature variables corresponding to the 1st, 2nd, ..., 11th principal component, respectively.

Table 15: List of significant features based on PCA score

Principal Components	Significant Features
1st component	Motor Current (THD)
2nd component	Motor Current (CF)
3rd component	Motor Current (peak2peak)
4th component	Motor Current (Shannon entropy)
5th component	Vibration (Mean)
6th component	Vibration (Spectral mean)
7th component	Vibration (Wavelet energy)
8th component	Fx (Mean)
9th component	Fy (Variance)
10th component	Fz (Spectral mean)
11th component	Wavelet energy ratio (Fx/Fz)

5.5. Discussion

This chapter analyzes the features recorded in the sensor database. Features from the sensor signal were extracted in a different domain. Fast Fourier transform (FFT) and wavelet transform analysis (WT) were employed to extract the signal. To reduce the feature dimensionality of the dataset, two types of techniques, PCC and PCA, were adopted. Correlation analysis describes each feature's relationship with the system response, which in this case is the cutting tool state (tool-wear). In this analysis, 10 features were selected based on the coefficient score. PCA was employed to reduce the features' dimension. Further PCA analysis showed that 11 features can be selected to identify systemic faults (tool wear classifier).

In both cases, features from the motor current signal and vibration sensor show promising correlations with tool wear states. The spindle motor current sensor is a promising candidate for combination with the vibration sensor during a turning test, due to its low cost and simple installation.

Chapter 6. AI-based Decision-Making Module

6.1. Introduction to Artificial Intelligence (AI) in Machining

In the manufacturing process, various factors such as machining process parameters, fault characteristics, environmental factors and human error can influence the result of expected productivity, tooling cost and part-scrap rate. An indirect monitoring system can sometimes mislead by providing wrong information. In general, the relationship between features extracted from the sensor signal is difficult to investigate due to its complexity and non-linear nature of the process. Visualization of the sensor data is insufficient for a decision-making system due to this complexity. Therefore, it is necessary to design a wear monitoring method that can learn from previously established information and transmit the learned knowledge into a new cutting test dataset. Artificial intelligence (AI) methods have tremendous potential to perform such tasks.

In this chapter, two types of AI techniques were implemented to develop a data-driven tool wear monitoring system. In addition, background information of these techniques is provided in this chapter with detailed evaluations of input features. Finally, the best AI techniques identified using experimental data were selected for further validation and implementation in the machining process.

6.2. Multi-layer Perceptron based Artificial Neural Network

The multi-layer perceptron artificial neural network (MLP-ANN) is the most widespread machine learning technique that uses the feed-forward artificial neural network

model structure and the backpropagation method for establishing the parameters (weights). The feed-forward neural network (FFNN) consists of an input layer with some hidden layers and an output layer. The network's functional direction is oriented from the input to the output layer without forming any loop inside the network. Each node is connected to the next layer with a specific connection weight. Several training functions are available that modify the connection weights of the process. This method also adopts the backpropagation algorithm to train the neural network. The basic working principle of the feed-forward-back-propagation neural network (FF-BPNN) using the MATLAB 'transig' transfer function is described below [66].

If, W_{xy} represents the weight values between the input and the hidden layer and W_{yz} is the weights between the hidden layer and the output layer, then the first stage (feed-forward stage) of the operation can be expressed as follows:

$$V(n) = W_{yz}(n) b(n) \quad (20)$$

$$o(n) = \varphi(v(n)) = \frac{2}{1 + e^{-2v(n)}} \quad (21)$$

Here, the iteration number is expressed as 'n', the output as 'o', the hidden layer output as 'b' and the activation function as 'φ'. The output network for the present weights is derived with Equation (21). The second stage is called the back-propagation (BP) stage which is expressed by the following Equation (22).

$$\Delta(n) = e(n) \cdot \varphi[v(n)] = [d(n) - o(n)] \cdot [o(n)] \cdot [1 - o(n)] \quad (22)$$

Where ‘ δ ’ is the local gradient function with error function ‘ e ’. Also, the actual and desired output is represented as ‘ o ’ and ‘ d ’ respectively. The final stage is the weighted value modification stage. The expression of this stage is:

$$W_{xy}(n+1) = W_{xy}(n) + \Delta W_{xy}(n) = W_{xy}(n) + \eta \delta(n) \cdot o(n) \quad (23)$$

Here, ‘ η ’ represents the learning rate of the training. During neural network training, these three stages repeat. The entire procedure is usually concluded when the error function values reach either zero or any constant value indicating that the network is not benefiting from further training.

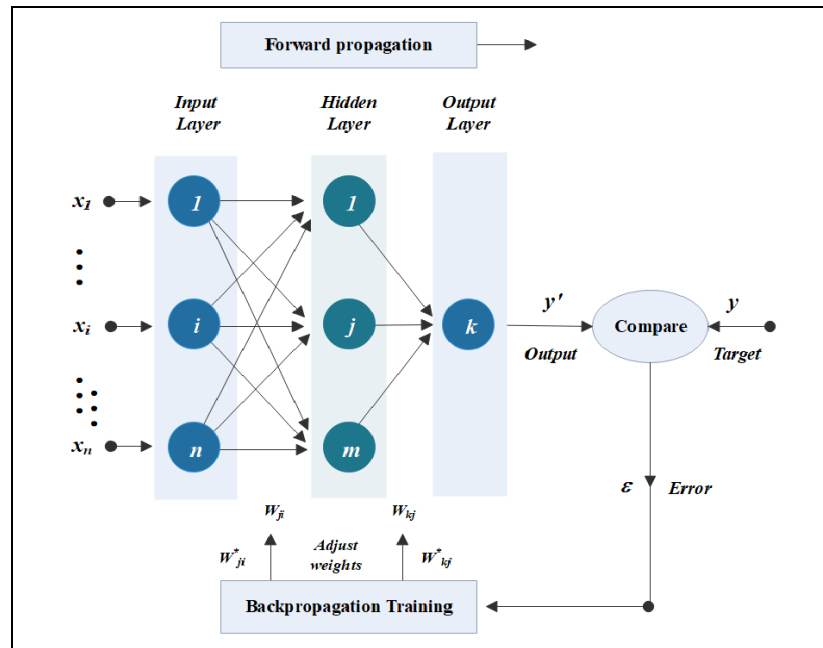


Figure 37: Three-layer feed-forward neural network

In this research, a 3-layered feedforward neural network with a backpropagation method was employed on the extracted features. The neural network implements several

input nodes, a single hidden layer with multiple neurons and an output layer for the prediction result. Figure 37 shows the basic structure of the neural network used in this study.

6.2.1. Comprehensive Evaluation of Major Clusters from PCC and PCA

In this section, the performance and effectiveness of the AI method (Artificial Neural Network) are investigated based on significant clusters of features extracted from the sensor signals (Section 5.4.1 and section 5.4.2). These clusters were obtained from the correlation analysis (Pearson correlation analysis) and PCA (Principal Component Analysis). Two types of clusters (Figure 38) from the correlation analysis and, three (3)- types from PCA were constructed (Figure 39) to use as the input dataset of the decision-making algorithm (AI techniques).

The clusters from each feature extraction method were used in the input dataset's (each dataset represented one machining cycle) of the Neural Network (NN). Each dataset consists of each machining cycle's cut five-channel signal (sensor set). The dataset's (a total of 884 datasets) was structured in such a way that 60% was assigned for training, 20% for testing and the remaining 20% to validate the model. Before training and testing, the input dataset was normalized to improve the training process. In addition, the dataset contained different machining parameters. Therefore, each training and testing process of the Neural Network (NN) algorithm contained three (3) machining parameters (cutting speed, feed, depth of cut) and the corresponding cluster of extracted features.

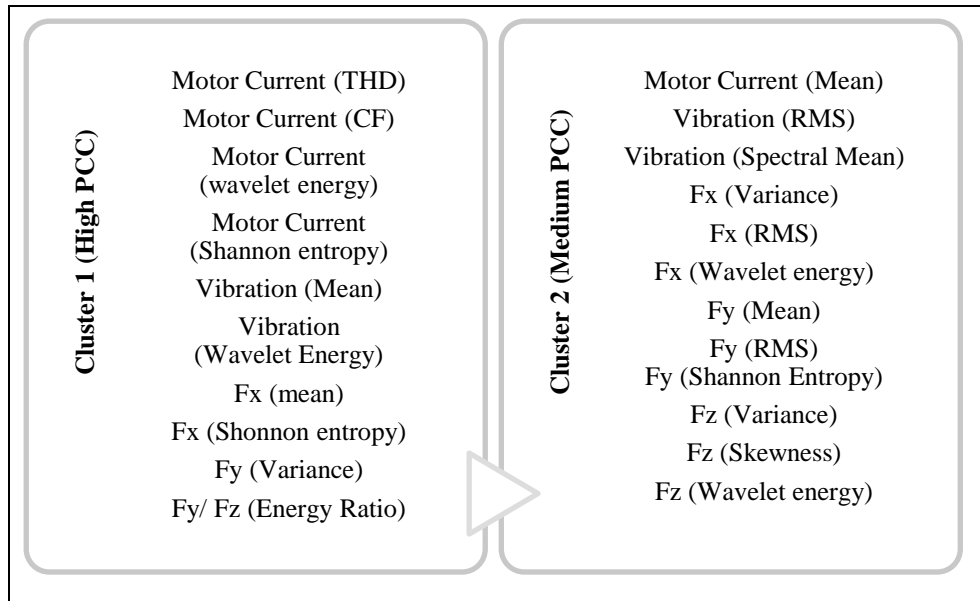


Figure 38: Major clusters from PCC analysis

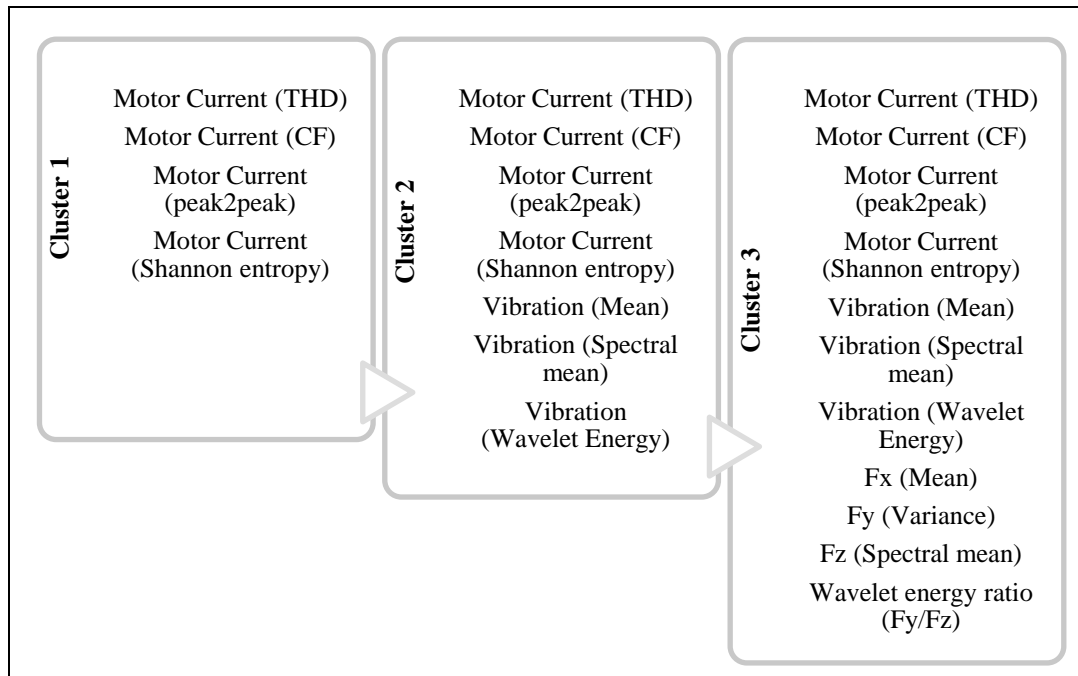


Figure 39: Major Clusters based on PCA

The comprehensive analysis was performed with a machine learning algorithm, the multi-layer perception based Neural Network (NN) in MATLAB©. Several characteristics played an important role in the investigation, such as the training algorithm, number of hidden layer nodes and corresponding clusters from the PCC analysis (Figure 38) and the PCA (Figure 39).

Training algorithm

To train the feed-forward neural networks, several machine learning training algorithms are available in MATLAB©. However, it is always difficult to identify which training algorithm is faster and will provide the best results for any given problem. This depends on many factors, such as input and output parameter, number of weights and biases, the error percentage and the objective of the training (pattern recognition or function optimization). Therefore, to identify the best training algorithm for this study, three types of machine learning training algorithms were employed, they are Levenberg-Marquardt (LM) [67], scaled conjugate gradient (SCG) [68] and gradient descent with momentum and adaptive learning rate backpropagation (GDX) [69].

The hidden layer node

Three different types of hidden layer node were also used, denoted as 10x, 15x, 20x number of nodes.

Statistics summary:

The effect of using the different machine learning algorithms and the hidden layer node number were considered as essential variables for the comparison analysis. The neural network success rate (NNSR%) determines the effectiveness of the model for data

prediction. Therefore, an overview of the NNSR% from the entire neural network model was presented in Figure 42. Extensive comparison analysis was conducted in this section based on the clusters from PCC (Figure 38) and PCA (Figure 39).

The objective of the analysis is to identify which machine learning algorithm and hidden layer node number provides a prediction model with the highest NNSR% and lowest RMSE (root mean squared error)- μm .

The Neural Network (NN) was trained with the cutting parameters (cutting speed, feed rate and depth of cut) and clusters 1 (Figure 38) and cluster 2 (Figure 38) from the PCC analysis, respectively.

- In all cases (different ML algorithm), cluster-1 from PCC analysis showed the higher NNSR (averaging 88.2%) and cluster-2 was observed to be lower (averaging 73.87%) (Figure 40)
- The effect of the hidden layer node number can be explained by Figure 41. In most cases, the 20x hidden layer node showed a promising rate of success. Though the higher hidden layer node number shows the highest level of NNSR%, the 10x hidden layer node number (LM algorithm) of cluster-1 reached the highest success rate (97.20 NNSR%). In general, cluster-1 of PCC based features showed a tremendous success rate in all types of hidden layer node numbers (Figure 42).

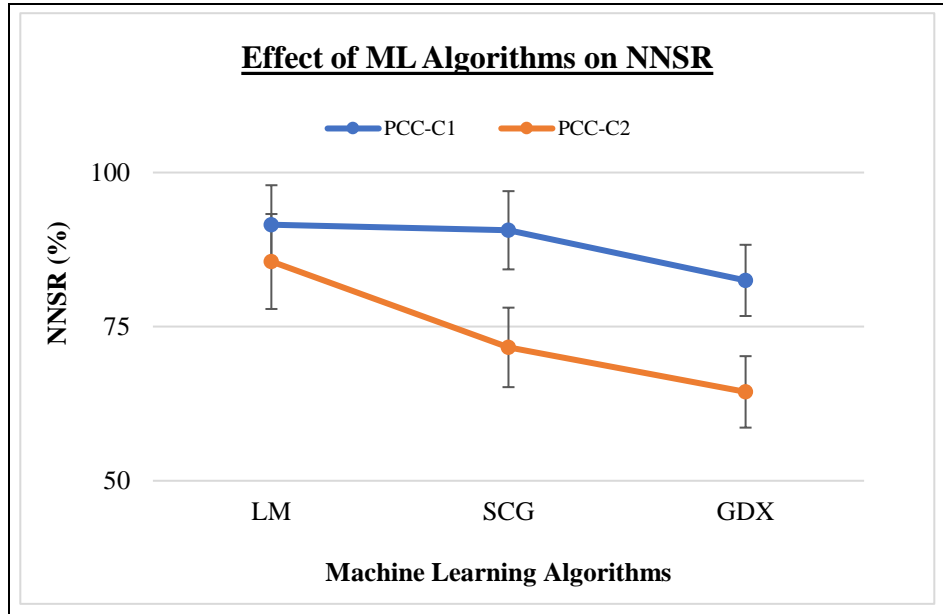


Figure 40: Effect of ML algorithms on the NN success rate

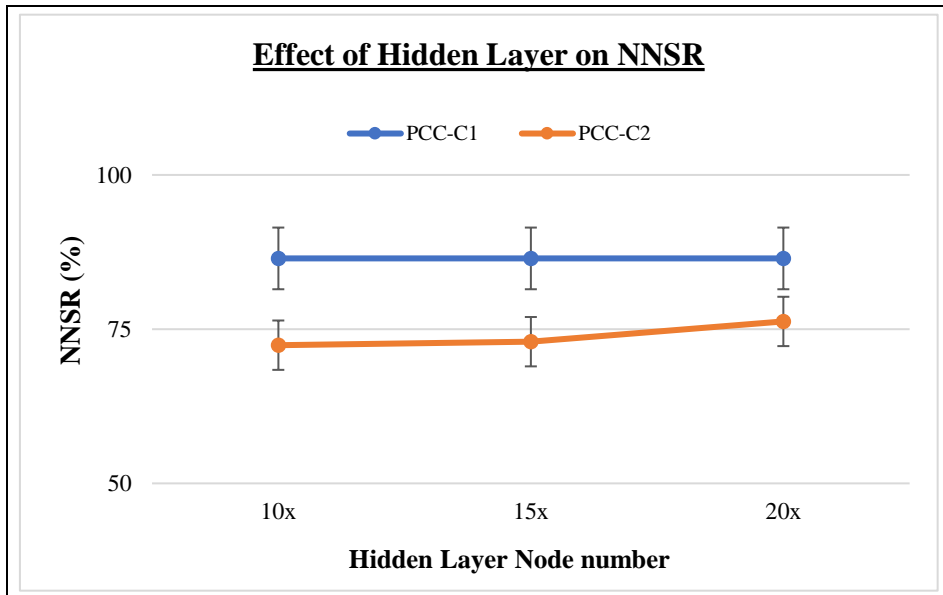


Figure 41: Effect of hidden layer node number on NN success rate

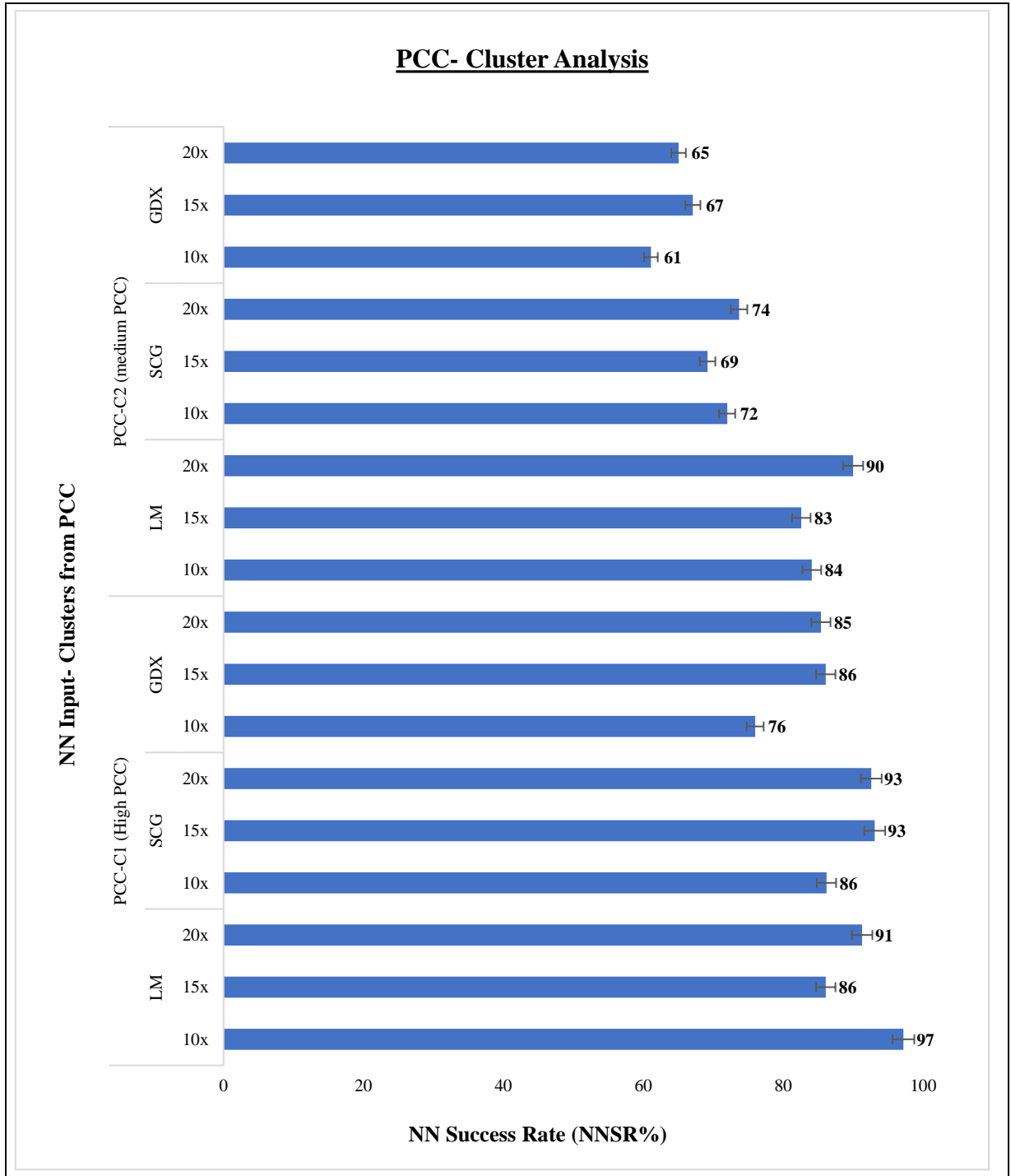


Figure 42: Evaluation of PCC based clusters in the Neural Network (NN)

To evaluate the PCA based clusters (Figure 39) used in the Neural Network (NN) training, a summary of NN modelling results (with NNSR%) is shown in Figure 44. In this study, the cutting parameters (cutting speed, feed rate and depth of cut) and cluster 1, cluster 2 and cluster 3 from the PCA analysis (Figure 39) were used as inputs for the NN model. The objective of this analysis was to monitor tool wear based on the clusters obtained from the PCA.

In most cases (ML algorithm and hidden layer nodes), the PCA cluster-2 showed the highest NN success rate (93.80% NNSR) (Figure 43). Cluster-2 from PCA is a combination of the features extracted from the spindle motor current sensor and the vibration sensor.

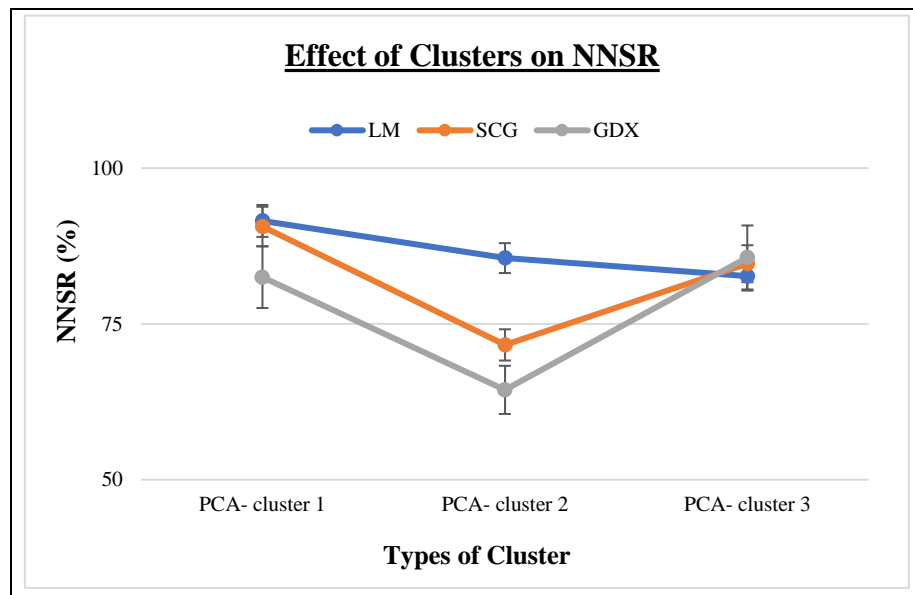


Figure 43: Effect of cluster type on NN success rate

- The GDX training algorithm showed the lowest success rate in the entire cluster analysis, whereas the SCG algorithm showed a consistent success rate (averaging

85.57% NNSR) under all types of PCA based cluster analysis in the neural network (NN) modelling (Figure 44).

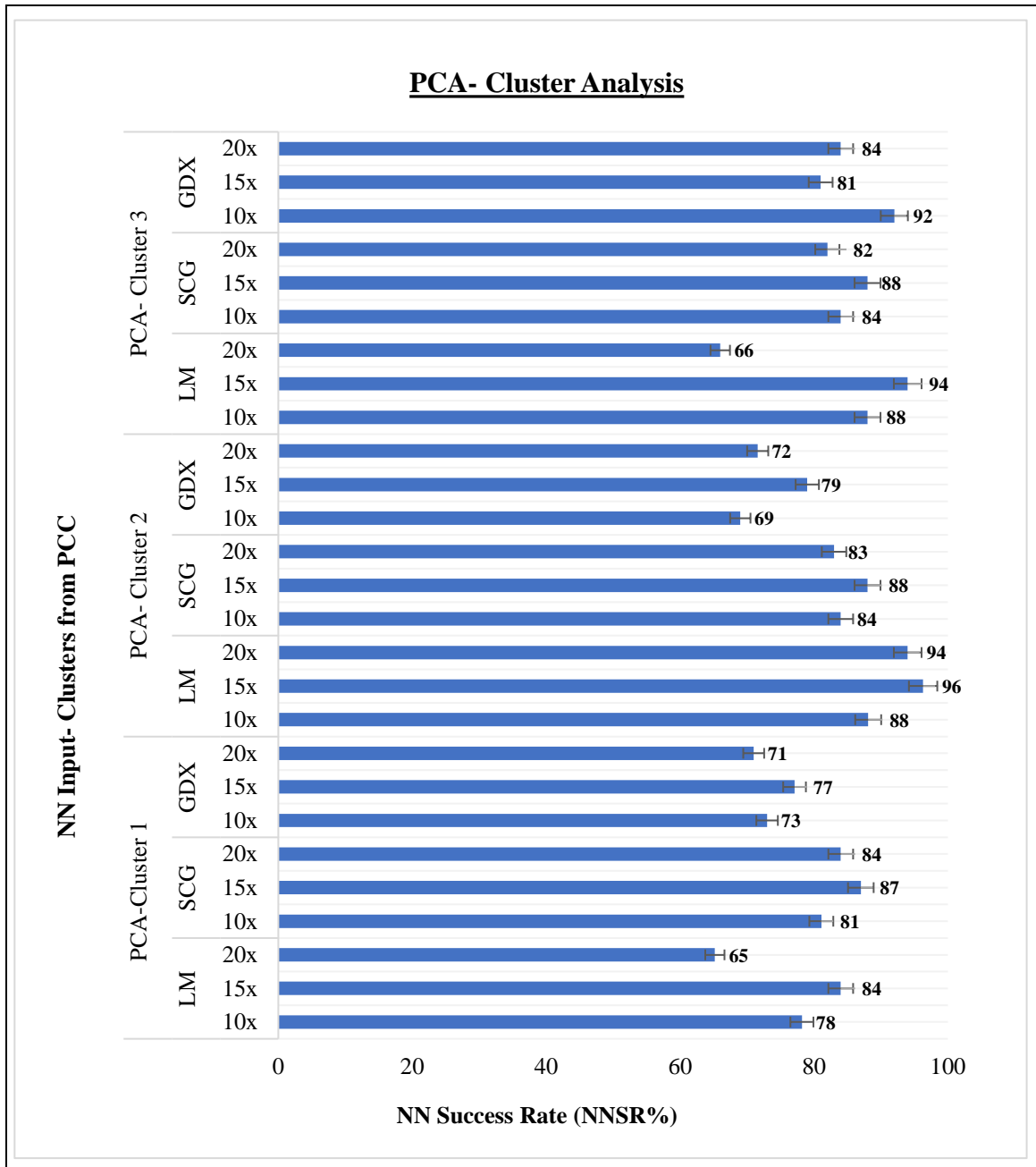


Figure 44: Evaluation of PCA based clusters in the Neural Network (NN)

- Cluster-1 attained the highest level of NNSR% in the (LM-10X) validation test (84% NNSR%). A neural network prediction model based on cluster-1 can provide a considerable amount of monitoring success. Therefore, a low-cost based spindle motor current sensor shows considerable potential for use in a tool wear monitoring system. However, system could be more successful under a cluster-2 based NN prediction model (Figure 44).
- Cluster-2 based NN validation results showed the highest level of success in comparison with Cluster-1 and Cluster-3. The LM training algorithm with 15x or 20x number of hidden layers was found to achieve the best success level (96.3% NNSR or 94.0% NNSR) (Figure 44).
- The RMSE (root-mean-square error) from the dataset validation was varied in all cases. Based on RMSE ($\sqrt{\frac{\sum_{i=1}^N (\text{Predicted}_i - \text{Experimental}_i)^2}{N}}$), cluster-1 (with LM based ML training algorithm) achieved the lowest level of error (RMSE= 1.43 μm) whereas, the PCA based cluster-1 had the highest level of error (RMSE= 11.1 μm) (Figure 45).
- In all cases, LM and SCG machine learning (ML) algorithms showed minimal RMSE compared with the GDX training algorithm (Figure 45).
- Based on RMSE analysis, PCC based cluster-1 input features and PCA based cluster-2 input features can be further studied during the model's implementation (Figure 45).

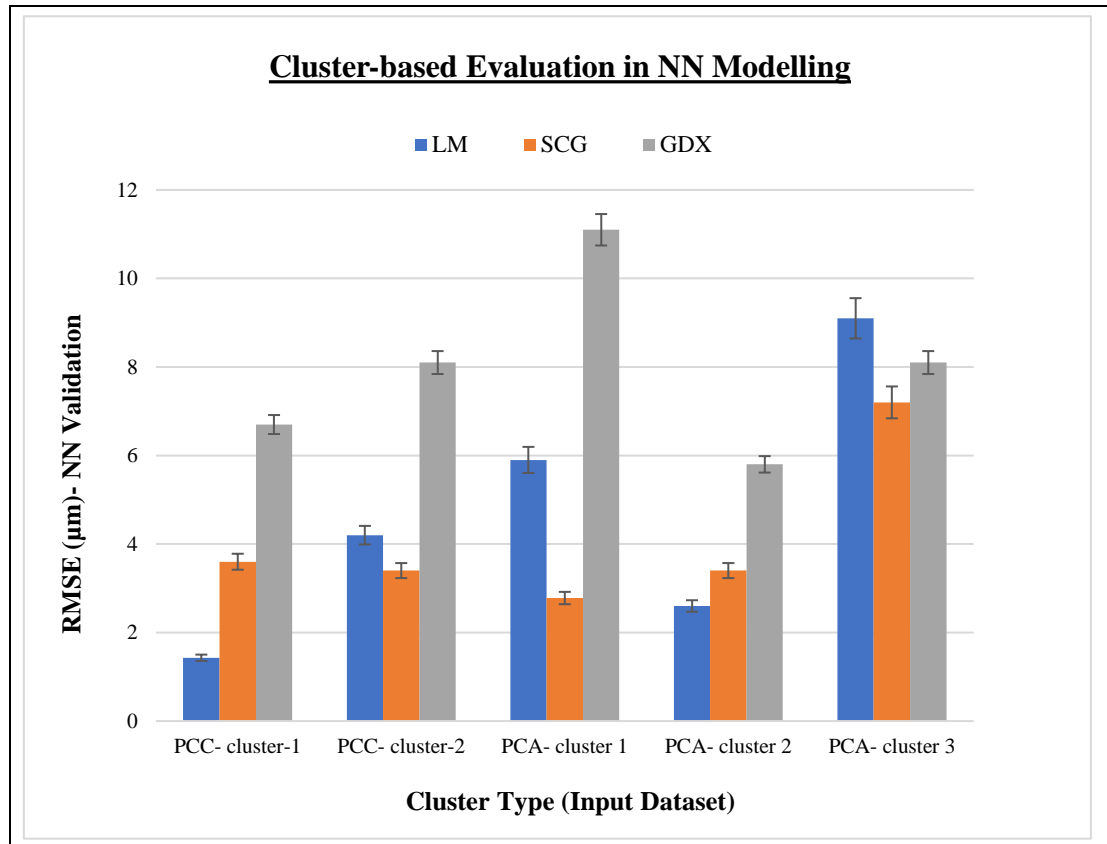


Figure 45: RMSE based evaluation of all cluster in NN modelling

6.3. Adaptive Neuro-Fuzzy Inference System (ANFIS)

ANFIS (Adaptive neuro-fuzzy inference system) is an artificial neural network-based ‘Takagi-Sugeno’ fuzzy inference system. It integrates the principles of ANN (artificial neural network) and fuzzy logic in a single frame. ANFIS prediction model use a ‘Sugeno’ FIS (Fuzzy Interface System) that presents knowledge from the dataset in an interpretable manner. The learning capability of the ANFIS model is derived from the use of a neural network in its structure. This learning capability can adjust the membership function parameters based on the trained input dataset. The objective of the ANFIS is to develop a

logical interpretation with membership functions and ANFIS rules based on the input dataset (trained and clustered) to predict the output variable.

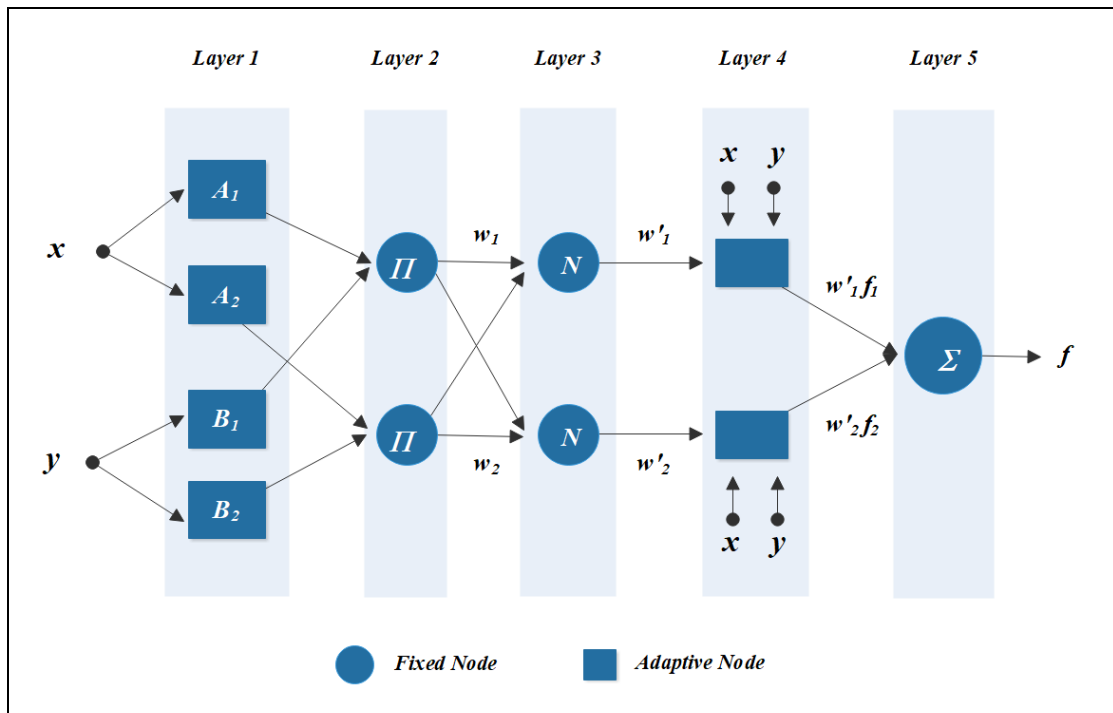


Figure 46: ANFIS architecture

The ANFIS architecture consists of several interconnected nodes that are characterised by fixed and adjustable parameters (Figure 46). The output signals from each layer are processed by the node functions. The ANFIS model processed by the node functions in each layer of the ANFIS architecture is explained below [70]:

Layer-1

The first layer's node consists of adaptive node functions. These nodes are typically used to fuzzify the inputs, 'x' and 'y', into the corresponding fuzzy linguistic values (small,

medium or high) using fuzzy membership functions (MFs). The fuzzified output from the 1st layer can be expressed by Equation (24).

$$O_i^1 = \mu A_i(x) ; \text{ where, } i=1, 2. \quad (24)$$

Where, $\mu A_i(x)$ defines the membership functions of the corresponding linguistic values for the first input. Each MF has parameters which depend on their respective curves (triangular, trapezoidal, bell-shaped, Gaussian or sigmoid).

Layer-2

In this layer, the fixed node function provides strength for the output signal rules by multiplying each of the input signals from the first layer with one another. The output signal rules, O_i^2 are expressed in Equation (25).

$$O_i^2 = \omega_i = \mu A_i(x) \times \mu B_i(y) ; \text{ where, } i=1, 2. \quad (25)$$

Here, ω_i is the output signal from the 2nd layer and $\mu B_i(y)$ are the corresponding MF's linguistic values for the second input.

Layer-3

The third layer calculates the normalized strength of the fuzzy rules, $\bar{\omega}_i$ which is obtained from the previous layer (2nd layer). This can be calculated as:

$$\bar{\omega}_i = \omega_i / \sum_{i=1}^n \omega_i ; \text{ where, } i=1,2. \quad (26)$$

Layer-4

In this layer, the defuzzification process is performed to solve the overall weighted output, $\overline{\omega}_i f_i$ using the normalized firing strength, $\overline{\omega}_i$. The defuzzification is accomplished through Equation (27).

$$\overline{\omega}_i f_i = \overline{\omega}_i (p_i x + q_i y + r_i) \quad ; \text{ where, } i=1,2. \quad (27)$$

Layer-5

The sum of all weighted signals from the 4th layer is used to calculate the overall output 'f' in the 5th layer, which is given by Equation (28).

$$\begin{aligned} f &= \overline{\omega}_1 f_1 + \overline{\omega}_2 f_2 \\ &= (\overline{\omega}_1 x) p_1 + (\overline{\omega}_1 y) q_1 + (\overline{\omega}_1) r_1 + (\overline{\omega}_2 x) p_2 + (\overline{\omega}_2 y) q_2 + (\overline{\omega}_2) r_2 \end{aligned} \quad (28)$$

Where, f_1 and f_2 are Takagi–Sugeno first order linear functions and p_1, q_1, p_2, q_2 are the linear coefficients of those functions. The network implements the first order Sugeno type fuzzy reasoning for learning and fine tuning. The first order Takagi–Sugeno fuzzy rules are shown in the Equation (29) and Equation (30).

$$R_1: \text{ IF } x \text{ is } A_1 \text{ AND } y \text{ is } B_1 \text{ THEN } z \text{ is } f_1(x, y); \quad (29)$$

$$\text{where, } f_1 = (p_1 x + q_1 y + r_1)$$

$$R_2: \text{ IF } x \text{ is } A_2 \text{ AND } y \text{ is } B_2 \text{ THEN } z \text{ is } f_2(x, y); \quad (30)$$

$$\text{Where, } f_2 = (p_2 x + q_2 y + r_2)$$

Where x and y are two inputs, R_i and f_i are the fuzzy rule base and the corresponding output. Meanwhile, A_1, A_2, B_1, B_2 are the linear or nonlinear parameters or fuzzy sets of

the MFs. These parameters are typically represented in terms of linguistic variables (words) of SMALL, MEDIUM or HIGH based on the selected MFs curves. Finally, p_1 , p_2 , q_1 , q_2 , r_1 and r_2 are linear coefficients of the Takagi–Sugeno first order models, f_1 and f_2 Figure 47 presents the flowchart of ANFIS modelling.

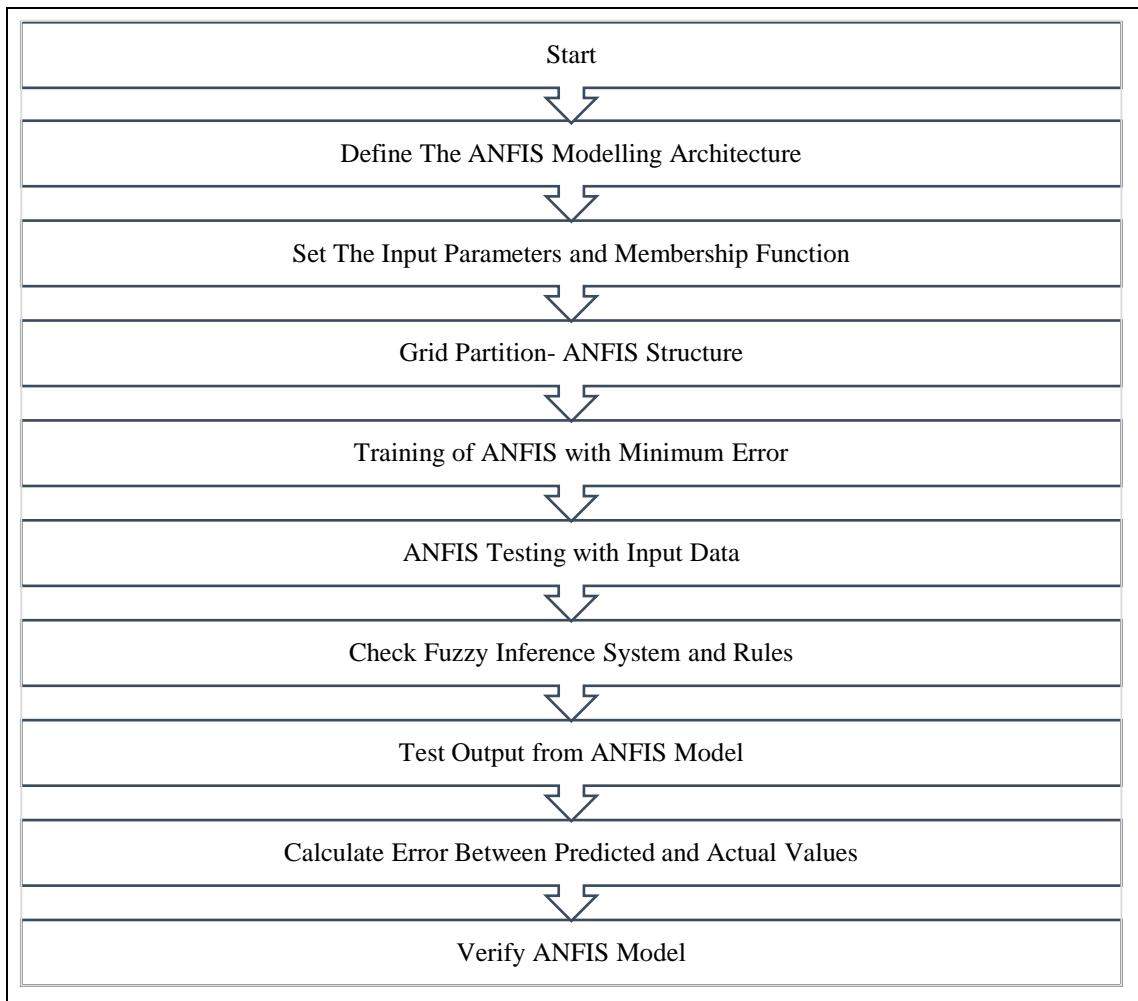


Figure 47: Flowchart of ANFIS modelling

In this study, MATLAB© software was used to develop the ANFIS model. The graphical user interface (GUI) of ANFIS in the software were used for training and testing

the experimental dataset from the turning test. Due to multivariate nature of the experimental data, 'gaussmf' was selected as the input membership function and a constant membership function was selected for the output data. The ANFIS model used a hybrid learning method to update the parameters of input & output data. The sub-clustering method (anfis2) was adopted instead of the grid-partition method (anfis1) due to the higher dimension clustering issues of the dataset during the training. The training process was continued until it reached the desired minimum RMSE output. Figure 48(a) represents the membership function (gaussmf) viewer of the input dataset and Figure 48(b) is the rule viewer of the ANFIS interface in MATLAB®.

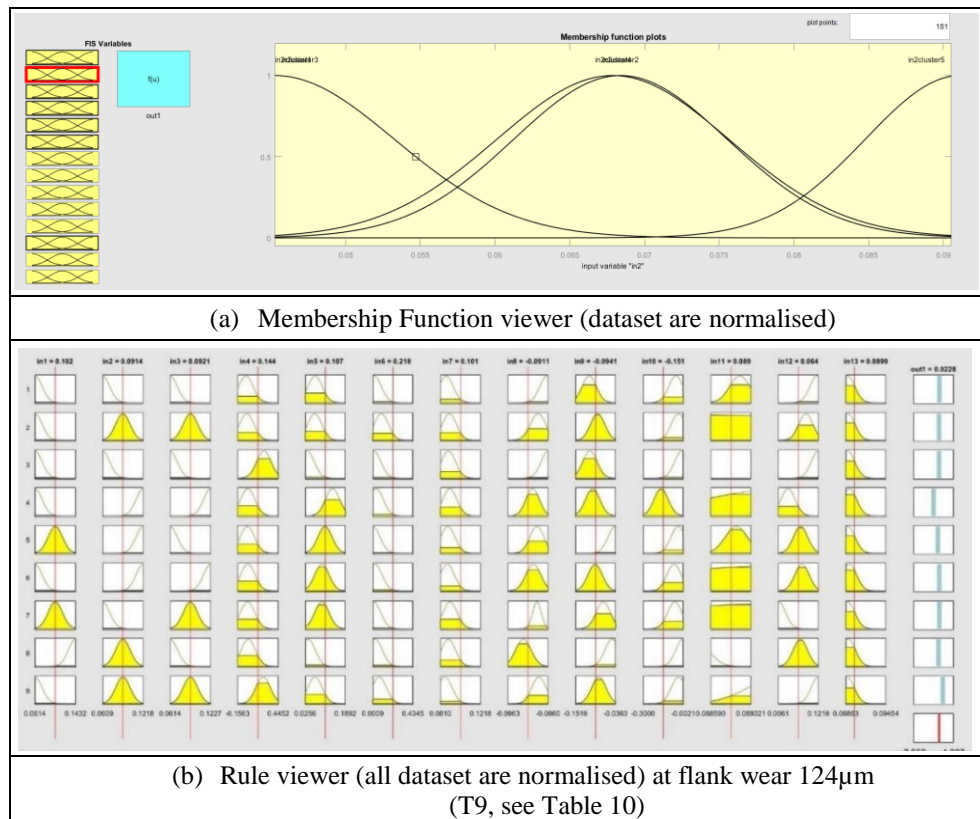


Figure 48: A general overview of the ANFIS interface

Table 16 shows the general overview of the ANFIS learning structure (based on all datasets)

Table 16: ANFIS Learning Structure

Maximum Number of nodes	456
Number of linear parameters	84
Maximum number of nonlinear parameters	156
Maximum number of parameters	240
Number of training data pairs	242
Number of fuzzy rules	84

6.3.1. Comprehensive Evaluation of Major Clusters from PCC and PCA

This section demonstrates the performance and effectiveness of the AI method (Adaptive Neuro-Fuzzy Inference System) based on the significant extracted feature clusters (Figure 38 and Figure 39) from the fusion of the sensor signal (section 5.4.1 and section 5.4.2).

During ANFIS training, the input dataset was consisted of feature cluster's (PCC or PCA) and the cutting condition (cutting speed, feed rate, depth of cut) and the predicted output (tool wear value) was compared with the actual test result's (offline results). In this

analysis, RMSE (root mean squared error) was used to account for training and validation error.

Figure 49 (a) shows that the ANFIS prediction error (RMSE) is $0.018 \mu\text{m}$ while cluster-1 of PCC (see Figure 38) based sensor features were used as an input variable. However, cluster-3 from PCA (Figure 39) based sensor features increased the error (RMSE= $0.20 \mu\text{m}$) of ANFIS prediction (Figure 49 (b)). In Figure 49, ‘index’ refers to the number of cuts (each machining pass during the turning operation).

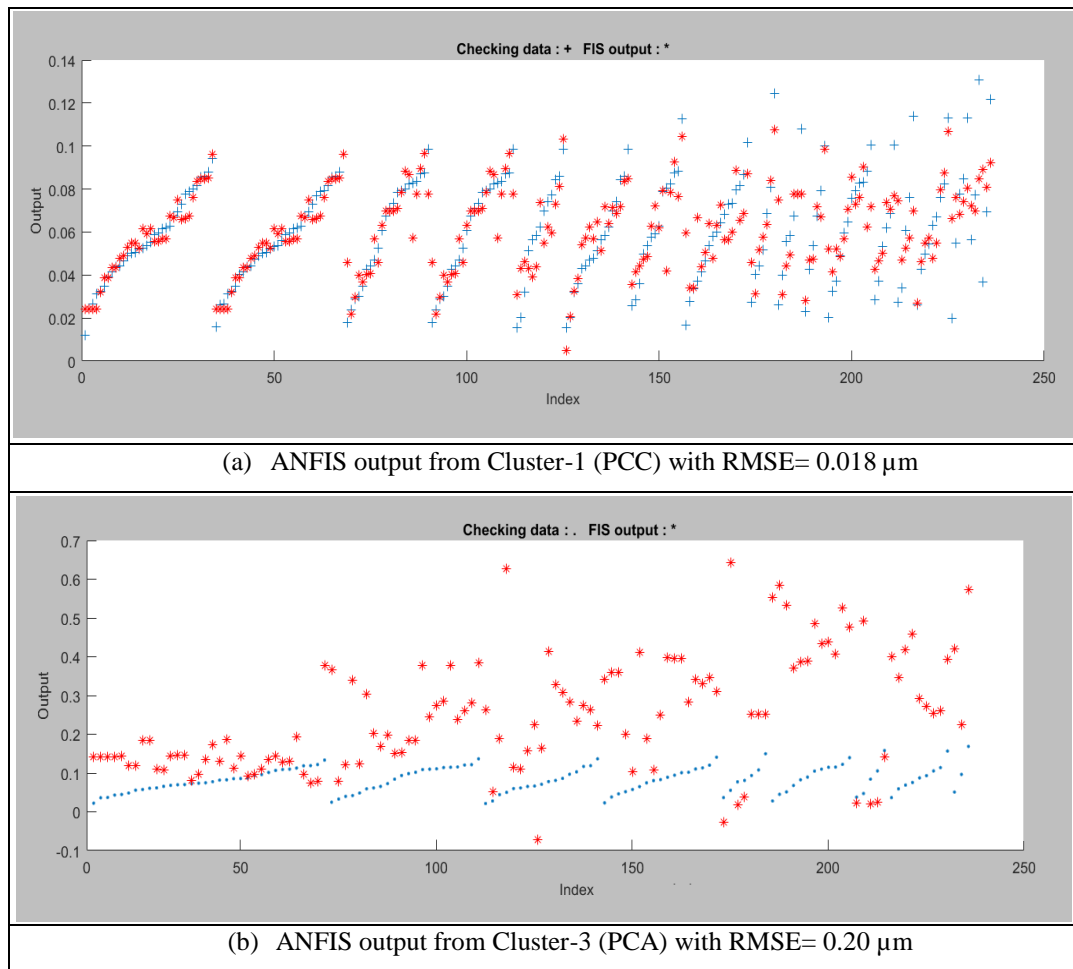


Figure 49: ANFIS validation results with RMSE

Though, PCC based cluster-3 features combines the features from all the sensors (sensor fusion), it shows higher prediction error. The reason for this discrepancy can be explained based on the PCC (Pearson correlation coefficient) analysis (see Table 14). Few features (especially from the Force channels) showed less sensitivity with the tool wear progression. Therefore, it results in higher prediction error when the PCA based cluster-3 were taken as input variable in ANFIS modelling. The ANFIS model was evaluated based on the structure provided depicted in Table 17.

Table 17: ANFIS structure Information

	Cluster Type				
ANFIS Parameter Type	PCC cluster-1	PCC cluster-2	PCA cluster-1	PCA cluster-2	PCA cluster-3
Number of input (with machining parameters)	14	16	7	10	14
Number of membership functions	9	7	9	6	5
Membership functions type	Gaussian Curve				
Fuzzy clustering type	Sub. Clustering (anfis2)				
Squash factor	0.15				
Epoch number	50				
Number of Fuzzy Rules	84				
RMSE (μm)	0.011	0.032	0.017	0.45	0.219

The model showed significant performance variations based on several factors, such as data sample, membership functions type and number. These factors play an essential role in evaluating the training and testing dataset that correlates the input membership functions with the output value.

The evaluation results of PCC and PCA cluster based ANFIS training and validation (RMSE) is presented in Figure 50. The purpose of this analysis is to represent the sensor fusion application in tool wear monitoring based on the input features (with cutting parameters) of different cluster type (Figure 38 and Figure 39) obtained from PCC analysis and PCA.

The input features obtained from PCC analysis (Figure 38) showed excellent results compared to PCA based features and (Figure 39) in ANFIS modelling. The average RMSE value (RMSE =0.02 μm) of PCC based features is significantly less in comparison with the average RMSE (Avg. RMSE= 0.23 μm) of PCA based features (Figure 50).

Cluster-1 and cluster-2 inputs from PCC based features (Figure 38) showed promising RMSE value. Cluster-1 (high correlations-based features) showed lowest RMSE (RMSE=0.0108 μm). Just as in NN modelling, the cluster-1 dataset from PCC analysis predominantly influences the ANFIS prediction model (Figure 50).

Cluster-1 input dataset from PCA (Figure 39) shows promising results compared to other PCA clusters. The features from this cluster (cluster-1 from PCA) were obtained only from the spindle current sensor and it shows a promising impact in ANFIS prediction.

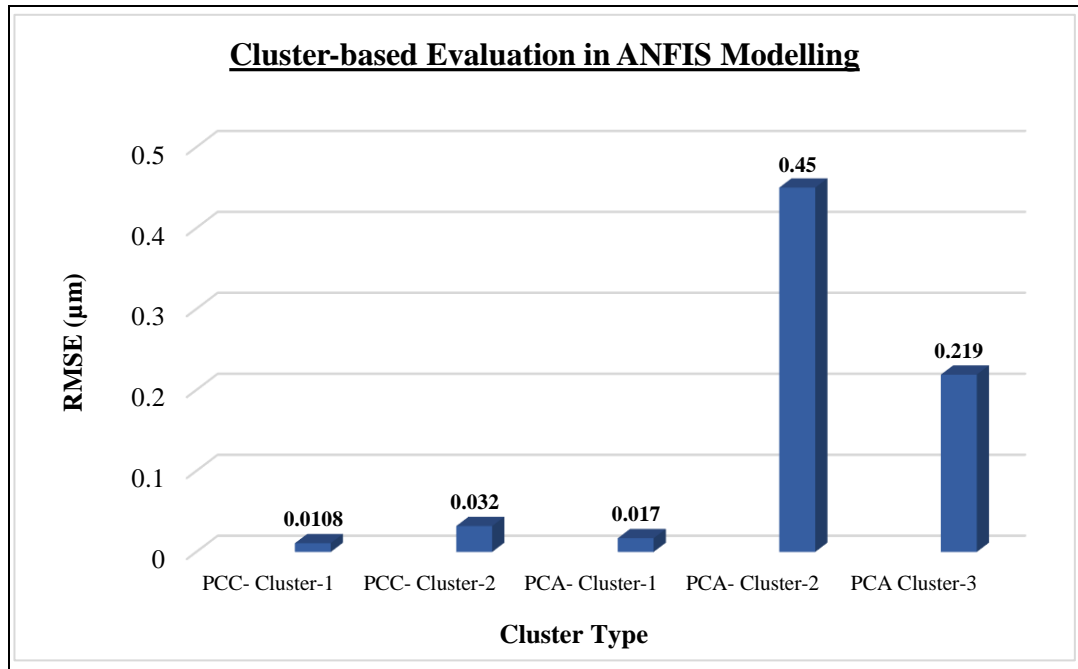


Figure 50: Evaluation of PCC and PCA based cluster on ANFIS modelling

6.4. Comparison between AI Techniques for TCM

A comparison of AI techniques presented in section 6.2 and section 6.3 is given in this section of the chapter. The purpose of this section is to obtain an AI-based data-driven tool-wear prediction model which can best predict the output result with minimum RMSE and maximum success rate (SR%). Two separate AI prediction models were developed based on the cutting test datasets. Figure 51 provides a comparison of AI techniques used in this research. This comparison draws from the entire cluster-based input dataset in these models. This input dataset also contains the machining conditions (cutting speed, feed rate and depth of cut).

Results reveal that the ANFIS model outperforms other artificial neural network-based prediction models. The ANFIS model with PCC based cluster-1 input features (Figure 38) showed the best overall result (RMSE= 0.013 μm). It should be noted that most of the PCC based cluster-1 features are from the motor current & vibration signal (Figure 38). As was shown earlier (section 5.4.1), most of the features from the spindle motor current sensor signal (i.e. THD, crest factor, mean) exhibit a strong correlation with the output result (tool wear). Moreover, PCA based cluster-1 which only consist of features from the spindle motor current sensor, also shows promising results (RMSE= 0.17 μm). The maximum RMSE (RMSE= 0.45 μm) ANFIS model was obtained with PCA cluster-2 input features (Figure 39).

Out of all ANN based prediction models, the PCA cluster-2 (Figure 39) input features showed the minimum error (RMSE= 2.46 μm). This cluster was constructed with the features obtained from the current and vibration sensors. The overall error in the ANN-based prediction model was comparatively higher than in the ANFIS model. Although the LM training algorithm-based ANN model showed the minimum RMSE (RMSE= 1.43 μm), whereas other ANN models were not as reliable (Figure 51).

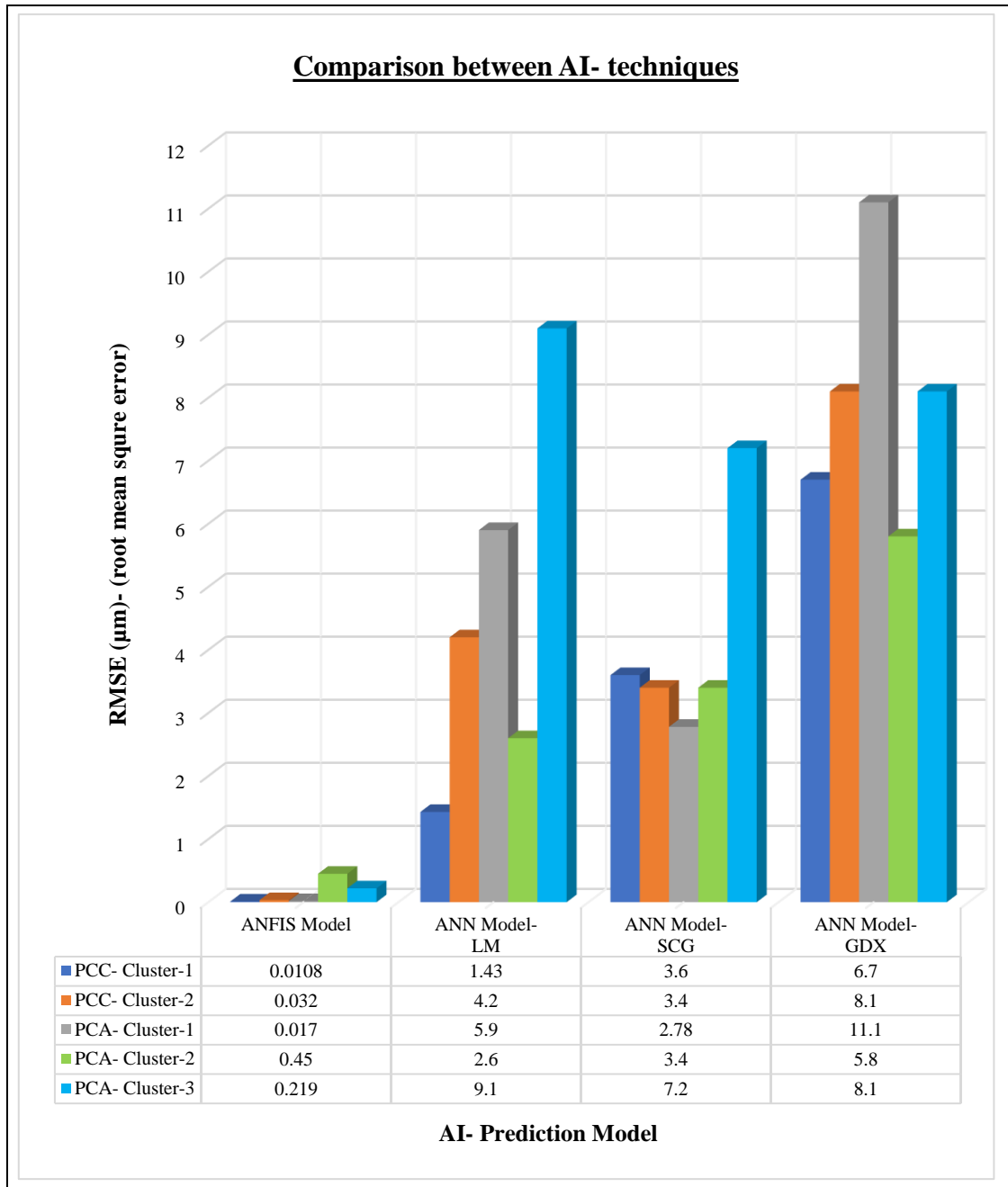


Figure 51: Comparison among AI based prediction model

Chapter 7. Implementation of the Developed TCM System

7.1. Introduction

In this study, an Artificial Intelligence (AI) based tool wear diagnosis and prognosis system was developed based on sensor fusion signal and indirect measurement of cutting tool wear (flank wear) during a turning operation. The experimental methodology of this research was carried out by a series of semi-finish turning and final-finish turning operations of AISI 4340 steel, along with online measurement of sensor fusion signals. Further expansion of this research was carried out on other material machining processes using a successful AI technique-based decision-making system. This chapter validates and implements the developed data-driven TCM system for other applications (different workpiece materials and cutting tools).

7.2. Implementation Methodology of the TCM System

To expand the developed TCM system, it is necessary to implement and validate it for different applications, cutting conditions and workpiece materials. Several factors were considered for implementing the TCM system, which reflects the main objectives and industrial applications of this research.

- A low-cost tool wear monitoring system.
- A supervised (previously trained system) AI-technique based tool wear monitoring system for different cutting tool material.

- A supervised (previously trained system) AI-technique based tool wear monitoring system for different workpiece material.

Therefore, the experimental design for the implementation test takes considered all these factors. The same experiment setup, machine tools and cutting tool holder (Kennametal© DCLNL 16 4D) was used for the designed system (Figure 52). Only the workpiece and cutting tool materials were different. In this chapter, the implementation test is listed as case study-1 and case study-2 (Table 18). The experiment details of the implementation and validation test are depicted in Table 18.

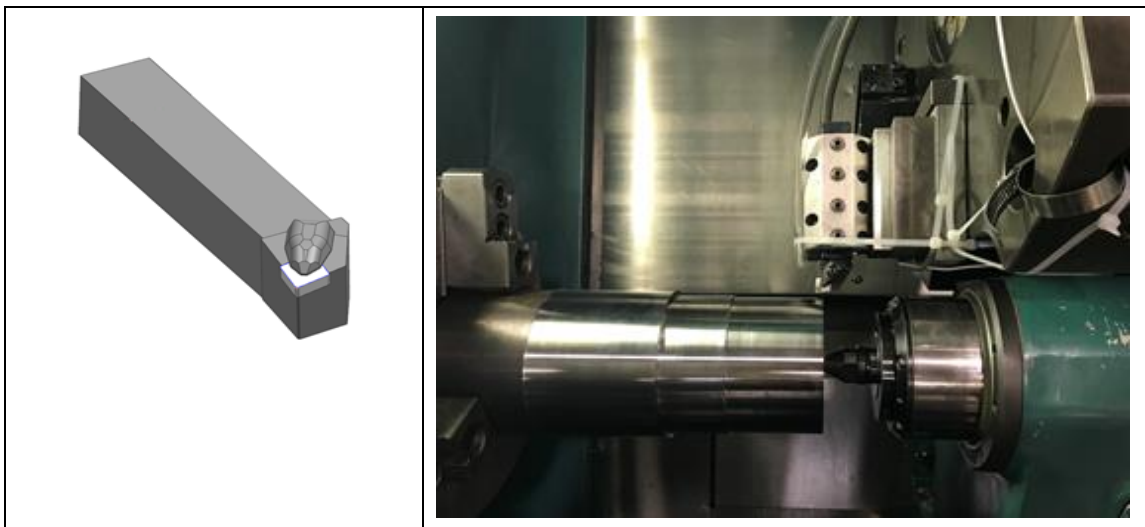


Figure 52: Experiment setup for validation (including tool holder)

Table 18: Experiment details for the TCM system implementation

Experiment Details	Case Study-1	Case Study-2
Workpiece Material	ASTM A536 Ductile Iron (24 ± 1.0 HRC)	AISI D2 Steel (46 ± 1.0 HRC)
Cutting Tool	CBN (Cubic Boron Nitride)	Pure Alumina (CC620)
Cutting Speed, V_c	250 m/min	120 m/min
Feed Rate, f	0.15 mm/rev	0.10 mm/rev
Depth of Cut, doc	0.25 mm	0.50 mm
Cutting Condition	Wet	Dry

Figure 53 flowchart shows the procedure of the developed TCM system implementation in both case scenario's (study-1 and study-2).

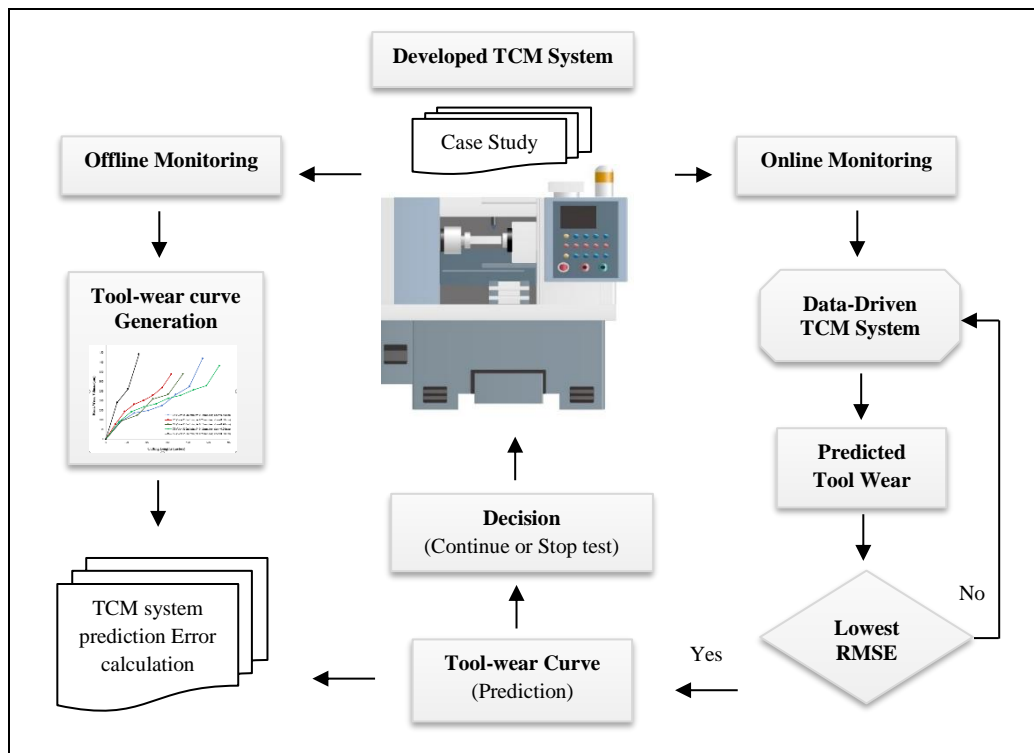


Figure 53: TCM system implementation flowchart

7.3. TCM System for Different Workpiece Material

In this section of the chapter, the data-driven AI based TCM system is implemented in two different case scenarios. Each test was carried out according to the flowchart shown in Figure 53. The first stage of each study was to extract the online monitoring dataset from the sensor fusion signal. These datasets represent the conditions of the cutting tool (flank wear). While analyzing the online signals from the sensors, the input features (Figure 38 and Figure 39) was selected based on the PCC result from section 5.4.1 and PCA result from the section 5.4.2. The input cluster (PCC-based cluster-1 and (PCA based cluster-1) was extracted to be feed into the data-driven TCM system to predict the output of each cut (one-pass in turning test).

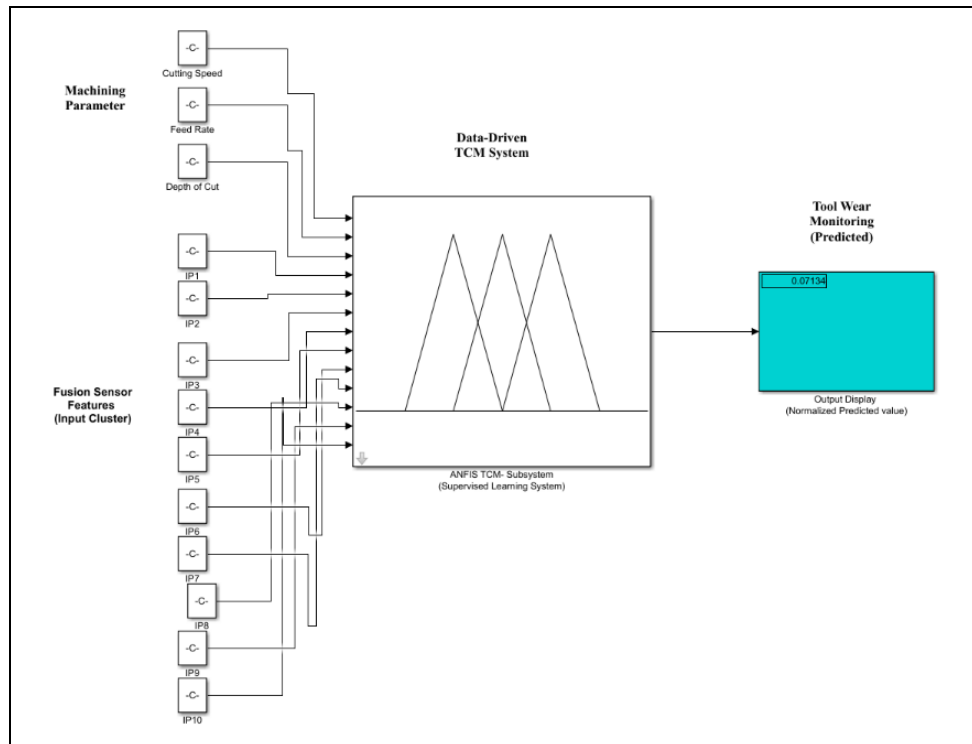


Figure 54: The architecture of the data-driven TCM system

Finally, the predicted data (flank wear value) given by the supervised data-driven ANFIS model were compared with offline monitoring results (flank wear value) through optical microscopy. Figure 54 shows the basic overview of the implementation procedure of the developed ANFIS- TCM system (in MATLAB© 2017) used for tool wear prediction (PCC based cluster-1 input features).

7.3.1. Case Study- 1

This case study's objective was to investigate the implementation of the data-driven AI based TCM system in the wet turning of ductile cast iron with a CBN tool. According to the industrial requirement, the cutting operation was semi-finish turning where the tool life was quantified as the number of cuts (total pass) accumulated when the maximum flank wear reaches 200 μm .

The input features were the PCC based cluster-1 (Figure 38), PCA based cluster1 features (Figure 39) obtained from the real-time sensor fusion signal and the cutting parameters (cutting speed, feed rate, depth of cut). The output values (predicted flank wear) were obtained from the data-driven TCM system (Figure 54) and compared with the offline monitoring dataset (flank wear values from optical microscopy) (Figure 55 and Figure 56).

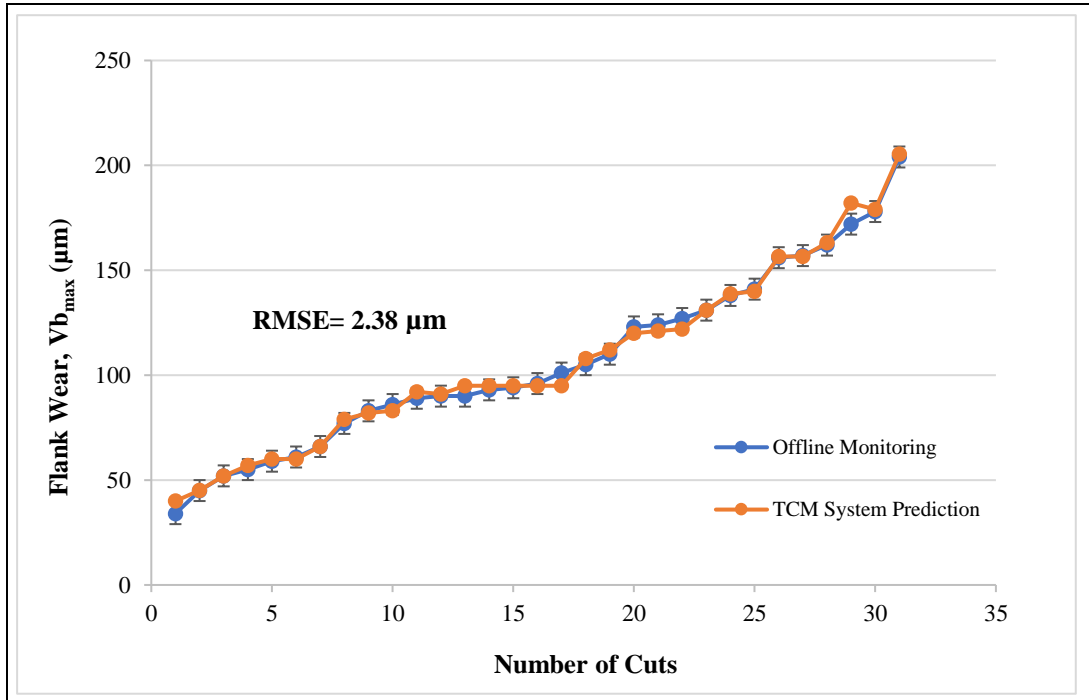


Figure 55: Prediction comparison of the TCM system (PCC-cluster-1 based)

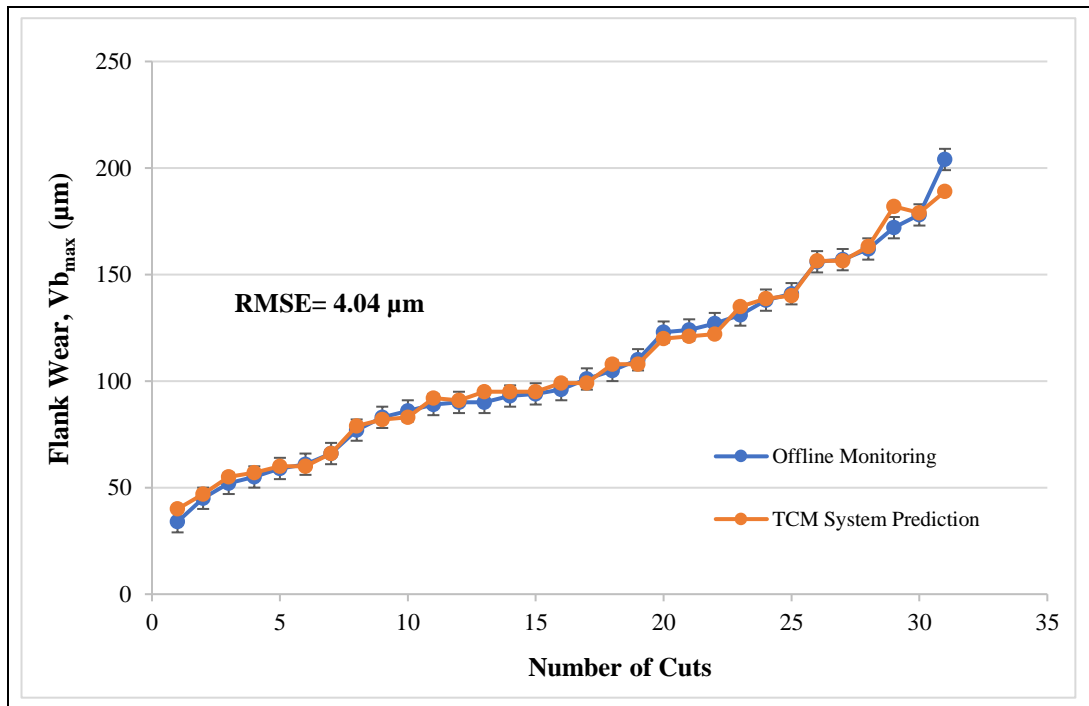


Figure 56: Prediction comparison of the TCM system (PCA-cluster-1 based)

7.3.2. Case Study- 2

The second case study was to investigate the implementation of the data-driven AI based TCM system in hard turning of AISI D2 steel with a pure alumina ceramic tool (cc620). In this experiment, the cutting tool life was quantified as the accumulated number of cut (total pass) upon reaching the maximum flank wear of 300 μm (tool failure). PCC based cluster-1 (Figure 38), PCA based cluster-1 features (Figure 39)) from the real-time sensor fusion signal and the cutting parameters (cutting speed, feed rate, depth of cut). The output values (predicted flank wear) were obtained from the data-drive TCM system (Figure 54) and compared with the dataset of offline monitoring (Figure 57 and Figure 58).

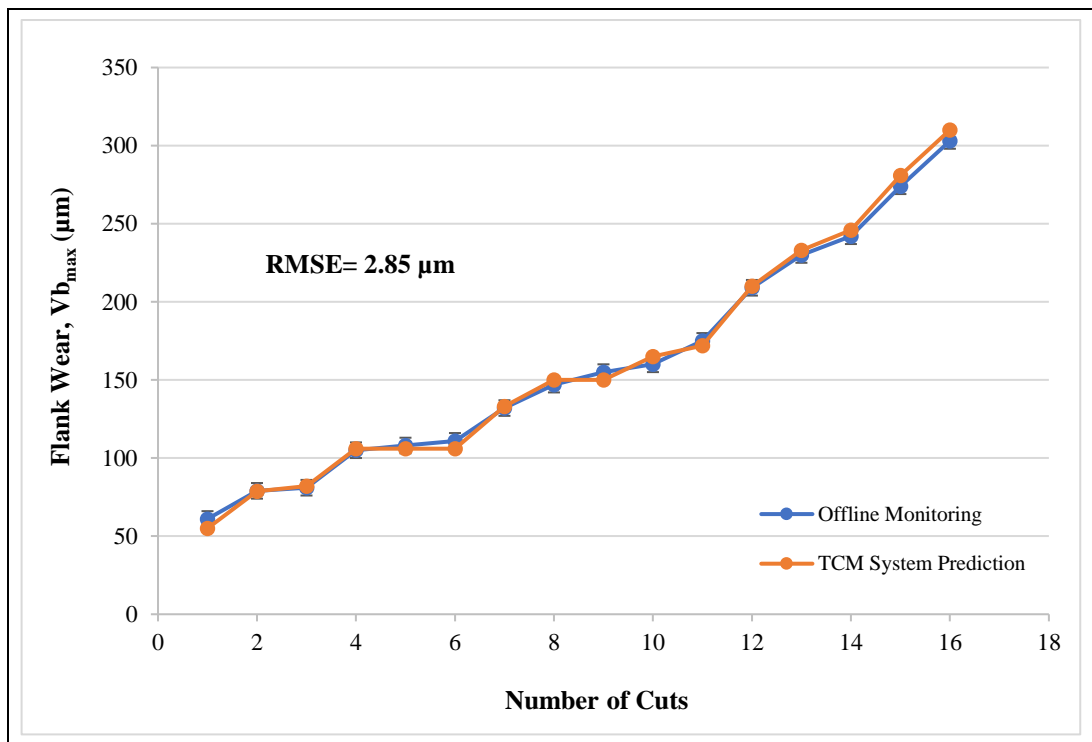


Figure 57: Prediction comparison of the TCM system (PCC-cluster-1 based)

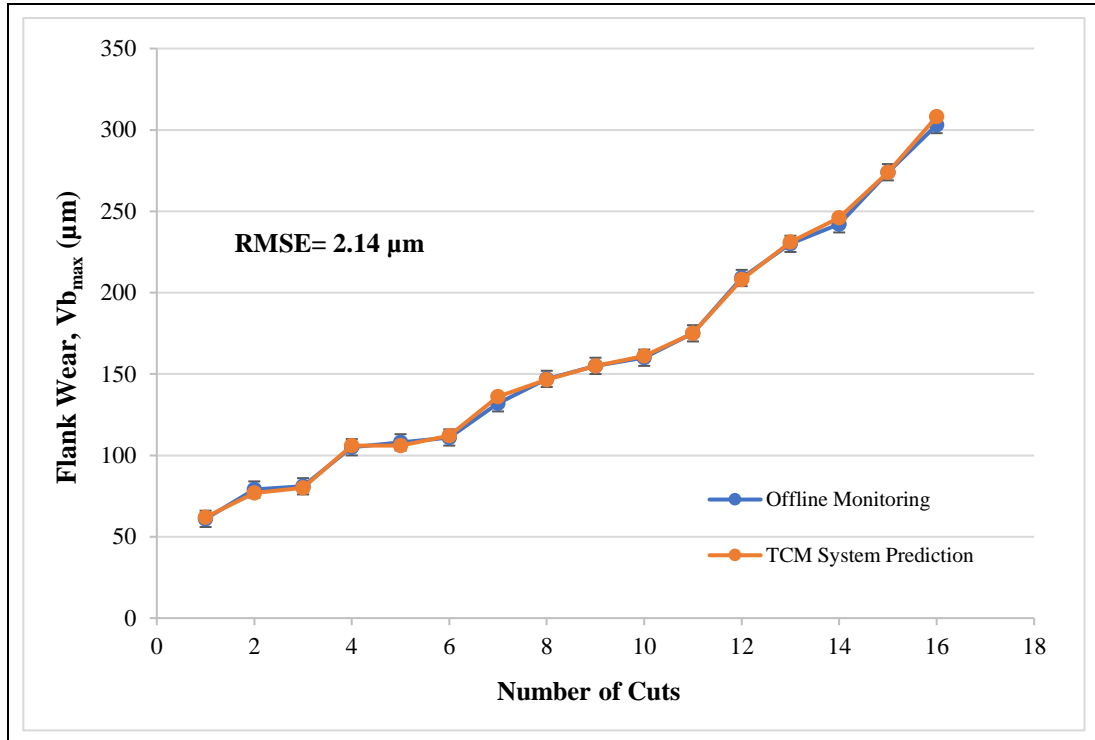


Figure 58: Prediction comparison of the TCM system (PCA-cluster-1 based)

7.3.3. Discussion

The data-driven AI technique based TCM system was implemented in two different case studies. In both cases, the developed TCM system’s implementation and procedure were the same. Also, predicted values of tool wear (flank wear) were compared with the offline monitoring data, and the error was calculated for comparative analysis.

In case study-1, Figure 55 and Figure 56 compare the predicted and offline data for PCC cluster-1 (Figure 38) and PCA cluster-1 (Figure 39) respectively. PCC based cluster-2 features being fed into the data-driven TCM system showed greater accuracy (RMSE of $2.38 \mu\text{m}$).

In case study-2, the developed TCM system was more successful than in case study-1. In each case, the RMSE value showed that promising results could be achieved using both types of clusters (Figure 57 and Figure 58).

Table 19 summarizes the offline monitoring results from the different case studies. The offline monitoring result shows that the wear progression is aggressive in case study-2 compared to the wear progression in case study-1. It should be noted that the hardness of the workpiece material (46 ± 1.0 HRC) of the case study-2 was close to the hardness of the workpiece material (50 ± 1.0 HRC) which were used to design and develop the TCM system.

Table 19: Summary of the offline monitoring results

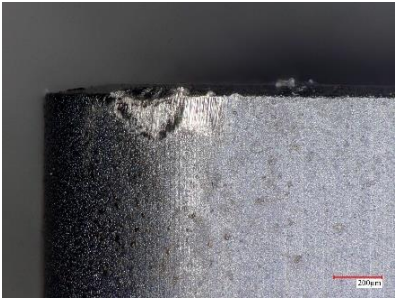

	Case Study-1	Case Study-2
Cutting Conditions	$V_c = 250$ m/min; $f = 0.15$ mm/rev; doc= 0.25 mm	$V_c = 120$ m/min; $f = 0.10$ mm/rev; doc= 0.5 mm
Offline Monitoring (From Optical Microscopy)		
Flank Wear	CBN Cutting Tool (Flank wear, $VB_{max} = 204$ μ m)	Pure Alumina Ceramic (cc620) Flank wear, $VB_{max} = 303$ μ m
End of Case Study	Total cut numbers= 31	Total cut numbers= 16

Figure 59 summarizes the comparison between these studies. In case study-2, the TCM system accuracy (prediction of tool wear) is higher than in study-1. The RMSE values

indicate the implementation accuracy of the system. Cluster-1 (PCC) based features (Figure 39) are sourced from the spindle motor current and the vibration sensor, which showed a promising result while the TCM system was implemented in study-2 (lowest RMSE). It's worth remarking that the maximum features from Cluster-1 (PCC) came from the current sensor and vibration sensor. Therefore, combination of the motor current sensor and vibration sensor can play a important role (low cost-based) in tool wear monitoring of different workpiece material during machining. Furthermore, PCA cluster-1 features are obtained from the current sensor only which also showed promising result in study 2. Further adaptability of the developed TCM system can reduce the prediction error in this case.

The overall accuracy of the developed system under different workpiece material turning operations means that it can play a promising role in industrial applications. Ideally, it can become a standard TCM system for turning operation of different workpiece materials.

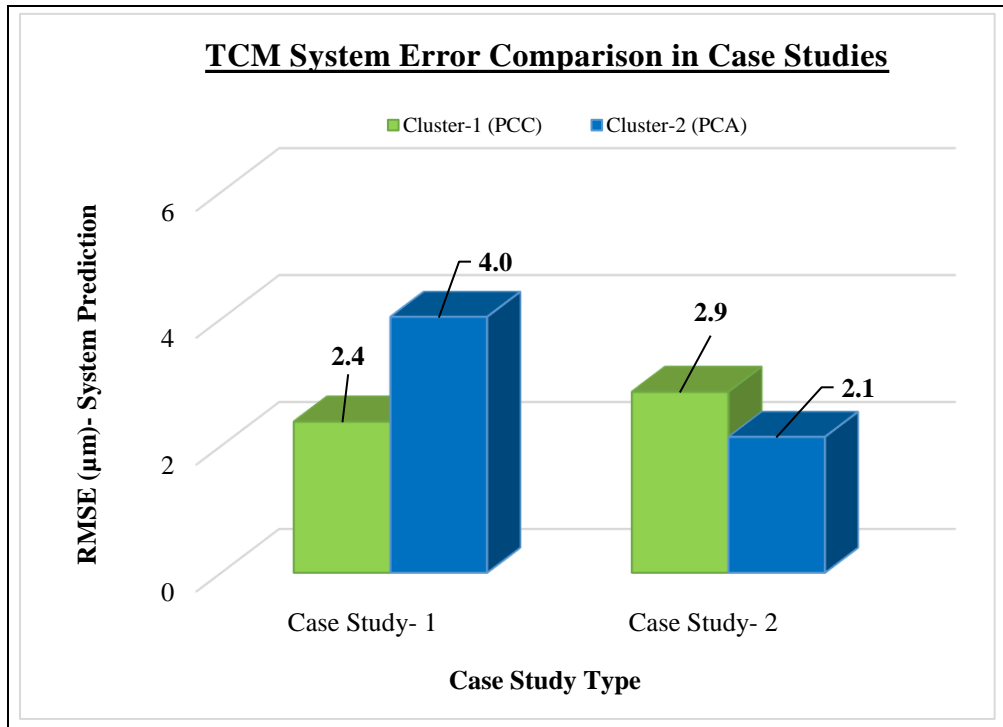


Figure 59: Error comparison of the TCM system

7.4. Adaptability of the TCM System

This section provides a general overview of the developed TCM system's adaptability for different workpiece material turning process. It demonstrates that the application of the TCM system can be wider due to its adaptive properties. The key objective of this research is to develop a low-cost TCM system which can be implemented for different workpiece machining processes. The case studies showed a promising result which can be carried out under different cutting conditions, cutting tools and materials during a turning operation.

Based on the result obtained from case studies, the further the existing TCM system can be trained (which means, more supervision of the developed TCM system), the more reliable it will become for further applications.

Furthermore, Material- 1, Material- 2 and Material-3 can be all used together to train the developed ANFIS based TCM system, which is defined as the ‘supervised learning’ of the developed TCM system. In this research, 65% of the entire online dataset from these workpiece materials were used to further train (Optimised training method used, hybrid) the model.

The supervised learning (training) modifies the membership functions (input-membership functions (gaussmf) which resulted in the lowest RMSE during the TCM system’s validation.

With the lowest RMSE, the supervised system can be implemented to online monitor tool wear in the machining of different workpiece materials. Therefore, the adaptability of the developed TCM system will increase its reliability and can establish it as the standard tool wear monitoring system for different workpiece materials.

Figure 60 provides a general guideline about the adaptability of the developed TCM system. The adaptability of the developed TCM system with reduced system RMSE can be further implemented in different workpiece material turning processes.

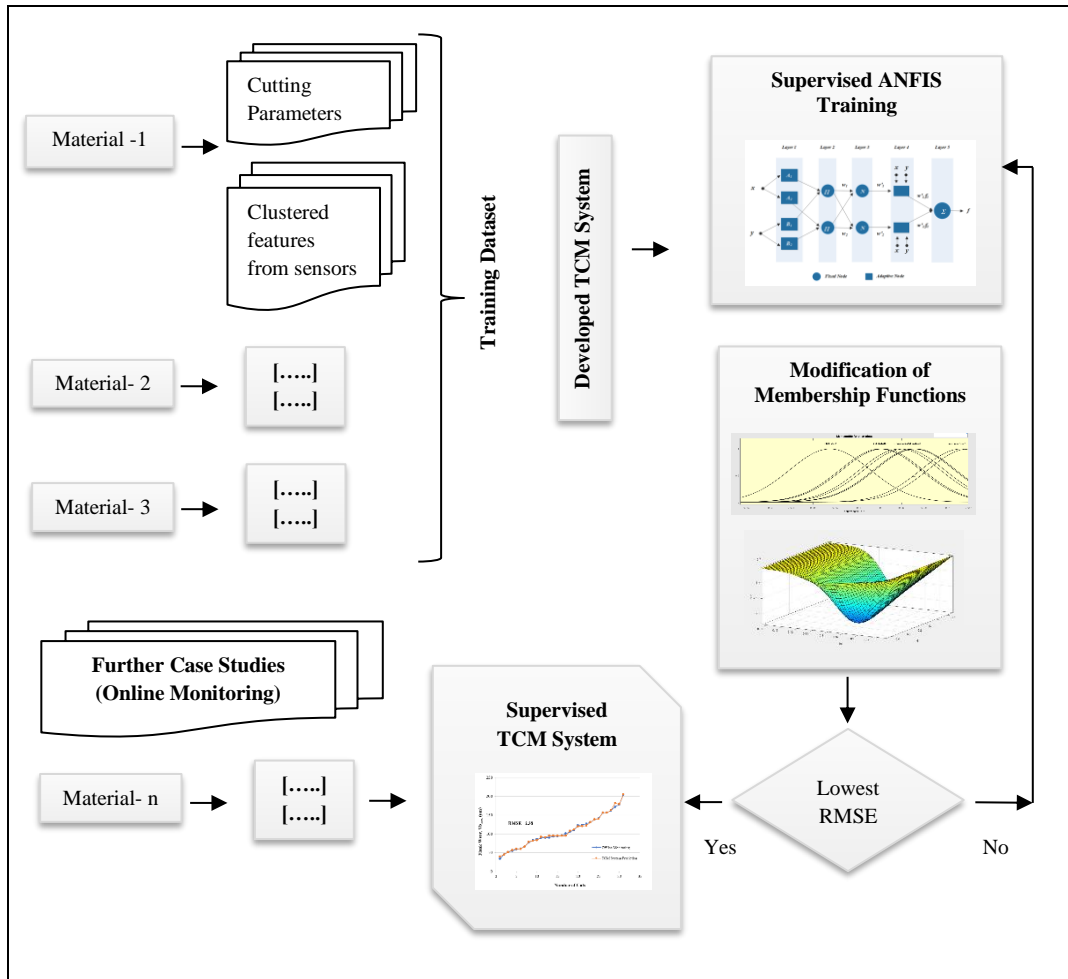


Figure 60: Adaptability of the Supervised TCM system

Chapter 8. Conclusions and Future Work

8.1. Summary of the Research

This research investigates the system level design and development of an automated, reliable tool condition monitoring system in the turning process using sensor fusion methodology, signal processing and artificially intelligent (AI) methods.

The research framework and the system level design are explained in Chapter 3. The main components of the TCM system's level design are: feature extraction, signal processing, dimensionality reduction and the AI-based decision making. This chapter describes the sensor fusion function, signal acquisition and preprocessing of the acquired signal.

Chapter 4 describes experimental work based on the design of experiment (DOE). A data acquisition system was used to detect the sensor fusion signals (five-channels) in every cutting test to generate a homogeneous dataset. All offline test results (tool flank wear measurement from the optical microscopy) were also presented in this chapter. Moreover, the effect of the cutting tool conditions on the sensor signals was also investigated to understand the relationship between sensor data and cutting tool conditions (tool flank wear).

Chapter 5 is composed of two sections. The first section investigates the application of modern digital signal processing in metal cutting processes. The current sensor, vibration sensor and force sensor were used in the sensor fusion setup of this research. Generally, these sensors have different properties and operating principles. Therefore, more insight is

required to build a complementary relationship between these sensors. Use of signal processing played a significant role here to transmit the information from the sensor fusion to a standard platform. Time-domain, frequency-domain and time-frequency domain analysis were implemented in this chapter to generate and extract the information from sensor.

The next section explores feature generation and extraction techniques from the acquired signal. A large number of features was extracted prior to analysis, which required dimensionality reduction techniques. Two types of dimensionality reduction techniques were implemented. Among them, PCC analysis provided the best result in this study. PCA results also considered that prompted further analysis. This chapter provided several cluster-based essential features from the extracted signal to serve as the basis for the decision-making system.

Chapter 6 investigates the application of artificial intelligence (AI) in the machining process. Two types of AI techniques were introduced in this chapter. Cluster-based features from the PCC analysis (Figure 38) and PCA (Figure 39) were used in this model. The AI techniques were comprehensively evaluated based on these different types of clustered features. The PCC based cluster-1 (Figure 38) comprised of features with the greatest correlation to cutting tool conditions. On the other hand, PCA features (Figure 39) consisted of signals obtained from the motor current sensor, combination of the motor current and vibration sensor and the combination of all sensors, respectively. In the first section, the ANN-based model was introduced based on the relationship between the extracted signal and the tool conditions (flank wear value). In the next section, the ANFIS based model was

introduced. Comparison analysis showed that the ANFIS model outperformed the ANN model in predicting the cutting tool conditions. The ANFIS model with the PCC based cluster-1 (Figure 38) input provided the best result with the lowest RMSE (0.013 μm) compared to the other model.

Moreover, the PCA based cluster-1 (Figure 39) showed a promising result (RMSE= 0.017 μm). This cluster only consists of spindle motor current sensor data and shows good reliability in tool wear prediction. Therefore, while using the ANFIS model, a low-cost current sensor can reliably detect the cutting tool conditions during the machining process.

Finally, the last chapter (Chapter 7) In this chapter, the developed TCM system based on the AISI 4340 steel hard-turning database was implemented to detect the cutting tool conditions in the turning operation of different material. The TCM system accuracy was analyzed in two case studies. In both cases, the TCM system based on the PCC based cluster-1 (Figure 38) type input (with machining conditions) and the ANFIS modelling showed high prediction accuracy.

The developed sensor fusion based TCM system can be applied for machining different materials under similar kinds of machining processes. The TCM system's adaptability ensures its successful implementation regardless of the workpiece material used in the turning process.

However, there are some limitations to this research. Only flank wear was considered. Though the pure alumina ceramic tool and CBN tool showed aggressive flank wear progression, other types of tool wear were also observed, such as crater wear and chipping in some cases. Also, the combinations of workpiece material and cutting tool were selected

based on the similar type of wear mechanism of the cutting tool. However, further study is currently ongoing in the stainless steel turning process (with a cemented carbide cutting tool) where the build-up edge (BUE), adhesion and chipping wear are significant wear criteria. Apart from flank wear prediction, the developed TCM system is currently being implemented to predict the build-up-edge during wet turning operation of stainless steel.

8.2. The contribution of the Research

The most significant contribution of this research work is introducing a low-cost tool condition monitoring (TCM) system for use as a standard at McMaster Manufacturing Research Institute (MMRI). Various aspects from different fields were applied in this research to investigate their relationship with the physics of the machining processes. Signal processing, data analytics and the application of AI techniques were used for design and development at the systemic level of tool condition monitoring.

The main contribution of this work is summarised as:

- Investigation of a multi sensor system tool wear monitor and comparative analysis of single, multiple and sensor fusions.
- Proposal of different data fusion strategies to obtain the most efficient sensor fusion setup, based on dimensionality reduction and correlation analysis results.
- Comprehensive cluster analysis of features extracted from the sensor fusion setup. Establishment of a standard data analysis procedure which will reduce the data analysis time in the future.

- Investigation of two AI decision-making algorithms. The results showed a promising outcome of ANFIS modelling implemented in the TCM system for machining different workpiece materials.
- Design of a low-cost TCM system for different workpiece materials in the turning process.
- Developing a standard method, via sensitivity analysis in which a combination of these sensors (particularly the motor current) can reliably monitor the progression of tool wear in machining. This development can significantly contribute to low cost and convenient monitoring of the cutting tool condition in the manufacturing environment.
- Design and development of a TCM system in the turning operation. The preliminary database was created from the cutting parameters of semi-finishing to finishing operations. A wide range of machining parameters was adopted in all experimental tests in this research to broaden the scope of the developed TCM system's implementation for a wide range of machining applications for different types of cutting tools and workpiece materials.
- Furthermore, it provides a standard tool wear monitoring guideline to be implemented online with the data acquisition software LabView©. Such as, the cluster-based features and successful prediction model can be used for monitoring parameter and data analytics during online tool wear monitoring through the LabView©.

8.3. Future Work and Recommendations

There are several directions in which the present research could be extended. The most relevant direction is to integrate the system into online monitoring program through LabView© data acquisition software and feedback control (based on decision-making system) of the machine. In this case, the decision from the TCM system can be conveyed to the machine without any presence of a human operator. This approach will extend the potential industrial applications of this research in a much broader way.

New advancements in the field of machine learning can also be adopted in the current research to enhance the model's adaptability to a highly dynamic manufacturing environment. In addition, further data analytic, big data training capability and smarter IoT hardware can be integrated into the TCM system.

Several material properties can be considered such as: the surface roughness, hardness, percentage of carbon (in steel) and stiffness of the material (which affects the measured current signal due to the change of non-linear loading) at a much wider scale. As a result, the developed TCM system can be implemented in the manufacturing industry considering reliability of the material properties in the same inventory lot.

References

1. Jantunen, Erkki. "A summary of methods applied to tool condition monitoring in drilling." *International Journal of Machine Tools and Manufacture* 42.9 (2002): 997-1010.
2. Rehorn, Adam G., Jin Jiang, and Peter E. Orban. "State-of-the-art methods and results in tool condition monitoring: a review." *The International Journal of Advanced Manufacturing Technology* 26.7-8 (2005): 693-710.
3. Martin, K. F. "A review by discussion of condition monitoring and fault diagnosis in machine tools." *International Journal of Machine Tools and Manufacture* 34.4 (1994): 527-551.
4. Scheffer, C., H. Engelbrecht, and P. S. Heyns. "A comparative evaluation of neural networks and hidden Markov models for monitoring turning tool wear." *Neural Computing & Applications* 14.4 (2005): 325-336.
5. Abellan-Nebot, Jose Vicente, and Fernando Romero Subirón. "A review of machining monitoring systems based on artificial intelligence process models." *The International Journal of Advanced Manufacturing Technology* 47.1-4 (2010): 237-257.
6. Siddhpura, A., and R. Paurobally. "A review of flank wear prediction methods for tool condition monitoring in a turning process." *The International Journal of Advanced Manufacturing Technology* 65.1-4 (2013): 371-393.
7. Heinemann, R., S. Hinduja, and G. Barrow. "Use of process signals for tool wear progression sensing in drilling small deep holes." *The International Journal of Advanced Manufacturing Technology* 33.3-4 (2007): 243-250.
8. Ertunc, Huseyin Metin, and Cuneyt Oysu. "Drill wear monitoring using cutting force signals." *Mechatronics* 14.5 (2004): 533-548.
9. Li, Xiaoli. "A brief review: acoustic emission method for tool wear monitoring during turning." *International Journal of Machine Tools and Manufacture* 42.2 (2002): 157-165.
10. Teti, Roberto, et al. "Advanced monitoring of machining operations." *CIRP Annals-Manufacturing Technology* 59.2 (2010): 717-739.
11. Dimla, Dimla Eric. "The correlation of vibration signal features to cutting tool wear in a metal turning operation." *The International Journal of Advanced Manufacturing Technology* 19.10 (2002): 705-713.

12. Wang, G. F., et al. "Vibration sensor-based tool condition monitoring using v support vector machine and locality preserving projection." *Sensors and Actuators A: Physical* 209 (2014): 24-32.
13. Rao, K. Venkata, B. S. N. Murthy, and N. Mohan Rao. "Cutting tool condition monitoring by analyzing surface roughness, work piece vibration and volume of metal removed for AISI 1040 steel in boring." *Measurement* 46.10 (2013): 4075-4084.
14. Ambhore, Nitin, et al. "Tool condition monitoring system: A review." *Materials Today: Proceedings* 2.4-5 (2015): 3419-3428.
15. Franco-Gasca, Luis Alfonso, et al. "Sensorless tool failure monitoring system for drilling machines." *International Journal of Machine Tools and Manufacture* 46.3-4 (2006): 381-386.
16. Lee, Kang-Jae, Taik-Min Lee, and Min-Yang Yang. "Tool wear monitoring system for CNC end milling using a hybrid approach to cutting force regulation." *The International Journal of Advanced Manufacturing Technology* 32.1-2 (2007): 8-17.
17. Constantinides, N., and S. Bennett. "An investigation of methods for the on-line estimation of tool wear." *International Journal of Machine Tools and Manufacture* 27.2 (1987): 225-237.
18. National Instruments, How to Choose the Right DAQ Hardware for Your Measurement System, 2012, pp. 1–5.
19. Liu, Xianbing, et al. "Adaptive interpolation scheme for NURBS curves with the integration of machining dynamics." *International Journal of Machine Tools and Manufacture* 45.4-5 (2005): 433-444.
20. Chen, Xiaozhi, and Beizhi Li. "Acoustic emission method for tool condition monitoring based on wavelet analysis." *The International Journal of Advanced Manufacturing Technology* 33.9-10 (2007): 968-976.
21. Abukhshim, N. A., P. T. Mativenga, and M. A. Sheikh. "Heat generation and temperature prediction in metal cutting: A review and implications for high speed machining." *International Journal of Machine Tools and Manufacture* 46.7-8 (2006): 782-800.
22. Vallejo, Antonio G., et al. "Tool-wear monitoring based on continuous hidden Markov models." *Iberoamerican Congress on Pattern Recognition*. Springer, Berlin, Heidelberg, 2005.

23. Al-Habaibeh, A., and N. Gindy. "Self-learning algorithm for automated design of condition monitoring systems for milling operations." *The International Journal of Advanced Manufacturing Technology* 18.6 (2001): 448-459.
24. Jeong, Gi-Bum, Dong Hwan Kim, and Dong Young Jang. "Real time monitoring and diagnosis system development in turning through measuring a roundness error based on three-point method." *International Journal of Machine Tools and Manufacture* 45.12-13 (2005): 1494-1503.
25. Abu-Mahfouz, Issam. "Drilling wear detection and classification using vibration signals and artificial neural network." *International Journal of Machine Tools and Manufacture* 43.7 (2003): 707-720.
26. Fu, Pan, A. D. Hope, and G. A. King. "A neurofuzzy pattern recognition algorithm and its application in tool condition monitoring process." *Signal Processing Proceedings, 1998. ICSP'98. 1998 Fourth International Conference on*. Vol. 2. IEEE, 1998.
27. Saravanan, S., G. S. Yadava, and P. V. Rao. "Condition monitoring studies on spindle bearing of a lathe." *The international journal of advanced manufacturing technology* 28.9-10 (2006): 993-1005.
28. Chelladurai, H., V. K. Jain, and N. S. Vyas. "Development of a cutting tool condition monitoring system for high speed turning operation by vibration and strain analysis." *The International Journal of Advanced Manufacturing Technology* 37.5-6 (2008): 471-485.
29. Elbestawi, Mo A., Mihaela Dumitrescu, and Eu-Gen Ng. "Tool condition monitoring in machining." *Condition Monitoring and Control for Intelligent Manufacturing*. Springer, London, 2006. 55-82.
30. Burke, Laura I., and Sabbir Rangwala. "Tool condition monitoring in metal cutting: a neural network approach." *Journal of Intelligent Manufacturing* 2.5 (1991): 269-280.
31. Sokołowski, Andrzej. "On some aspects of fuzzy logic application in machine monitoring and diagnostics." *Engineering Applications of Artificial Intelligence* 17.4 (2004): 429-437.
32. Jemielniak, Krzysztof, Leszek Kwiatkowski, and Paweł Wrzosek. "Diagnosis of tool wear based on cutting forces and acoustic emission measures as inputs to a neural network." *Journal of Intelligent Manufacturing* 9.5 (1998): 447-455.

33. Beggan, C., et al. "Using acoustic emission to predict surface quality." *The International Journal of Advanced Manufacturing Technology* 15.10 (1999): 737-742.
34. Wong, Y. S., et al. "Tool condition monitoring using laser scatter pattern." *Journal of Materials Processing Technology* 63.1-3 (1997): 205-210.
35. Sun, J., et al. "Effective training data selection in tool condition monitoring system." *International Journal of Machine Tools and Manufacture* 46.2 (2006): 218-224.
36. Pontuale, G., et al. "A statistical analysis of acoustic emission signals for tool condition monitoring (TCM)." *Acoustics Research Letters Online* 4.1 (2003): 13-18.
37. Gao, Hongli, and Mingheng Xu. "Intelligent tool condition monitoring system for turning operations." *International Symposium on Neural Networks*. Springer, Berlin, Heidelberg, 2005.
38. Choi, Yonghoon, Ranga Narayanaswami, and Abhijit Chandra. "Tool wear monitoring in ramp cuts in end milling using the wavelet transform." *The International Journal of Advanced Manufacturing Technology* 23.5-6 (2004): 419-428.
39. Stachowiak, G. P., P. Podsiadlo, and G. W. Stachowiak. "Shape and texture features in the automated classification of adhesive and abrasive wear particles." *Tribology Letters* 24.1 (2006): 15-26.
40. Zeng, Hao, et al. "Multi-modal sensing for machine health monitoring in high speed machining." *Industrial Informatics, 2006 IEEE International Conference on*. IEEE, 2006.
41. Li, Xiaoli, and Xin Yao. "Multi-scale statistical process monitoring in machining." *IEEE Transactions on Industrial Electronics* 52.3 (2005): 924-927.
42. Li, Xiaoli, Shiu Kit Tso, and Jun Wang. "Real-time tool condition monitoring using wavelet transforms and fuzzy techniques." *IEEE Transactions on Systems, Man, and Cybernetics, Part C (Applications and Reviews)* 30.3 (2000): 352-357.
43. Bradley, C., and Y. S. Wong. "Surface texture indicators of tool wear-a machine vision approach." *The International Journal of Advanced Manufacturing Technology* 17.6 (2001): 435-443.

44. Jurkovic, J., M. Korosec, and J. Kopac. "New approach in tool wear measuring technique using CCD vision system." *International Journal of Machine Tools and Manufacture* 45.9 (2005): 1023-1030.
45. Kerr, David, James Pengilley, and Robert Garwood. "Assessment and visualisation of machine tool wear using computer vision." *The International Journal of Advanced Manufacturing Technology* 28.7-8 (2006): 781-791.
46. Vilcek, Igor, and Jan Madl. "Cepstral Analysis in Tool Monitoring." *Emerging Solutions for Future Manufacturing Systems*. Springer, Boston, MA, 2005. 507-512.
47. Barker, R. W., G. Klutke, and M. J. Hinich. "Monitoring rotating tool wear using higher-order spectral features." *Journal of engineering for industry* 115.1 (1993): 23-29.
48. Spiewak, S., and S. M. Wu. "Tool wear monitoring and breakage detection based on "intelligent filtering"." *International Journal of Machine Tools and Manufacture* 28.4 (1988): 483-494.
49. Wang, Zhijun, et al. "Feature-filtered fuzzy clustering for condition monitoring of tool wear." *Journal of Intelligent Manufacturing* 7.1 (1996): 13-22.
50. Chen, Zhong, and XianMing Zhang. "Monitoring of tool wear using feature vector selection and linear regression." *International Conference on Natural Computation*. Springer, Berlin, Heidelberg, 2005.
51. Sick, Bernhard. "Classifying the wear of turning tools with neural networks." *International Conference on Artificial Neural Networks*. Springer, Berlin, Heidelberg, 1997.
52. Du, R. X., M. A. Elbestawi, and S. Li. "Tool condition monitoring in turning using fuzzy set theory." *International Journal of Machine Tools and Manufacture* 32.6 (1992): 781-796.
53. Kwon, Won-Tae, and Kornel F. Ehmann. "Tool wear monitoring by using the imaginary part of the transfer function of the cutting dynamics." *International Journal of Machine Tools and Manufacture* 34.3 (1994): 393-406.
54. Gao, Hongli, et al. "The investigation of a self-adjusting tool wear monitoring system." *Mechatronics and Automation, Proceedings of the 2006 IEEE International Conference on*. IEEE, 2006.

55. Elbestawi, Mo A., and Mihaela Dumitrescu. "Tool condition monitoring in machining-neural networks." *Information Technology for Balanced Manufacturing Systems*. Springer, Boston, MA, 2006. 5-16.
56. Jie, Sun, et al. "Feature extraction and selection in tool condition monitoring system." *Australian Joint Conference on Artificial Intelligence*. Springer, Berlin, Heidelberg, 2002.
57. Sun, Jie, et al. "The application of nonstandard support vector machine in tool condition monitoring system." *Electronic Design, Test and Applications, Proceedings. DELTA 2004. Second IEEE International Workshop on*. IEEE, 2004.
58. "Module ACT005-42L-S technical datasheet," AcuAMP
59. ISO, ISO. "3685: Tool-Life Testing with Single-Point Turning Tools." *International Organization for Standardization (ISO): Geneva, Switzerland* (1993).
60. Astakhov, Viktor P. "The assessment of cutting tool wear." *International Journal of Machine Tools and Manufacture* 44.6 (2004): 637-647.
61. Jung, Jee-Hoon, Jong-Jae Lee, and Bong-Hwan Kwon. "Online diagnosis of induction motors using MCSA." *IEEE Transactions on Industrial Electronics* 53.6 (2006): 1842-1852.
62. Misiti, Michel, et al. "Wavelet toolbox." *Matlab User's Guide* 64 (1997).
63. Welch, P. (1967). The use of fast Fourier transform for the estimation of power spectra: a method based on time averaging over short, modified periodograms. *IEEE Transactions on audio and electroacoustics*, 15(2), 70-73.
64. He, Q., Yan, R., Kong, F., & Du, R. (2009). Machine condition monitoring using principal component representations. *Mechanical Systems and Signal Processing*, 23(2), 446-466.
65. Tong, F., Tso, S. K., & Hung, M. Y. Y. (2006). Impact-acoustics-based health monitoring of tile-wall bonding integrity using principal component analysis. *Journal of sound and vibration*, 294(1-2), 329-340.
66. Rumelhart, D. E., & McClelland, J. L. (1986). Parallel distributed processing: explorations in the microstructure of cognition. volume 1. foundations.
67. Hagan, M. T., & Menhaj, M. B. (1994). Training feedforward networks with the Marquardt algorithm. *IEEE transactions on Neural Networks*, 5(6), 989-993.

68. Møller, M. F. (1993). A scaled conjugate gradient algorithm for fast supervised learning. *Neural networks*, 6(4), 525-533.
69. Moreira, M., & Fiesler, E. (1995). *Neural networks with adaptive learning rate and momentum terms* (No. EPFL-REPORT-82307). Idiap.
70. Jang, J. S. (1993). ANFIS: adaptive-network-based fuzzy inference system. *IEEE transactions on systems, man, and cybernetics*, 23(3), 665-685.